The Dissertation Committee for Albina Rifovna Khasanova Certifies that this is the approved version of the following Dissertation:

Genetic architecture of trait divergence in *Panicum hallii* ecotypes

Committee:

Thomas E. Juenger, Supervisor

Craig R. Linder

Philip A. Fay

Jose R. Dinneny

Caroline E. Farrior

Stanley J. Roux Jr.

Genetic architecture of trait divergence in *Panicum hallii* ecotypes

by

Albina Rifovna Khasanova

Dissertation

Presented to the Faculty of the Graduate School of

The University of Texas at Austin

in Partial Fulfillment

of the Requirements

for the Degree of

Doctor of Philosophy

The University of Texas at Austin

May 2021

Dedication

I dedicate this work to my husband Jason Edward Bonnette for his unwavering support in my journey to accomplish this goal.

Acknowledgements

The works presented here came to be in large part due to the invaluable support and input from the many individuals that I had an opportunity to interact with during my time as a graduate student. Firstly, I want to acknowledge and express my utmost gratitude to my graduate adviser Dr. Thomas Juenger: for providing me with an opportunity to be a part of his lab, creating a positive and interactive learning environment, leading me through this journey and being a supportive source of inspiration over the years. This work would not have been completed without him. I want also to thank all of my committee members: Dr. Philip Fay, Dr. Jose Dinneny, Dr. Randy Linder, Dr. Caroline Farrior and Dr. Stan Roux for being part of my committee and giving me important feedback, timely guidance and support during the course of this research.

Each of the three works in this thesis were aided by key collaborators and I am very thankful for their expertise and guidance: Dr. John Lovell (Chapter 1), Dr. Xiaoyu Weng (Chapter 1), Dr. Jerry Jenkins (Chapter 1), Dr. Yuko Yoshinaga (Chapter 1), Jason Bonnette (Chapter 1, 2, 3), Jeremy Schmutz (Chapter 1, 3), Joseph Edwards (Chapter 2, 3), Esther Singer (Chapter2). Additionally, I want to thank all of the Postdocs and my fellow grad students in the Juenger lab that I was lucky to interact with during graduate school and who also become my friends: Dr. Brandon Campitelli, Dr. Michael Aspinwall, Dr. Eugene Shakirov, Dr. Grace John, Dr. John Lovell, Dr. Xiaoyu Weng, Dr. Bhaskara Govinal Badiger, Dr. Robert Heckman, Dr. Alice MacQueen, Dr. Li Zhang, Dr. Weile Chen, Dr. Elizabeth Milano, Dr. Juan Diego Palacio-

Mejia, Taslima Haque, Samsad Razzaque. A special thanks to Dr. Joseph Edwards who become my mentor in microbial genetics.

I also want to thank all of the members of the Juenger lab for help in large scale studies and providing a positive learning environment, support, guidance, and sharing their expertise. The field and large scale greenhouse experiments would not have happened without Jason Bonnette and his team who assisted in experiment preparation, plant phenotyping and sample collection: Allison Hutt, Nick Ryan, Ben Anderson, Dallas Miller, Justin Shih, Matthew Donahue and Bethany Watson. Undergraduate students Jack Dwenger and Brady Lee also provided valuable help in greenhouse experiments along with all of the Juenger lab members.

I want to thank the Plant Biology graduate school and Integrative Biology department for travel awards that allow me to share my work at numerous conferences. Special thanks to Tamra Rogers, the departments graduate coordinator, for her help with all things organizational and administrative during graduate school.

Lastly, I want to thank my family, my mother Nailya and brother Nail for their support though this endeavor. And finally, my deepest thanks are to my husband Jason Bonnette for his constant help and emotional support all these years.

This research was supported by the DOE Office of Science, Office of Biological and Environmental Research (BER), grant no. DE-SC0008451 to TEJ. Additional funding sources included a NSF Plant Genome Research Program Grant (IOS-0922457) to TEJ and an NSF postdoctoral fellowship (IOS-1402393) to JTL. The work conducted by the U.S. Department of Energy Joint Genome Institute is supported by the Office of Science of the U.S. Department of Energy under Contract No. DE-AC02-05CH11231.

Abstract

Genetic architecture of trait divergence in *Panicum hallii* ecotypes

Albina Rifovna Khasanova, PhD

The University of Texas at Austin, 2021

Supervisor: Thomas E. Juenger

Environmental heterogeneity across a species range can drive functional trait variation and lead to the formation of locally adapted ecotypes. Plant ecotypes are often differentiated by suites of correlated root and shoot traits that share common genetic, developmental, and physiological relationships. This divergence requires coordination between multiple plant organ systems. This research predominantly examines the genetic architecture underlying root-shoot trait relationships and their interaction with the environment in order to develops a more complete picture of the adaptive differences that arise between ecotypes. We used a recombinant inbred line population derived from upland and lowland ecotypes of the diploid C4 perennial bunch grass *Panicum hallii* to examine the following: 1. The quantitative genetics of root and shoot trait coordination. 2. The quantitative genetics of the impact of plant root microbiomes collected from natural environments on plant root and shoot traits. 3. How plant host genetics shape root microbiomes. Utilizing extensive phenotyping of plant traits and a quantitative genetic approach, we identified several genomic 'hotspots' which control suites of correlated root and shoot traits, thus indicating genetic coordination between plant organ systems in the process of ecotypic divergence. In addition, we

found that genomic regions of colocalized quantitative trait loci (QTL) for the majority of shoot and root growth related traits were independent of colocalized QTL for shoot and root resource acquisition traits. The allelic effects of individual QTL underscore ecological specialization for drought adaptation between ecotypes and reveal possible hybrid breakdown through epistatic interactions. We show that the growth and development of ecotypes and their trait divergence depends on soil microbiomes and find that broad-sense heritability is modified by soil microbiomes, revealing important plant genotype-by-microbiome interactions for quantitative traits. We detected a number QTL interacting with the soil microbiome, including epistatic interactions dependent on soil microbiome context. We also show that microbial inocula habitat of origin changes the heritability for individual microbes (ASVs) and that different plant genomic regions are associated with abundance of individual microbes and community level structure. Our results highlight the genetic architecture underlying trait divergence and the importance of microbial interactions in C4 perennial grasses.

Table of Contents

List of Tables

List of Figures

Chapter 1: The genetic architecture of shoot and root trait divergence between mesic and xeric ecotypes of a perennial grass[1]

ABSTRACT

Environmental heterogeneity can drive patterns of functional trait variation and lead to the formation of locally adapted ecotypes. Plant ecotypes are often differentiated by suites of correlated root and shoot traits that share common genetic, developmental, and physiological relationships. For instance, although plant water loss is largely governed by shoot systems, root systems determine water access and constrain shoot water status. To evaluate the genetic basis of root and shoot trait divergence, we developed a recombinant inbred population derived from mesic and xeric ecotypes of the perennial grass *Panicum hallii*. Our study sheds light on the genetic architecture underlying the relationships between root and shoot traits. We identified several genomic 'hotspots' which control suites of correlated root and shoot traits, thus indicating genetic coordination between plant organ systems in the process of ecotypic divergence. Genomic regions of colocalized quantitative trait locus (QTL) for the majority of shoot and root growth related traits were independent of colocalized QTL for shoot and root resource acquisition traits. The allelic effects of individual QTL underscore ecological specialization for drought adaptation between ecotypes and reveal possible hybrid breakdown through epistatic interactions. These results have implications for understanding the factors constraining or facilitating local adaptation in plants.

[1]Khasanova A, Lovell JT, Bonnette J, Weng X, Jenkins J, Yoshinaga Y, Schmutz J, Juenger TE. 2019. The genetic architecture of shoot and root trait divergence between mesic and xeric ecotypes of a perennial grass. Frontiers in Plant Science 10: 1–10. Albina Khasanova designed and conducted glasshouse and field experiments, analyzed the results and wrote the chapter.

INTRODUCTION

Adaptations to abiotic stress have been implicated as driving factors in ecological speciation (Lexer and Fay, 2005; Stebbins, 1952), where populations have diverged across a number of traits, exhibit different niche characteristics, and eventually become reproductively isolated (Yardeni et al., 2016; Lowry, 2012; Clausen, 1951). Local adaptation to soil water availability is an especially important driver of plant evolution (Kooyers et al., 2015; Rajakaruna, 2004; Stebbins, 1952) and can impose strong natural selection on populations, leading to the formation of ecotypes that are differentially adapted to xeric and mesic habitats (Kumar et al., 2008; Joly et al., 1989). Xeric and mesic ecotypes are often characterized by the divergence of common suites of morphological and phenological traits (Lowry, 2012; Clausen, 1951) related to maintaining water status and tolerating drought (Juenger, 2013; Markesteijn and Poorter, 2009; Chapin et al., 1993).

While leaf and shoot traits are important drivers of adaptation to drought (Juenger, 2013; Carmo-Silva et al., 2009), the properties of root systems determine plant water access and can place constraints on shoot water status (Hund et al., 2009; Price et al., 2002). Shoot traits may be related to root traits through genetic correlation (Bouteille et al., 2012) or be dependent upon root traits through resource allocation tradeoffs (Hammer et al., 2009), including changes in carbon allocation between root and shoot systems (Hummel et al., 2010). Higher root mass ratio (RMR) increases water foraging capability to maintain plant water status, which can be accomplished by allocating more resources towards roots (Knights et al., 2006) or by inhibiting above ground growth (Hendricks et al., 2015). Specific leaf area (SLA, the ratio of leaf area to leaf dry mass) and specific root length (SRL, the ratio of root length to root dry mass) are both important plant

traits linked to resource acquisition (Cheng et al., 2016; Reich, 2014) and SRL is typically thought of as the below ground analog of SLA (Reich, 2014; Eissenstat et al., 2000). These traits are often positively correlated (Valverde-Barrantes et al., 2017; Reich, 2014; Withington et al., 2006) and associated with rapid growth (Pérez-Harguindeguy et al., 2016; Reich, 2014)—where an acquisitive root strategy (high SRL) can be aided by an acquisitive leaf strategy (high SLA; Pérez -Ramos et al., 2013). Despite evidence that root and shoot trait covariance is an important driver of plant adaptation, few studies have documented how combinations of specific shoot and root traits generate locally adapted ecotypes. The genetic basis of such trait complexes and the implications of recombining adaptive shoot and root traits in hybrids are poorly understood.

Quantitative genetic analyses and the mapping of quantitative trait loci (QTL) permit exploration of the genetic basis of trait correlations and trait divergence (Milano et al., 2016; Lovell et al., 2015; Fishman et al., 2002). Importantly, by simultaneously analyzing multiple traits, QTL mapping can infer the loci and genetic interactions that drive ecological trait correlations. Functional traits with a high degree of correlation that underlie divergence can result from pleiotropy through shared developmental genetics or genetic linkage (Lovell et al., 2013; Via and Hawthorne, 2005) as a result of correlational selection (Brodie et al., 1995). For example, colocalized QTL for root and shoot traits including root biomass, root volume, shoot biomass and plant height have been identified in a wheat recombinant inbred line population (Iannucci et al., 2017) likely resulting from pleiotropy or tightly physically linked genes. Overall, there is growing evidence for substantial genetic variation in root system architecture and root/shoot relationships. However, the loci driving these trait correlations and the degree to which these patterns impact plant productivity are largely unknown.

Panicum hallii is a small, self-fertilizing, C4 perennial bunch grass native to North America that occurs across a large geographical range comprised of diverse habitats and climates. Average annual precipitation ranges from 127 cm per year on the eastern border of its distribution to 13 cm per year on the west. *P. hallii* occurs as two distinct ecotypes (xeric upland and mesic lowland) that are classified as separate varieties, *P. hallii* var. *hallii* (hereafter referred to as *hallii*) and *P. hallii* var. *filipes* (hereafter referred to as *filipes*). *Hallii* is typically found in xeric upland habitats with shallow, dry, calcareous and rocky soils in the American southwest and northern Mexico; while *filipes* occurs in mesic lowland areas on clay and silt soils mostly along the Gulf Coast Plain of Texas and Mexico (Waller, 1976; Gould, 1975). The xeric upland ecotype, *hallii*, is smaller in stature and overall size than the mesic lowland ecotype *filipes*: with smaller leaves, fewer tillers, earlier flowering time, fewer flowers per inflorescence, but larger seed size and seed mass (Lowry et al., 2013; Waller, 1976). This is consistent with its polyploid relative, *Panicum virgatum* (an important biofuel candidate), where upland ecotypes are typically smaller, flower earlier (Lowry et al., 2014a) and have less leaf area (McMillan, 1965) than lowland ecotypes. Previous analyses of shoot traits in a F2 population of *P. hallii* (Lowry et al., 2014b) demonstrated that a few large-effect loci drove multivariate shoot trait divergence between *hallii* and *filipes*, and complete genomes has been assembled and compared (Lovell et al., 2018). Here, we investigate the genetic architecture of multidimensional root phenotypic traits and their relationship with shoots to develop a more complete picture of the adaptive differences between these ecotypes.

In this study, we cross xeric and mesic ecotypes of *P. hallii*, to generate a population of recombinant inbred lines (RIL) at the F7 generation and subsequently constructed a new genetic map based on whole genome re-sequencing. We utilized extensive phenotyping of root and shoot

traits and a quantitative genetic approach to identify the genetic architecture of trait relationships and their divergence among ecotypes. We discovered shared QTL clusters involved in genetic correlations between root and shoot growth related traits that were independent of QTL clusters for carbon allocation and phenology related traits. The allelic effects of individual QTL underscore ecological specialization for drought adaptation between *hallii* and *filipes* and reveal possible hybrid breakdown through epistatic interactions.

MATERIALS AND METHODS

Morphological shoot and root phenotyping under greenhouse conditions

We developed a population of recombinant inbred lines (RILs) derived from a cross of *hallii* and *filipes* and constructed a genetic map from whole genome re-sequencing (see Supplementary Appendix A1). Seedlings of 174 F7 RILs and the two parental genotypes were planted to 6 cm x 30 cm Cone-Tainers (Stuewe and Sons, Tangent, OR) filled with Field and Fairway Profile (The Turf Trade, NJ, USA) media. Plants were grown in completely randomized block design within three blocks on a single bench at the University of Texas greenhouse (see Supplementary Appendix A2). Plants were harvested within three days of a common developmental stage defined as when a fully expanded flag leaf with a visible ligule was observable on any tiller with an emerging panicle. Harvest dates across the population ranged from 27-51 days after germination. The tiller height, leaf length and area of the flag leaf of the main tiller were measured and tiller number was counted at the time of harvest. Total root number was counted and then the root system was spread out in a clear acrylic water filled tray and scanned at a 600 dpi resolution using an EPSON Scanner (Model 12000XL, Epson America, Inc., San Jose,

CA, USA) calibrated for use with WinRhizo Pro 2015 root image analysis software (Regent Instruments Inc., Canada). Leaf, shoot and root tissue was dried and weighed to obtain biomass. Specific leaf area (SLA) was calculated (Supplementary Appendix A2).

Root trait data was obtained from scans using WinRhizo Pro 2015 software and included total root length (cm), total root volume (cm3), and average root diameter (mm). Specific root length (SRL; cm g-1)), root tissue density (RTD, g cm-3), and root mass ratio (RMR) were calculated for each plant (Supplementary Appendix A2).

Data and QTL analysis

Data analyses centered on fitting linear mixed models and considered RIL genotype as a fixed effect (proc mixed, SAS) for the measured phenotypic traits. Block was also included as a fixed effect covariate when it had a significant impact on measured traits (emergence day, specific root length and root diameter). The SAS procedure PROC CORR was used to calculate genetic correlation coefficients of traits based on RIL line means. Broad-sense trait heritability was calculated using h2boot software using one-way ANOVA among inbred RILs with 1000 bootstrap runs (Phillips and Arnold, 1999). Trait divergence between parental lines was evaluated with a t-test in SAS.

The majority of the measured traits were continuously distributed with relatively strong multivariate structure based on pairwise correlational analyses. As such, we also used genetic principal component analysis (PCA) to obtain a multidimensional overview of shoot and root trait variation and integration. PCA was performed on the trait means of each line for the following phenotypic variables: emergence day, tiller number, root number, root biomass, shoot biomass, root diameter, root tissue density, specific root length, specific leaf area, tiller height, leaf length,

root volume and total root length. PCA was completed using SAS with the proc princomp function. The first three principal components that together explained 75% of total variation were retained for QTL analysis.

QTL mapping was completed in R using the R/qtl package (Broman and Sen, 2009) on the RIL breeding values as described above. When quantitative trait data distributions were not normally distributed, data was log (emergence day, tiller number) or square root (shoot biomass) transformed. Two functions were used to determine the position of QTL and to conduct the calculation of estimates for additive effects and epistasis (an additive-by-additive interaction between quantitative trait loci) (script: https://github.com/AlbinaKh/P.hallii_RIL_RootShoot_QTLmapping). The scantwo function with 1000 permutations was used to calculate penalties for main effect and interactions for each phenotypic trait, and the stepwise QTL function was used to conduct a forward-backward search and account for epistasis with a maximum of 6 QTL (at least two QTL peaks in addition to those detected with the scanone function) that optimized the penalized LOD score criterion. Threshold values for type 1 error rates were set at alpha = 0.05 for all traits based on permutation. 1.5 LOD drop intervals of QTL were calculated using the qtlStats function (Jtlovell/qtlTools, 2018). In addition, QTL analysis was performed on the first three principal components following the above procedure.

Confirming root and shoot biomass QTL in a field study

To further confirm and evaluate major QTL detected in our greenhouse study, we conducted a follow up field experiment on a focal QTL during the 2016 growing season. Ten RILs homozygous at the shared QTL region for root and shoot biomass were selected for this experiment

(5 with *filipes* alleles and 5 with *hallii* alleles). Eight biological replicates of each selected RIL line and eight replicates of the two parental genotypes were planted on May 10, 2016 under both restrictive and well-watered irrigation treatments ((10 RILs + 2 parents) x 8 biological replicates x 2 irrigation levels = 192 plants; see Supplementary Appendix A2). Plants were harvested towards the end of the summer growing season in August. Shoots were separated from roots, dried at 55°C for 4 days before weighing for biomass. Trait values more extreme than 1.5x the interquartile range were removed as outliers prior to analysis. For statistical analysis, we used linear mixed models with proc mixed in SAS. The main effect for the model was genotype at the focal QTL (*filipes* or *hallii* alleles at the marker position), treatment and genotype-by-treatment interaction. RIL line was used as a random effect to control for background genetic variance.

RESULTS

Heritable shoot and root trait differences between mesic and xeric ecotypes

The RIL parents representing mesic and xeric ecotypes of *Panicum hallii* (HAL2 and FIL2) had significantly different shoot and root trait mean values (Table 1.1). The xeric genotype, HAL2, had 2.3-fold earlier first panicle emergence (t values at 5 dfs and P values; t=2.87, P=0.035), 3.3-fold less shoot biomass (t=4.39, P=0.007) and 2.8-fold less root biomass (t= 3.08, P=0.028), 1.8-fold shorter plant height (t= 3.43, P=0.018), 2.2-fold shorter leaf length (t=6.3, P=0.001), 2-fold shorter total root length (t=3.29, P=0.022), 2.5-fold lower total root volume (t=3.41, P=0.02), and 1.3-fold increased specific root length (t=-2.5, P=0.05) relative to the mesic genotype FIL2 (Table 1.1).

We estimated broad-sense trait heritability (H2) as the proportion of observed phenotypic variance due to genetic differences among RILs in the population. In the RIL population, all measured traits were heritable, with H2 ranging from 18% to 66% for shoot traits and from 34% to 60% for root traits (bootstrap based significance, in all cases $P<0.001$). The most heritable traits were leaf length (66%), plant height (64%), shoot biomass (60%), root length (60%) and root biomass (58%; Table 1.1). Transgressive segregation, where the range of recombinant phenotypes extends beyond the range of parental values (Rieseberg et al., 1999), was found among the majority of traits except shoot biomass, plant height, leaf length, root biomass and root number, where FIL2 had trait values that were the highest or close to the highest of population wide values, while HAL2 values were generally in the middle of the population trait distribution (Table 1.1).

Many shoot and root phenotypic traits showed remarkably strong genetic correlations in the RIL population (Table A1). For example, shoot and root biomass ($r=0.92$, $P<0.0001$), tiller and root number ($r=0.67$, $P<0.001$), shoot biomass and root volume ($r=0.91$, $P<0.0001$), and shoot biomass and total root length ($r=0.90$, $P<0.001$) were all positively genetically correlated. We performed principal component analysis (PCA) to characterize the multivariate structure of our data. The first three PCA axes explained 75% of the overall trait variance. Principal component one (PC1; 45.5% variance explained) was composed of general plant size traits (shoot biomass, root biomass, number of tillers, number of roots, tiller height, leaf length, root volume and root length). Principal component two (PC2; 16.5%) was mainly composed of root resource acquisition traits (SRL, root diameter and root tissue density). Principal component three (PC3; 12.6%) was composed of carbon acquisition and allocation traits (SLA, RMR and panicle emergence; Table A2; Figure A1).

Paragraphs with the style *Heading 3,h3* applied can be extracted to appear in the table of contents with the style *TOC 3*.

QTL underscore root and shoot trait divergence between *hallii* and *filipes*

Given high H2 values, it is not surprising that QTL were detected for all measured traits. A total of 32 QTL were identified for 14 phenotypic traits: two QTL for one phenological trait, 14 QTL for five shoot traits and 16 QTL for eight root traits (Table 1.2, Figure 1.1, Figure A2). QTL for all traits showed additive effects in the direction of parental divergence, except for one of three QTL for tiller number, one of four QTL for root diameter, and one of three QTL for SRL. *Filipes* alleles had later panicle emergence and increased trait values for plant size related traits, including: emergence day, root number, root tissue density, root biomass, shoot biomass, tiller height, leaf length and root volume. *Hallii* alleles increased trait values associated with water acquisition (SRL) and carbon acquisition and allocation (RMR, SLA).

The additive effects of each QTL explained from 5.25% to 15.4% of phenotype variation for shoot traits, and from 5.9% to 18.6% for root traits (Table 1.2). Of these 32 QTL, eight QTL occupied unique positions in the genome: root tissue density on chr1, leaf length on chr2, tiller number on chr3, root number on chr3, SLA on chr5 and chr8, tiller height on chr6, and root diameter on chr8. As expected, three of these single QTL were also identified by principle component QTL (Table A3, Figure 1.1). The confidence intervals of all other QTL are shared or colocalized with at least one other QTL.

Trait-specific QTL cluster into genomic 'hotspots'

We identified three major and five minor clusters of root and shoot trait QTL occurring over five different chromosomes (Table 1.2, Figure 1.1). Here we identify QTL clusters (CL) by chromosome and numerical order from the telomere for each chromosome. As expected, we found that positions of QTL for principle components were highly indicative of the locations of QTL clusters for the traits loading on particular PC axes (Table A3, Figure 1.1, Figure A2).

QTL for PC1 localized to three genomic clusters of QTL for plant size traits. CL9.1 contains shoot biomass and leaf length QTL. CL5.1 contains root biomass, shoot biomass, root volume, total root length and panicle emergence QTL. CL5.3 contains root biomass, shoot biomass, root volume, total root length, tiller number and root number QTL. A separate QTL pair for tiller height and root diameter not identified with PC1 lies between these two large clusters. PC2 QTL localized with one of two genomic clusters of QTL for root resource acquisition traits. CL1.1 and 3.1 both contain SRL and root diameter traits. PC3 QTL localized to a single genomic cluster (CL7.2) related to carbon allocation traits. CL7.2 contains panicle emergence day, leaf length, number of tillers, RMR and SLA. Near this PC3 associated QTL is a minor cluster (CL7.1) of leaf length and SRL (Table 1.2, Table A3; Figure 1.1).

Four pairwise epistatic interactions, where the effect of one QTL depends on the allelic state of an unlinked QTL, were detected (Table 1.2, Table A3; Figure 1.2). Three QTL from cluster CL5.3 (shoot biomass, root biomass and PC1) interacted with other QTL for these traits located in CL5.1. In addition, the root number QTL from CL5.3 interacted with the root number QTL on chr3. Individuals that possess the *hallii* allele for these QTL at CL5.3 mask the positive effects of their interactive QTL.

A Major Pleotropic Effect QTL is Confirmed in the Field

To confirm the effects of QTL observed in a controlled greenhouse study, we phenotyped two sets of RILs homozygous for different parental alleles at the loci for shoot and root biomass (CL5.2) in a field experiment. While the magnitude of increased biomass for lines with *filipes* alleles at the selected QTL observed in the field is 24% less for the root biomass and 11% less for the shoot biomass relative to the greenhouse, the effects are significant and in the same direction as those observed in the greenhouse. Field grown lines with *filipes* parental alleles produced 1.9-fold more root biomass (P=0.0024) and 2.7-fold more shoot biomass (P=0.0002) relative to field grown lines with *hallii* parental alleles (Figure 1.3). In addition, the HAL2 parental line showed a 1.8-fold increase trend in RMR (P=0.09) over the FIL2 parental line under field conditions compared to the 1.2-fold difference observed in the greenhouse (P=0.018). There were no significant differences between the irrigation treatments or the interaction of treatment by genotype for RILs or the parental genotypes. However, root biomass showed a 1.2-fold increase trend under the dry treatment relative to the wet treatment (P=0.08).

DISCUSSION

Ecotypes are often differentiated by suites of correlated root and shoot traits that may share common genetic and developmental architectures as a result of adaptive differentiation. One of our major findings was several genomic 'hotspots' of colocalized QTL for multiple shoot and root traits. This is consistent with a previous study of a *P. hallii* F2 population covering a suite of ecotype differentiating shoot trait QTL which clustered on chr5 (Lowry et al., 2014b). In addition to confirming this important locus, we discovered additional root traits linked to this region along

with additional regions of clustered loci for root and shoot traits. Colocalized QTL controlling traits such as root biomass, shoot biomass, among others, has also been shown in RIL populations of wheat and sorghum (Mace et al., 2012; Iannucci et al., 2017). These findings indicate that specific loci can shape both shoot and root morphological traits, through tight linkage of several genes controlling individual traits or a single pleiotropic gene that controls several traits.

PC1 QTL localized to three genomic regions controlling several size related root and shoot traits (shoot biomass, root biomass, root volume, and other). We found that the *hallii* allele had additive effects in the direction of ecotype divergence and contributed to smaller root and shoot phenotypes in every case compared to the *filipes* allele. This finding is consistent with the global pattern observed in angiosperm plants whose shoot and root biomass are positively correlated (Enquist and Niklas, 2002) and with other studies on perennial grasses where total biomass is decreased under water limited conditions (Tozer et al., 2017; Weißhuhn et al., 2011; Baruch, 1994). Importantly, we show that one of the main growth QTL effects is robust to the environment and persists under natural field conditions.

In addition to differences in absolute size, there are expected differences in carbon acquisition and allocation between xeric and mesic ecotypes. PC3 resulted from cluster of carbon allocation and phenology related traits (SLA, RMR, tiller number and panicle emergence). Plants with *hallii* alleles had greater SLA, RMR, tiller number, and faster panicle emergence. Thinner leaves (high SLA) have lower carbon cost and are associated with increased photosynthetic capacity (Cornelissen et al., 2003; Reich et al., 1997). Increased RMR helps to maintain plant water status and productivity under drought (Comas et al., 2013). Faster flowering time along with greater tiller number allows for rapid production of seeds when resources are available for short

time periods. These factors combined may indicate that *hallii* employs a fast acquisitive strategy for drought escape; acquiring nutrients rapidly and flowering quickly to enter a dormant state before periods of summer drought. Acquisitive shoot and root strategies have been associated with fast growth strategies and summer dormancy in other perennial grasses (Balachowski et al., 2016). This contrasts with the lower SLA, and RMR of the mesic *filipes*, which may employ a slow strategy of thicker longer lasting leaves, larger more persistent roots, and abundant above ground foliage. This common genetic control of ecotype differentiating traits involving shoot and root organs suggests that these factors evolved in tandem. Variously, we found a relatively weak genetic correlation between SLA and SRL, which are important plant traits linked to resource acquisition (Cheng et al., 2016; Reich, 2014) and associated with fast growth (Pérez-Harguindeguy et al., 2016; Reich, 2014). Each of these traits had three independent QTL. Thus, divergence of these traits is likely due to independent loci which become structured across ecotypes as a result of strong directional or correlational selection. In this case, our crossing scheme was able to largely decouple these traits through recombination.

Observed pairwise epistatic interactions for root biomass, shoot biomass and root number showed that *hallii* alleles mask the effects of *filipes* alleles in all cases. When lines are homozygous for *hallii* parental alleles at CL5.3, it contributes to smaller phenotypes for these traits, regardless of the genotype at their respective interactive QTL. This suggests that the CL5.3 loci could include a pleiotropic gene with major effect that controls the development of multiple shoot and root size related traits. Natural populations of *P. hallii* ecotypes are largely homozygous, thus these linked QTL likely work together in a positive direction and contribute to the phenotypic trait correlations that underlie ecotype divergence. The observed epistasis in the RIL population could be involved

in ecological speciation (Burke and Arnold, 2001), and these interactions in hybrid plants could be deleterious and impact survivorship by undermining synergistic trait relationships. For example, the combination of reduced root and shoot size effected by *hallii* alleles may be desirable in xeric environments, but deleterious in natural hybrids or under the higher competition mesic environments that *filipes* inhabits.

Greenhouse detected genetic correlations confirmed under field conditions

There is persistent concern that effects observed in greenhouse studies are not representative of plant performance in natural or agronomic environments. Although greenhouse and growth chambers may be able to replicate a wide range of temperature and light conditions, other differences between these artificial and natural environments can be significant. Furthermore, greenhouse studies are often conducted on very young plants and in smaller than optimal pots, which can significantly alter root architectures compared to natural environments. Several recent studies have highlighted how differences in conditions between glasshouse and natural settings can affect the mapping of genetic architectures for various plant traits (Poorter et.al., 2012; reviewed in Lovell et al., 2016).

We sought to overcome this concern by confirming the glasshouse detected genetic architecture of two of our chief traits of interest (root biomass and shoot biomass) in selected RILs and parental genotypes in a field setting at full plant maturity. In the RILs, we found that our glasshouse observed QTL were confirmed. For the parental lines, we found that root mass ratio differences between the xeric and mesic ecotypes nearly doubled under field conditions as compared to the glasshouse study. This suggests that adaptive allocation of biomass to roots increases with plant age and can also be constrained by pot limitations in the glasshouse. More

importantly, these results provide credence to the assumption that our glasshouse study is predictive of plant performance in a natural setting. Future studies with *P. hallii* should explore the genetic architecture of shoot:root traits over multiple perennial seasons in additional field studies. These data will help to clarify the lifetime fitness consequences of allocation strategies and potential ecological tradeoffs that arise in natural habitats.

CONCLUSION

In the process of ecotype formation, populations can diverge across many functional traits and exhibit different niche characteristics, which requires coordination between plant organ systems. Root traits are involved in adaptive differentiation to abiotic stresses by their direct effects on water acquisition, and through correlation, tradeoffs or constraints with shoot traits (Mace et al., 2012; Hammer et al., 2009). Our study sheds light on the genetic architecture underlying the relationships between root and shoot traits involved in ecotype divergence of *Panicum hallii* and demonstrates that some correlated traits are under common genetic control as a result of QTL colocalization and interaction, while other traits are controlled by independent loci. We found several genomic hotspots relating to multiple root and shoot traits and a striking pattern of epistatic interaction impacting overall plant growth. Further insight into the molecular basis of these loci will be an important step in understanding the genetic coordination and ecological importance of root and shoot systems involved in ecotype divergence.

DATA ACCESSIBILITY

The raw sequencing data was deposited at NCBI (Table A4).

TABLES

Table 1.1. FIL2 and HAL2 root and shoot trait value means with SE and t-statistics; and RIL root and shoot trait value means, range and broad-sense heritability (H2) with SE. t-statistics given at 5 degrees of freedom with statistically significant P-values indicated in bold text.

Phenotypic Trait	**FIL2**	**HAL2**	***t***	***P*-value**	**RIL mean**	**RIL range**	H^2±**SE**
Panicle Emergence (day)	9.25±1.19	4.00±1.38	2.87	**0.035**	7.01±1.74	1.00 – 18.33	0.51±0.05
Shoot Biomass (g)	4.74±0.49	1.41±0.57	4.39	**0.007**	1.65±0.33	0.29– 4.74	0.59±0.05
Tiller Number	6.25±0.48	5.00±0.56	1.68	0.150	6.00±0.83	3.00 – 14.50	0.50±0.05
SLA	325.62±18.15	382.77±20.96	-2.06	0.094	381.58±33.17	264.67 – 499.36	0.18±0.08
Plant Height (cm)	21.18±1.82	11.63±2.11	3.43	**0.018**	12.57±1.56	4.30 – 23.65	0.63±0.04
Leaf Length (cm)	30.77±1.72	14.23±1.98	6.30	**0.001**	15.66±1.46	4.75– 24.27	0.66±0.04
Root Biomass (g)	1.38±0.18	0.51±0.21	3.08	**0.028**	0.54±0.10	0.12 – 1.60	0.58±0.06
Root Number	14.00±0.97	8.33±1.11	3.84	**0.012**	8.87±1.39	2.50 – 15.00	0.38±0.05
SRL (cm g^{-1})	10.14±0.85	13.37±0.98	-2.50	0.055	12.27±1.11	6.12 – 17.95	0.43±0.06
RTD (g cm^{-3})	0.06±0.01	0.05±0.01	1.31	0.247	0.05±0.01	0.03 – 0.08	0.39±0.07
Root Diameter (mm)	0.46±0.01	0.44±0.02	1.27	0.259	0.45±0.01	0.37 – 0.55	0.37±0.05
Root Volume (cm^3)	2.43±0.28	0.98±0.32	3.41	**0.019**	1.00±0.17	0.26 – 2.90	0.56±0.05
Root Length (m)	1.37±0.14	0.67±0.16	3.29	**0.022**	0.65±0.11	0.12 – 1.64	0.59±0.04
RMR	0.22±0.01	0.27±0.01	-3.44	**0.018**	0.25±0.02	0.16 – 0.39	0.34±0.09

Table 1.2. Main and epistatic effects of QTL for the *Panicum hallii* RIL population.

Phenotype	Chr	Peak (cM)	1.5 Lod Interval	LOD	% var	Effect	SE	Positive allele donor	QTL Cluster (CL)
Panicle Emergence	5	52.1	40-59	4.59	9.85	-0.044	0.009	*filipes*	CL5.1
(day)	7	80.0	31-83	4.31	9.2	-0.039	0.008	*filipes*	CL7.2
Shoot Biomass	5	58.6	56-60	7.43	14.8	-0.044	0.007	*filipes*	CL5.1
(g)	5	136.0	128-142	5.08	9.82	-0.031	0.007	*filipes*	CL5.3
	9	66.1	60-71	4.78	9.19	-0.027	0.005	*filipes*	CL9.1
	Epi5:5			2.86	5.36	0.027	0.007		
Tiller Number	3	40.5	38-48	7.23	14.74	-0.054	0.009	*filipes*	
(count)	5	137.0	128-142	3.47	6.73	-0.037	0.009	*filipes*	CL5.3
	7	73.6	46-81	4.84	9.56	0.039	0.008	*hallii*	CL7.2
SLA	5	13.3	0-26	3.15	5.25	9.772	2.543	*hallii*	
(cm^2g^{-1})	7	66.0	60-74	8.56	15.37	16.394	2.494	*hallii*	CL7.2
	8	19.8	16-23	8.33	14.90	16.077	2.484	*hallii*	
Tiller Height	5	76.0	74-77	6.16	13.34	-1.765	0.320	*filipes*	CL5.2
(cm)	6	83.9	69-88	3.82	8.05	-1.096	0.256	*filipes*	
Leaf Length	2	89.7	76-96	4.28	8.56	-1.19	0.264	*filipes*	
(cm)	7	43.6	35-64	4.39	8.80	-1.293	0.283	*filipes*	CL7.1
	9	63.4	59-75	3.41	6.76	-0.985	0.246	*filipes*	CL9.1
Root Biomass	5	58.6	56-60	8.81	18.61	-0.012	0.002	*filipes*	CL5.1
(g)	5	136.0	135-142	8	16.71	-0.010	0.002	*filipes*	CL5.3
	Epi5:5			4.61	9.21	0.008	0.002		
Root Number	3	88.0	69-104	6.18	13.9	-1.08	0.199	*filipes*	
(count)	5	125.7	125-130	5.36	11.94	-0.81	0.196	*filipes*	CL5.3
	Epi3:5			2.79	5.99	0.73	0.202		
SRL ($cm\ g^{-1}$)	1	91.5	82-94	5.3	11.02	0.66	0.131	*hallii*	CL1.1

Table 1.2 (continue)

Phenotype	Chr	Peak (cM)	1.5 Lod Interval	LOD	% var	Effect	SE	Positive allele donor	QTL Cluster (CL)
	3	18.8	17-36	5.16	10.7	0.78	0.156	*hallii*	CL3.1
	7	44.7	34-49	3.16	6.4	-0.55	0.145	*filipes*	CL7.1
RTD (g cm^{-3})	1	6.3	0-20	3.15	7.9	-0.001	0.0004	*filipes*	
Root Diameter	1	86.0	82-94	4.73	8.68	-0.009	0.002	*filipes*	CL1.1
(mm)	3	34.2	30-36	5.36	9.91	-0.011	0.002	*filipes*	CL3.1
	5	71.9	66-75	3.78	6.84	0.010	0.002	*hallii*	CL5.2
	8	47.9	43-52	4.65	8.50	-0.009	0.002	*filipes*	
Root Volume	5	58.6	56-63	3.96	8.85	-0.134	0.030	*filipes*	CL5.1
(cm^3)	5	117.2	109-142	3.07	6.77	-0.119	0.032	*filipes*	CL5.3
Root Length	5	58.6	44-138	3.12	7.85	-0.82	21.29	*filipes*	CL5.1,2,3
RMR (ratio)	7	67.0	62-74	6.36	15.34	0.0137	0.002	*hallii*	CL7.2

Chr, chromosome; Peak, cM (centimorgan) position of the QTL peak; LOD, logarithm of odds; % var, percent of variance; SE, one standard error; SLA, specific leaf area; SRL, specific root length; RTD, root tissue density; RMR, root mass ratio; Epi, epistasis.

FIGURES

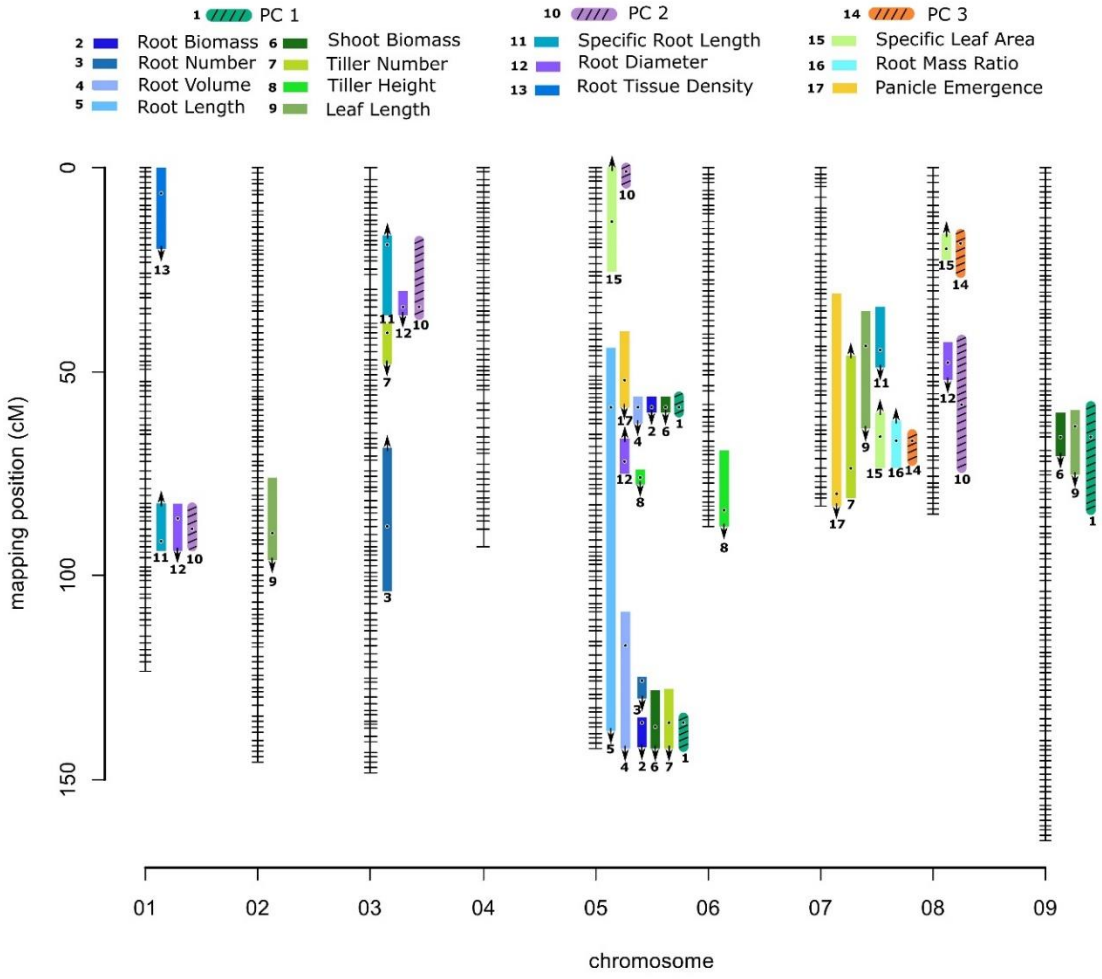

Figure 1.1. Genetic map of the *Panicum hallii* RIL population with location of trait QTL. Colored bars indicate 1.5-LOD drop confidence intervals. Location of dots within the bars is the location of QTL peaks. Arrow represents the direction of additive effect, with up or down arrows indicating that the hallii allele increases or decreases the trait value.

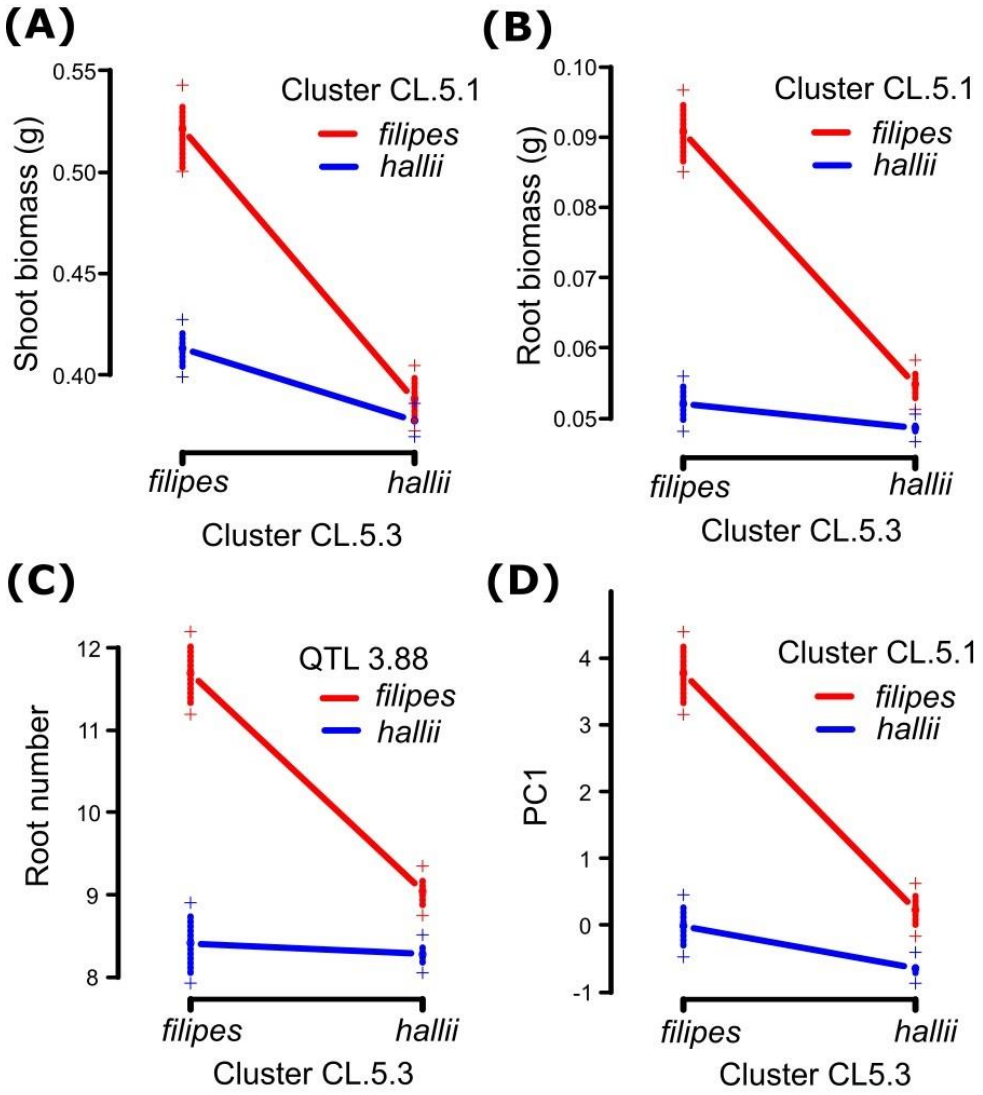

Figure 1.2. Pairwise epistatic QTL in the *Panicum hallii* RIL population. Plotted points indicate two-locus genotype means ± 1SE for the two loci containing root biomass between CL.5.1 and CL.5.3 (A), shoot biomass between CL.5.1 and CL.5.3 (B), root number between QTL 3.88 and CL.5.3 (C) and PC1 between CL.5.1 and CL5.3 (D).

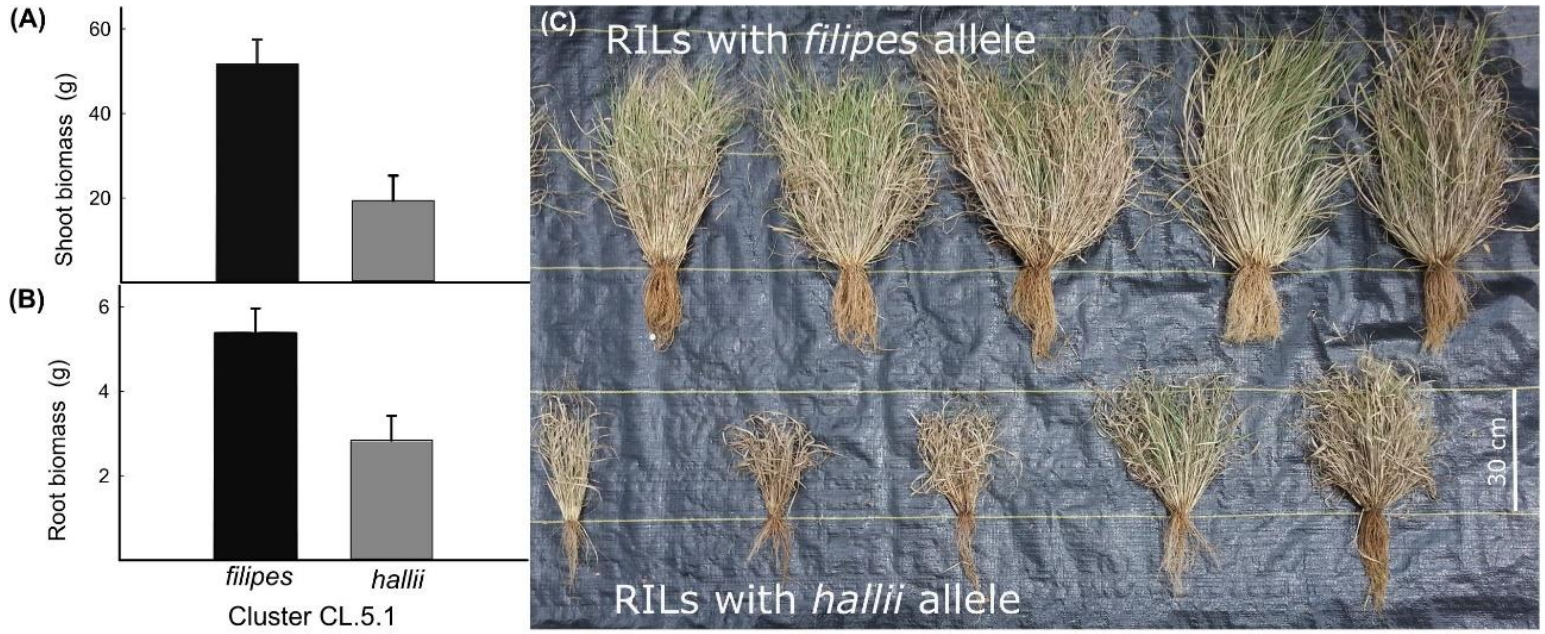

Figure 1.3. Mean ± 1SE of shoot biomass (A) and root biomass (B) for field grown *Panicum hallii* RILs homozygous for either *filipes* or *hallii* parental alleles at shoot and root biomass QTL located in cluster CL5.1. Picture of field grown RILs homozygous at CL5.1 for *filipes* allele (top row) and *hallii* allele (bottom row) (C).

Chapter 2: Quantitative genetic-by-soil microbiome interactions in a perennial grass affect functional traits

ABSTRACT

- Plants interact with microbiota that can impact plant growth, performance, and local adaptation. However, few studies have explored the impact of microbial communities from distinct native locations on plant functional traits, and less is known about how host-microbe interactions affect the quantitative genetics of plant traits.
- We used a recombinant inbred line (RIL) mapping population derived from upland and lowland ecotypes of the diploid C4 perennial bunch grass *Panicum hallii* to explore quantitative genetic responses to soil microbiomes. Our experimental design included contrasts of RILs grown in the presence and absence of microbial communities derived from native habitats. We collected data for multiple traits thought to be important in ecotype divergence.
- We show that the growth and development of ecotypes and their trait divergence depends on soil microbiomes. Moreover, we find that broad-sense H2 is modified by soil microbiomes, revealing important plant genotype-by-microbiome interactions for quantitative traits. We detected a number of quantitative trait loci (QTL) that interact with the soil microbiome, including epistatic interactions that depend on the context of the soil microbiome.
- Our results highlight the importance of microbial interactions in ecotypic divergence and trait genetic architecture in C4 perennial grasses.

INTRODUCTION

Plants have evolved alongside microbes for millions of years and have formed intricate relationships with soil microbial communities via their root systems. Soil microbial community composition is shaped by soil abiotic conditions and varying soil types contain microbiomes with distinct taxonomic distributions (Hartman & Tringe, 2019; Fierer, 2017). Plant host genetics also drive the assembly of rhizosphere and endosphere microbial communities (Trivedi et al., 2020; Jones et al., 2019), and crop varieties or natural ecotypes (or genotypes) grown in a common environment can differ in root and rhizosphere community structure (Bowsher et al., 2020; Li et al., 2018; Perez-Jaramillò et al., 2017; Wagner et al., 2016). To some degree, the root microbiome can be thought of as an extended phenotype of the plant. Plant-soil-microbiome relationships can influence plant traits and there is strong evidence that microbes can yield positive effects on plant performance directly or indirectly by impacting plant functional traits (Egamberdieva et al., 2017; Wagner et al., 2014; Lau & Lennon, 2012). Plant root associated microbiomes impact root traits, can increase nutrient acquisition, provide indirect impacts on shoot traits (such as increasing shoot biomass) and promote tolerance to abiotic and biotic stress (Santhanam et al., 2015; Mendes et al., 2013; Sukumar et al., 2013; Friesen et al.,2011). In synthetic community research, growing the same genotype in the presence or absence of differing sets of selected microbiomes produces a wide range of plant trait modulation (De Souza et al., 2020; Vorholt et al., 2017). Given the growing evidence of microbial effects on plant growth and development, it's possible that plant microbial interactions also play a role in the process of local adaptation, where plant populations diverge and exhibit different niche characteristics and habitat preferences.

Many plant species are composed of highly varied ecotypes across their range, each of which may show a high degree of trait divergence. Traits under strong genetic control can be profoundly influenced by environmental factors and the degree to which these factors influence plant traits can vary widely across genotypes. These types of interactions are termed genotype-by-environment interaction (GxE; Des Marais et al., 2013). Many studies focus on local adaptation and GxE in response to changing conditions (Midolo & Wellstein, 2020; Leimu & Fischer, 2008), however, the relative contribution of abiotic and biotic factors is often unclear (Runquist et al., 2020). Plants encounter diverse biotic factors including competition, herbivory, pathogens and an array of microbial communities (Bischoff et al., 2006; Järemo et al., 1999), but little is known about how specific interactions between plants and microbial communities contribute to adaptation. The vast majority of studies exploring plant-microbe interactions focus on pairwise interactions with strong effects, often involving nitrogen fixing symbionts, model beneficial bacterial strains, or agronomically important pathogens. However, plants often grow better in novel or foreign soil microbial communities compared with those found in their native range (Benning & Moeller, 2020; Lankau & Keymer, 2018), which could indicate maladaptation derived from the presence of specialized pathogens or host microbiome mismatching. Additional experimental studies exploring the impact of microbial communities are critically needed to fully elucidate aspects of plant-microbe interactions and local adaptation.

Several difficulties arise in studying plant-microbe interactions in both laboratory and field settings. Microbial communities are highly diverse and dynamic and many of their constituent strains are difficult to isolate and culture independently. Synthetic community approaches utilize small groups of isolated microbes for use in research, but such communities are incomplete

representations of real-world conditions and are often grown in unrealistic conditions (e.g., on agar plates or in Magenta boxes). Conversely, manipulating microbial communities in natural conditions is nearly impossible due to a plethora of uncontrollable factors. A hybrid approach of introducing microbial communities to lab grown plants through controlled and quantified inoculum derived directly from natural sources can bridge these two solutions (Wagner et al., 2014). While not without limitations, such studies allow an evaluation of the impact of the microbiome on plant traits that vary quantitatively in response to the presence of microbes in more controlled environments and help introduce tools like high throughput phenotyping, genetic mapping, and genomic analyses to plant-microbiome studies (Singer et al., 2020).

Numerous QTL mapping studies have explored the genetic architecture of GxE in natural and crop populations for a number of abiotic factors and this approach has become widely utilized to study plant responses to abiotic stress and to understand plant trait plasticity (Des Marais et al., 2017; Vij & Tyagi, 2007). Far less work has been directed at the influence of biotic factors, specifically microbiomes. QTL involved in the recruitment of mycorrhizae have been studied for a variety of crops such as maize, poplar, and winter wheat (Lehnert et al., 2017; Labbé et al., 2011; Kaeppler et al., 2000). While mycohorrizal fungi are widely studied and their function is better known, microbiomes are a diverse assemblage of many bacterial and fungal clades, and approaches which examine whole microbiomes may be more reflective of how plant adaptation is shaped through these interactions in natural environments.

Panicum hallii is a diploid, C4, self-fertilizing, North American native perennial bunch grass that occurs across a large geographical range with diverse habitats and climate. There are two naturally occurring ecotypes of *P. hallii* that are classified as separate varieties: an upland

xeric ecotype, *P. hallii* var. *hallii* (hereafter referred to as *hallii*) and a lowland mesic ecotype, *P. hallii* var. *filipes* (hereafter referred to as *filipes*). These ecotypes display trait divergence in a similar direction and magnitude to other perennial grass species with upland and lowland ecotypes which is thought to be driven by adaptive evolution along precipitation gradients across the species range (Khasanova et al., 2019; Gray et al., 2014; Lowry et al., 2014a). Many observations have shown that both ecotypes of *P. hallii* display a large degree of plasticity in several shoot traits in response to changes in abiotic factors including light (Weng et al., 2019) and precipitation (Lovell et al., 2018), yet these differences are minor in comparison to the differences inherent between the ecotypes. However, little is known about the importance or relative contribution of biotic factors including microbial influences in shaping plant shoot and root traits in this system and plants in general compared to these more widely studied abiotic factors.

Here, we used quantitative genetics to understand the impact of soil microbiomes on root and shoot traits. By using a recombinant inbred population derived from a cross between two ecotypes, we can identify plant genomic regions contributing to these microbial-mediated traits. To overcome the limitations of synthetic community approaches and the complexity of natural soils, we took a hybrid approach of inoculating sterilized soils with naturally derived microbial communities in a glasshouse setting. In this study, we analyze a population of recombinant inbred lines (RILs) derived from a cross between the upland and lowland ecotypes of *P. hallii*. Specifically, we sought to answer four questions: 1) Does the native soil microbiome drive plasticity in *P. hallii* above- and below-ground traits? 2) Are microbiome effects general, or specifically related to the location of origin of the microbiome? 3) Do *P. hallii* ecotypes exhibit GxE in response to variable soil microbiomes? And, 4) Can we map genetic effects and their

interactions with the microbiome to the genome? Overall, our experiment demonstrates the impact of living soil microbiomes on the quantitative genetic architecture of both root and shoot traits in *P. hallii* and highlights the potential importance of microbiomes in local adaptation.

MATERIALS AND METHODS

Plant Material

We used a population of recombinant inbred lines (RILs) derived from a cross between *P. hallii* var. hallii (HAL2 ecotype) and *P. hallii* var. *filipes* (FIL2 ecotype) to evaluate the genetic basis of plant-microbiome interactions. A single F1 hybrid individual was used to generate a large population of F2 plants which were bred by single seed descent to the F7 generation (Khasanova et al., 2019). Both parental lines have full genome assemblies that are publicly available (https://phytozome-next.jgi.doe.gov/; Lovell et al., 2018). The RIL population genetic linkage map was constructed by shallow whole-genome resequencing and is congruent with the physical genome. Seeds of 293 F7 RILs and the two parental ecotypes were sterilized with 50% bleach for five minutes, rinsed with sterile water, treated with 30% ethanol for 30 seconds and finally given five sterile water rinses. Seeds were then scarified with sandpaper and placed on wet sterilized sand in petri dishes sealed with parafilm in August 2018 and allowed to germinate for five days on a bench in a glasshouse located at the University of Texas at Austin (16-h days at 500 μE m −2 s −1, 28°C; 8-h nights at 24°C). Germinated seedlings were then transferred haphazardly over a three-day period to prepared treatment pots.

Microbial Inoculum Collection and Treatment Soil Preparation

RIL plants and parental replicates were grown in the presence and absence of native microbiome inoculations. Inoculum consisted of soils obtained from the same locations where we obtained the parental lines used in the creation of the RIL mapping population (Lady Bird Johnson Wildflower Center in Austin, TX for var. *hallii* and the Corpus Christi Botanical Garden, in Corpus Christi, TX for var. *filipes*). The Austin soil is a reddish rocky clay/silt and the Corpus soil is a grey sandy loam; specific nutritional and mineral contents are given in Table A5. Soils were collected from areas where *P. hallii* was present by clearing the soil surface of plant matter, collecting soil by shovel to a depth of 25 cm and subsequently removing any root material present in the sample.

To create the four treatments, we mixed 1% by volume of native soil inoculum (to minimize the effect of nutritive and textural soil properties from the inoculum) with a twice-autoclaved horticultural soil mix of compost, decomposed granite and vermiculite (Thunder Dirt, Geo Growers, Austin, TX) and left it for two weeks to incubate in closed 400-liter plastic containers (Edwards et al., 2019). We selected this particular commercial soil mix because it homogenizes well and facilitates root extraction and cleaning. For soils utilized in the control treatments, the 1% soil inoculum was twice autoclaved over a 24-hour period before mixing and incubation. Given the nature of this large-scale glasshouse experiment under an open-air environment, true sterility of the control treatments is not possible and thus we refer to the treatments by their inoculum source: microbiome treatments as Austin Inoculated (AI) and Corpus Inoculated (CI), and control treatments as Mock Austin Inoculated (MAI) and Mock Corpus Inoculated (MCI). Our Mock treatment combinations are likely to obtain their living microbiome through incomplete or

inadequate sterilization, by dispersal from adjacent pots, or from inoculation through the general glasshouse environment. Our goal is simply to use sterilization and inoculation as tools to manipulate the microbiome, and we acknowledge that our treatments levels will be far from sterile controls or natural microbiomes. Nevertheless, we feel this experimental system allows us to assess the holistic impact of soil microbes, above and beyond what could be obtained from studies of individual microbes or experiments under more artificial conditions.

Microbial DNA extraction and 16S rRNA gene sequencing

To characterize the microbial community composition at each native location, we collected samples of rhizosphere and root from eight haphazardly selected *hallii* individuals growing at Austin and nine *filipes* individuals growing at Corpus. Additionally, five bulk soil samples (all plant material removed) from each site were collected in areas adjacent to living *hallii* plants (44 samples total). DNA extraction of these samples was performed with the DNeasy PowerSoil Pro Kit (Qiagen, Hilden, Germany). 16S ribosomal RNA gene regions were amplified using the 515F-806R primer pair, barcoded and sequenced on the Illumina Novaseq platform on the SP flowcell using 250x250. To characterize treatments in the glasshouse experiment, this procedure was performed again on rhizosphere, root and soil samples taken at harvest from seven replicates of each parent in each treatment (four treatments x 14 parents x three compartments = 168 samples).

Experimental Design

Each treatment consisted of all 293 RILs and seven replicates of each parent for a total of 307 plants per treatment in the experiment (four treatments x 293 RILs + 56 parents =1,228 plants). Incubated soil for treatments and controls was transferred to 950 ml 3" x 8" Mini-Treepots (Stuewe

and Sons, Tangent, OR). Treepots were lined with sterile plastic bags perforated at the bottom to allow water drainage and facilitate easy root system removal. Pots for all four treatments were randomized in a single block design in a glasshouse and left for acclimation in open air for two weeks before seedlings were transplanted. Plants were watered with UV sterilized tap water for the duration of the experiment.

Harvest and Phenotyping

Plants were harvested prior to first panicle emergence after six weeks of growth over a five-day period. Individual plants were extracted from pots by gently pulling the plastic bag from the pot to prevent damage to the root system. Next, the plastic bag was cut open and plants with their attached root system were removed from the soil by gently shaking them over a wire mesh. Soil rhizosphere samples for parental lines were collected by dipping each root system into sterilized 50 ml tubes filled with 1X phosphate buffered saline (PBS) buffer. Plants were then hung by the shoot base on a clamping apparatus and soil particles were removed from the root system with a spray of UV-sterilized water. Roots were then separated from shoots and preserved in 90% ethanol for future phenotyping. Tillers were counted and flag leaf area of the main tiller was measured. Shoot and leaf tissue were dried at 55°C and weighed separately to obtain aboveground biomass, and to calculate Specific leaf area (SLA; fresh leaf area / dry mass of the leaf (cm2 g-1)).

For each plant, we calculated number of roots produced and then the entire intact root system was carefully spread out in a clear acrylic tray filled with UV sterilized water and then scanned on an EPSON 12000XL flatbed scanner (Epson America, Inc., San Jose, CA, USA) calibrated for use with WinRhizo Pro 2019 root image analysis software (Regent Instruments Inc., Canada). In addition, one representative nodal root with attached lateral roots was haphazardly

selected and scanned separately to facilitate collection of 1st order root length and lateral root length. Following scanning, a small portion of the central root system for parental lines was sampled into Eppendorf tubes and frozen for DNA extraction and PCR amplification to determine root endosphere microbial community composition. The remaining root tissue was collected and dried for 96 hours in an oven at 55°C, and weighed to obtain root system biomass.

Scans of the root systems and selected single roots were analyzed with WinRhizo Pro 2019 software to determine total root length (cm), total root volume (cm3), and average root diameter (mm), for intact root systems; and lateral root length and the 1st order root length for selected individual roots. Lagarde's local threshold parameter was used to facilitate recognition of thin and pale roots and the following traits were calculated: specific root length (SRL; total root length / root biomass (cm g-1)), root tissue density (RTD; root biomass / total root volume (g cm-3)), and root mass ratio (RMR, root biomass / total biomass).

Sequence Analysis

Demultiplexed sequences were trimmed to remove adapter and primer binding sites using Cutadapt (Martin, 2011). Amplicon sequence variants (ASVs) were inferred using DADA2 (Callahan et al., 2016). Errant ASVs due to chimerization were detected using the "consensus" method in DADA2 and discarded. Any ASV with a sequence length of greater than 256 bp or less than 250 bp were discarded. Taxonomic classifications were assigned to each ASV using DADA2's assignTaxonomy () function using the Silva reference database (version 132, Quast et al., 2013).

Microbiome data was analyzed using the software package R (R Core Team, 2020). ASVs assigned to mitochondrial and chloroplast lineages were discarded from the data prior to

normalization. For principal coordinates analysis (PCoA) and phylum level abundance statistics, the raw counts were normalized to account for differences in sequencing depth between samples by dividing each ASV count by sequencing depth of a particular sample and multiplying by 1000 to place the counts on a per mille scale. Principal coordinate analyses were conducted using the capscale () function in the package Vegan (Oksanen et al., 2020). Bray Curtis dissimilarity on log2 transformed abundances was used for all PCoAs unless otherwise noted. Alpha diversity was calculated using Shannon Entropy from the diversity () function in Vegan. Differential abundance of aggregated phylum abundances was performed using linear models on log2 transformed abundances. Differential abundance of ASVs between conditions was conducted using DESeq2 on raw counts (Love et al., 2014).

Plant trait data from all replicates of parental ecotypes was analyzed to test the genotypic and microbial treatment effects on plant morphological traits. We fit factorial linear mixed models using PROC MIXED in SAS (Littell et al., 1996) consisting of Ecotype, Treatment, and Ecotype x Treatment interactions as fixed effects. Preliminary analysis did not show any significant differences (in all cases, $P > 0.113$ between MAI and MCI treatments for parental ecotypes and RILs), thus the average between them was used for this and all subsequent analyses (hereafter referred to as the Mock Inoculated (MI) treatment).

To explore the impact of the microbiome on the quantitative genetic architecture of our measured traits, we fit linear mixed models testing for GxE using the sommer package (Covarrubias-Pazaran, 2018) in R based on the additive and epistatic relationship matrix determined from the genotypic data of the RIL. Our approach competed a simple “base” model including additive genetic variance (Va), additive*additive epistatic variance (Vaa) and a fixed

treatment effect to more complex models that allowed either the additive genetic variance (Va), additive*additive epistatic variance (Vaa) or the residual to vary by the microbiome treatment (AI, CI, MI). Models were compared with AIC and LIK and assumed no covariance among treatments. We calculated broad-sense H2 as Va+ Vaa/Vp and present variance components and model comparisons.

The observation of different QTL effects under different treatment conditions provides evidence for QTL x environment interactions. There are a number of potential statistical strategies for detecting the occurrence of QTL x environment interactions (Des Marais et al., 2013). To detect QTL present in the AI, CI and MI treatments, we completed QTL mapping on RIL values in R using the R/qtl package (Broman & Sen, 2009) in each environment separately. When quantitative trait data distributions were not normally distributed, data was log transformed (Tiller Number, Root Number, Shoot Biomass, Root Biomass, Root Diameter, RMR, Lateral Root Length). We used calc.genoprob with step=2 and map.function="kosambi" to calculate genotype probabilities every two cM. Penalties for main effects were calculated with the scantwo function on 1000 permutations and the stepwise QTL function was used to conduct a forward-backward search accounting for epistasis (additive-by-additive interaction between QTL) with a maximum of seven QTL (QTLs detected with scanone function plus at least two QTL peaks) that optimized the penalized LOD score criterion. For all traits the alpha was set at 0.05 as a threshold for type 1 error rates based on permutation to detect main QTL. We also lowered our threshold to alpha = 0.1 to detect suggestive QTL, and the qtlStats function was used to calculate the 1.5 LOD drop interval of QTL.

We further tested for QTL x environment interactions in a full linear model incorporating the data from the three treatments using the PROC MIXED procedure of SAS. First, in R, we used fill.geno with the method = "maxmarginal" and min.prob = 0.95 to fill in missing genotypic data. These data were then used in a series of linear models in SAS including the main and interactive effects of all significant markers detected in the initial QTL analysis and the interaction of these markers with the experimental treatments (Lynch & Walsh, 1998). Marker x treatment interaction indicates QTL x environment interaction, marker x marker interaction represents epistasis averaged over the environments, and marker x marker x treatment interaction indicates environment specific epistasis. We performed this analysis to test GxE interaction effects by contrasting the AI, CI and MI microbiomes (e.g. potentially identifying different soil or residual microbiome impacts). To test the significance of individual marker alleles at each treatment, we used the slice function in SAS as tests of simple effects (Winer, 1971) for all significant marker x treatment and marker x marker x treatment interactions.

RESULTS

Treatment drives bacterial community composition

We used 16S rRNA gene amplicon sequencing classified into ASVs to characterize both the native microbial communities and the communities generated by our experimental inoculations. For parental ecotypes growing under natural habitats, PCoA revealed strong location/ecotype and compartment effects (i.e. soil, rhizosphere, and root) across axes one and two, respectively (Figure 2.1 a). Permanova mirrored these results with location/ecotype explaining the most variance ($R2 = 0.21$, $P < 0.001$) and compartment explaining the second most

($R2 = 0.15$, $P < 0.001$; Table 2.1). Microbiota varied significantly in alpha diversity between the compartments, but not between location (Figure 2.1 b). Phylum level distributions were overall consistent between microbiota of plants growing at the two natural locations with *Proteobacteria*, *Actinobacteria*, and *Acidobacteria* being dominant members (Figure 2.1 c), which is congruent with results from previous root-associated microbiome studies (Singer et al., 2019; Wagner et al., 2016; Edwards et al., 2015; Lundberg et al., 2012). Only three relatively low abundance phyla displayed significant differences between location-ecotype: WPS-2 and *Entotheonellaeota* in the rhizosphere and *Rokubacteria* in the root (Figure A3). Conversely, microbiota from the two locations were much more divergent at the ASV level and we identified a total of 735 unique ASVs which were differentially abundant by compartment (440 in soil, 251 in rhizosphere, and 401 in roots; Figure 2.1 d).

We next analyzed microbiota acquired under experimental conditions in the glasshouse by sampling roots and rhizosphere from the parents of the RIL population, along with soil from unplanted pots. PCoA revealed that inoculum and compartment significantly impacted microbiota composition (Figure 2.2 a). Alpha diversity was also impacted by compartment and inoculum: in general, we found that plants inoculated with native soil slurries hosted microbiota with greater Shannon diversity compared to plants with heat-killed, mock microbiota (Figure 2.2 b). As expected, when comparing the effect of inoculum source within heat killed or native conditions, we found that microbial communities of plants and soil with heat-killed inocula were significantly more similar than if the inoculum was unsterilized and this effect was consistent independent of compartment (Figure A4). Similar trends were observed at the phylum level: there were many more differentially abundant phyla by soil source when the inoculum was intact rather than heat

treated (Figure 2.2 c, d). When identifying ASVs whose abundance was impacted by soil inoculation source, many more ASVs were differentially abundant in comparisons between native soil inoculum compared to the heat killed versions (Figure 2.2 e). These results indicate that heat sterilization of inoculum dampens the effect of soil source on compositions of the resulting microbiome and that plants inoculated with native microbiota host significantly different microbial communities in the rhizosphere and roots.

When analyzed together, we found that glasshouse and field microbiomes formed distinct communities, yet were still identifiable by soil source (Figure A5a). These patterns were evident at the phylum level. For example, when comparing the relative abundance of phyla between field microbiota and treated glasshouse microbiota, *Acidobacteria*, *Actinobacteria*, and *Patescibacteria* were significantly more abundant under field conditions while *Bacteroidetes*, *Firmicutes*, *Gemmatimonadetes*, and *Gammaproteobacteria* were more abundant under glasshouse conditions (linear model on log transformed relative abundances for each phylum, adjusted P value < 0.05, Figure A5b). Taken together these results indicate that while the microbiomes resulting from inoculations of field soil could not fully recapitulate microbiota under field conditions, the experimental treatments retained significant differences in bacterial community structure between Austin and Corpus inoculations. Furthermore, our mock inoculated treatments (heat sterilized microbiota) resulted in bacterial communities with minimal differences compared to plants inoculated with live microbiota.

Effect of microbiome on parental traits

Differences in traits among parents were driven by plant ecotype (genotype), environment and genotype by environment interactions (GxE). Parental ecotypes differed in shoot and root traits

across all treatments. For example, FIL2 produced 1.64-fold more shoot biomass (P<0.0001), 1.98-fold more root biomass (P<0.0001), 1.46-fold higher RTD (P<0.0001) and 1.80-fold lower SRL (P<0.0001) relative to HAL2 (Figure 2.3 a, d, e; Table A6; Table A7). These results mirrored earlier descriptive studies of *P. hallii* ecotypes (Palacio Meija et al., 2021; Lowry et al., 2014b), including earlier studies of the shoot and root traits studied here (Khasanova et al., 2019). Treatment also had a significant effect on plant traits (Figure 2.3 a-c, e, f; Table A6, Table A7). For example, plants grown in inoculated soils had greater shoot biomass (1.35-fold more biomass in CI and 1.17-fold more in AI treatments relative to the MI treatment (P=0.027)), lower lateral root length (1.2-fold less in CI and 1.53-fold less in AI relative to MI (P=0.046)), and showed changes in SLA dependent upon treatment (1.05-fold increase in AI and 1.06-decrease in CI relative to MI (P=0.039)). Importantly, we also identified several ecotype x microbiome interactions (Figure 2.3 d-f; Table A6, Table A7). For example, SRL of FIL2 decreased 1.17-fold under AI and 1.33-fold under CI relative to MI soil, while HAL2 showed 1.1-fold increase in SRL under AI and no change under CI relative to MI (P=0.039; Figure 2.3 d; Table A6, Table A7). RTD of FIL2 increased 1.1-fold under AI and 1.36-fold under CI relative to MI, while HAL2 showed 1.1-fold decrease under AI and 1.1-fold increase under CI relative to MI (P=0.046; Figure 2.3 e; Table A6, Table A7). In total, seven traits showed ecotype differences between parental lines, five traits were affected by microbial treatment and three traits had significant ecotype x microbiome interaction (Figure 2.3; Table A6, Table A7).

The impact of the microbiome on the quantitative genetic architecture of our measured traits was evaluated by comparing “base” and “GxE” linear mixed models. In 11 out of 12 cases, the GxE models were favored by AIC and log likelihood ratio tests (Table A8). Broad-sense

heritability was low for most traits (ranging from 0.01 to 0.18; Table A6). Overall, we document considerable evidence that the microbiome modifies the expression of quantitative genetic variation in *P. hallii*.

QTL across and between microbial treatments

A total of 32 QTL were identified for 12 traits across all environments (Figure 2.4; Table A9, Table A10). The additive effects of each QTL explained from 2.9 - 22% of trait variation (Table A9). Of these 32 QTL, six QTL occupied unique positions in the genome. The confidence intervals of all other QTL overlapped or colocalized with at least one other QTL. Eight traits (shoot biomass, tiller number, SRL, lateral root length, root diameter, root number, root biomass and total root length) had 16 QTL with overlapping confidence intervals grouped into two genomic hotspots on chromosome three (Figure 2.4; Table A9). The hotspot located on 3@4.3 (chromosome number @ centimorgan) showed an additive effect in the direction of parental ecotype divergence, while the other hotspot located on 3@58 showed an additive effect opposite the direction of parental divergence. Pleiotropic genes or linked genes with correlated effects may drive these genomic hotspots of correlated traits. We also found significant epistatic interaction between these two hotspots. Individuals possessing the *hallii* allele for the QTL on 3@58, masked the effects of their interactive QTL on 3@4.3 (Table A9).

We detected 11 ecotype x microbiome QTL for 10 traits (Figure 2.5 a-k; Table A9, Table A10). Each of these QTL were analyzed to directly test in which treatment they were present, and to estimate the direction and magnitude of their effects (Figure 2.5 a-k; Table 2.2, Table A11). In the MI treatment, QTL for shoot biomass, root biomass and root number were detected with the *hallii* allele contributing to a higher trait value (Figure 2.5 a, i, j). In the CI treatment, QTL for

RMR and SRL were detected with the *filipes* allele contributing to a higher trait value (Figure 5b, c). In the AI treatment, QTL for tiller number, root number, root diameter, lateral root length, shoot biomass, root biomass, root length and first order root length had allelic effects with the *hallii* allele contributing to a higher value for all traits except root diameter (Figure 2.5 d-k). Of these QTL, four have overlapping confidence intervals and are grouped into a hotspot on chromosome seven and three are grouped together on chromosome nine (Figure 2.5 e-k; Table 2.2, Table A11). Two of the three QTL present on chromosome nine were also detected in the MI treatment (Figure 2.5 i, j; Table 2.2, Table A11). Epistatic interactions between two QTL for root diameter (chr 1@68 and 2@78.8) were present only in AI and CI (Figure 2.6 a-c, Table 2.2, Table A11) and individuals possessing genotypes at the two loci from the same parent (recovering the ecotypic configuration) produced traits with the smaller magnitude (Figure 2.6 b, c).

DISCUSSION

There is growing appreciation for the important and often complex interactions that exist between plants and their associated microbial communities. Exploring the genetic architecture of plant trait-microbiome interactions is an important step in determining if these interactions may play a role in local adaptation and evolution. Here, we conducted a QTL study with a *P. hallii* RIL mapping population in soils inoculated with microbiomes from native *P. hallii* habitats to observe the impact of microbiomes on plant traits and genetic architecture. We found that the microbiota in the natural habitat of the RIL parental lines are distinct and served as suitable experimental treatments to quantify the effects of different microbiota on host-plant traits. In this study, soils inoculated with native microbiomes drive trait plasticity in both, above and below ground traits, and these effects were both general and location specific with respect to the origin of the microbial

inoculum. We found QTL that displayed GxE for ten of twelve measured traits, suggesting widespread genetic variation in trait responses to plant-microbiome interaction. We also identified epistatically interacting QTL for root diameter present only in microbiomes from native locations, indicating that hybridization may disrupt genes and their interaction with microbes through root characteristics. Overall, our study suggests that plant-microbe interactions play an important role in plant genetic architecture and impact plant functional traits.

It is clear that host traits are impacted by microbial communities. Although soil microbes interact directly with the root system, they can induce changes that affect entire plant. The presence of microbiomes from native soil inoculum induced trait plasticity in above and belowground traits for the parental lines that was general and location specific (Figure 2.3). For example, traits linked to resource acquisition such as specific leaf area (SLA) and specific root length (SRL) were altered in responses to the presence of microbiomes. High SLA correlates with high nitrogen contents and low structural investments in leaves, which yields high rates of photosynthesis to promote rapid growth (Cornelissen et al., 2003; Reich et al., 1997), a trait necessary in xeric environments with short seasons terminated by drought (Balachowski et al., 2016). This is consistent with high SRL, where plants produce longer and thinner roots with less structural input to search for water (Balachowski et al., 2016). SLA showed a plastic response to location specific native microbiomes: SLA was increased for plants with the AI microbiome and decreased for plants with the CI microbiome. This pattern is consistent with the directionality of ecotypic divergence. Moreover, SRL showed GxE in response to microbiomes that was also concordant with the direction of parental trait divergence: with xeric adapted *hallii* showing higher SRL in the presence of native microbiomes while mesic adapted *filipes* showed lower SRL.

We detected two groups of QTL interacting with native microbiomes. The first included QTL which responded to native soil inoculums regardless of their origin and a second where QTL interacted with native soil inoculum from only one site. For example, QTL for root number 8@33.1 was present only in the MI treatment and not detected in native treatments, suggesting that native microbiomes reduce variation for this trait (Figure 2.5 a). This could be explained by microbial taxa which flourished under MI treatment given that the niche competition was relaxed. QTL for SRL (4@19.1) and RMR (3@74.9) showed location specific GxE (Figure 2.5 b, c); plants with the *filipes* allele in the CI treatment resulted in a higher trait value. This is opposite to the direction of SRL trait divergence in parental ecotypes and to their response to the CI treatment. Eight QTLs showed location specific GxE to the AI treatment (Figure 2.5 d-k). Our previous study conducted at the panicle emergence stage suggested that xeric *hallii* employs a fast-acquisitive strategy for drought escape by acquiring nutrients rapidly and flowering quickly to enter dormancy before the onset of summer drought (Khasanova et al., 2019). This is consistent with current study conducted at the tillering stage where plants with the *hallii* allele in interaction with the AI microbiome produced more root and shoot biomass. This is accomplished by the increased production of tillers with roots to support them. Root systems of plants with these *hallii* QTL hotspots produced longer and thinner roots, putatively allowing increased foraging and resource acquisition. Four of these QTL present in interaction with AI clustered in the genomic "hotspot" on chromosome seven and three QTL clustered on chromosome nine. This common genetic control of ecotype differentiating traits involving above and below ground traits suggests that these factors interact with the AI microbiome in tandem, potentially contributing to ecotype divergence and local adaptation. The effects of QTL with GxE are small in our study, possibly due to the fact that the data was collected

at the early seedling stage. Future studies at later life stages may shed the light on whether these impacts are amplified over time.

We also identified epistatically interacting QTL for root diameter present only in treatments with microbiomes from native locations (Figure 2.6). When lines are homozygous for either *hallii* or *filipes* alleles at both of the interacting QTL, individuals produce smaller diameter roots. In contrast, individuals with mismatched genotypes (HH/FF) at the pair of interacting loci develop larger diameter roots. This indicates that hybridization may disrupt genes and their interaction with microbes through root characteristics. Epistatic interactions involving effector host-sensitivity systems are not uncommon in plant-microbiome interactions (Jeuken et al., 2009). It may be that mismatched sensing of pathogens and disrupted downstream immune system responses underlie our discovery. However, we observed no obvious damage or necrosis in our roots and the observed epistatic QTL effects did not translate to decreases in aboveground biomass. Additional studies, perhaps based on fine-mapping or transcriptomic experiments, will be needed to further evaluate links between epistasis-microbiome interactions and root developmental responses.

A strength of our approach to treatment inoculation was prioritizing community effects, as opposed to the effect of single bacterial inoculants. However, given the exciting experimental advances of isolated bacterial strains in synthetic communities, targeted communities using locally adapted bacterial strains or combinatorics (Paredes, 2018) could be used to address how the presence / absence of particular microbial members impact plant phenotypes. In addition, it is intriguing to speculate on the type of plant genes and molecular mechanisms underlying the host x microbiome QTL detected in our study. It could be that these QTL harbor genes that interact

only indirectly with the host microbiome, perhaps through abundance of soil nutrients as modified by microbes. For example, certain soil microbes in our inoculates may alter the abundance or availability of soil nutrients with subsequent consequences for genetic variation in root or shoot growth. It may be that QTL are related to root exudates or metabolites released that may recruit or amplify key beneficial microbes with subsequent impacts on available nutrients. There are many examples of soil resource abundances of key nutrients impacting plant growth, including genes that demonstrated plastic responses to nutrient availability (Brumbarova & Ivanov, 2019). Alternatively, it may be that the genes within QTL intervals are involved in more direct interactions with microbes. For example, recent studies have shown that phytohormones, microRNAs and secreted peptides are known to recruit and foster the establishment of symbiotic arbuscular mycorrhizal fungi (Muller & Harrison, 2019). Moreover, Finkel et al. (2020) recently discovered an important role of the bacterial genus *Variovorax* in plant root growth by modification of auxin concentration gradients in the rhizosphere, which subsequently modulates other microbiota members. Plants also deploy extensive immune systems to ward off pathogens and control access of microbes to endophytic compartments (Chen et al., 2020) and some of our interactions may be related to ecotypic specific resistance or susceptibility. Our observation of an epistatic interaction is especially interesting as they may represent sensing and signaling pathways that are triggered or directed by microbes. In our case, epistatic interactions may also represent hybrid incompatibilities between ecotypes that are driven by the microbial community. Given the broad confidence intervals of our genome wide scans, we resist the temptation to consider and discuss specific candidate genes. Nevertheless, we emphasize that our approach leads to a direct pathway of fine-

mapping and the identification and cloning of new genes involved in plant-microbiome interactions.

Our results show that microbiomes impact the influence of genetic architecture on plant traits in two locally adapted ecotypes of *Panicum hallii*. These effects were broadly divided into two categories, effects dependent upon the presence of inoculated microbiomes in general and effects dependent upon microbiomes originating from a specific location of origin. This pattern sheds light on the role biotic factors may play in ecotype divergence and raises questions about how the modification of plant genetic architecture by microbes leads to local adaptation and ultimately speciation. Further work in this system has several pathways forward. Broad characterization of microbial communities can be used to determine how genetic variation shapes microbial communities as well as individual microbes. For example, this approach may allow for differentiating the effects that are mediated by plant-fungal interactions vs. plant-bacterial interactions. Once more is known about specific members of the microbial community that play large roles in impacting plant traits, reductionist approaches including targeted inoculations of bacterial / fungal strains and reverse genetic approaches could be used to identify specific mechanisms underlying plant-microbe interactions.

TABLES

Table 2.1. PERMANOVA Partitioning and Analysis of 16S community composition of native populations of *P. hallii* ecotypes and experimental plants grown in glasshouse.

Collected	Effect	Df	SS	MS	F.Model	R^2	P-Value
native environment	Location/Ecotype	1	1.893	1.893	14.066	0.216	**0.001*** **
	Compartment	2	1.351	0.677	5.029	0.154	**0.001*** **
	Location/Ecotype x Compartment	2	0.395	0.197	1.469	0.045	0.079
glasshouse	Ecotype	1	0.105	0.105	1.655	0.004	0.085
	Treatment	3	7.835	2.611	40.960	0.370	**0.001*** **
	Compartment	2	4.313	2.156	33.824	0.203	**0.001*** **
	Ecotype x Treatment	3	0.241	0.080	1.261	0.011	0.151
	Ecotype x Compartment	2	0.095	0.047	0.750	0.004	0.804
	Ecotype x Compartment	6	1.209	0.201	3.161	0.057	**0.001*** **
	Ecotype x Treatment x Compartment	6	0.231	0.038	0.605	0.010	0.999

Table 2.2. Main and epistatic effects of GxE QTL for the *Panicum hallii* RIL population.

Trait	**TRT**	**Chr**	**Peak (cM)**	**1.5 Lod Inter-val**	**LOD**	**% var**	**Effect**	**SE**	**Donor of Positive allele**	**GxE (Mixed Model)**
RMR	CI	3	74.1	68-83	3.6	5.3	-0.02	0.006	*filipes*	CI
SRL	CI	4	19.1	16-32	2.7	3.5	-1.12	0.316	*filipes*	CI
Root Number	MI	8	33.1	16-39	2.8	3.8	0.03	0.008	*hallii*	MI
Tiller number	AI	7	17	2-22	4.4	6.5	0.06	0.013	*hallii*	AI
Root Diameter	AI	7	2.7	0-48	3.9	4.8	-0.01	0.003	*filipes*	AI
Root Number	AI	7	0.3	0-10	3.5	5.4	0.04	0.011	*hallii*	AI
Lateral Root Length	AI	*7	3.4	0-63	2.6	4.1	0.08	0.022	*hallii*	AI
Shoot Biomass	AI	*9	3.9	0-10	2.5	3.9	0.06	0.017	*hallii*	AI
Root Biomass	AI	9	3.9	0-8	3.2	4.5	0.07	0.018	*hallii*	AI, MI
Root Length	AI	9	3.9	0-12	2.8	4.1	135.40	37.720	*hallii*	AI
1st Order Root Length	AI	9	25.6	14-31	4	6.2	1.09	0.250	*hallii*	AI
Root Diameter	CI	Epi1@68*2@79.5			5.1	5.8	-0.02	0.003		AI, CI

* indicates suggestive QTL detected with alpha=0.1; GxE (Mixed Model – Treatment x Marker interactions using PROC mixed in SAS): indicates treatment in which QTL effect is significant; TRT – Detected in treatment; Chr – Chromosome; SE – Standard Error.

FIGURES

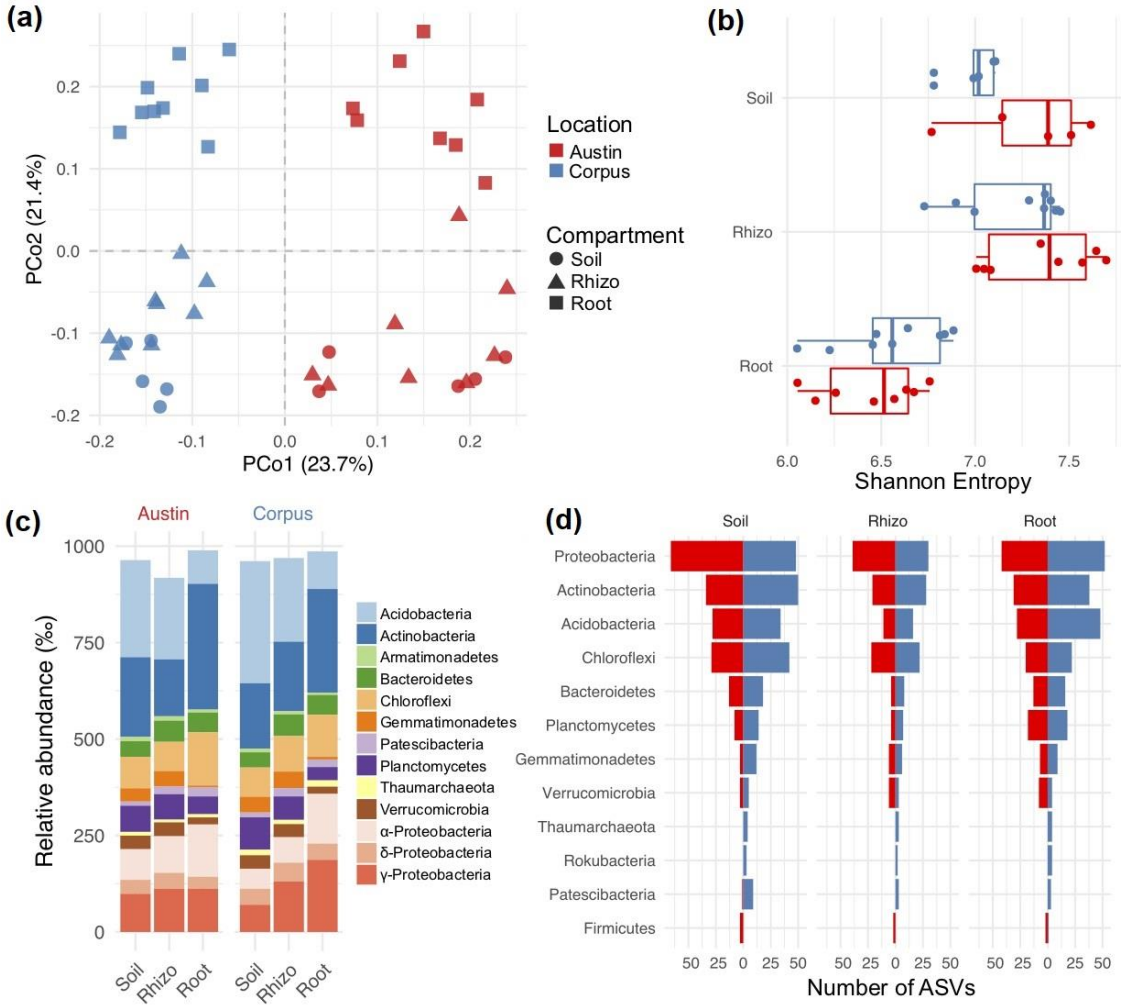

Figure 2.1. Parental genotypes grown under natural conditions host distinct microbiota. Panels: (a), principal coordinate graph based on Bray-Curtis dissimilarities; (b), Shannon diversity of samples from native parental habitats; (c), phylum level distribution of microbiota from natural habitats; (d), number of ASVs with differential abundance between parental habitats broken down by phylum where bars to the left indicate number of ASVs enriched in the Austin habitat, while bars to the right indicate number of ASVs enriched in the Corpus habitat. Color legends in b and d are consistent with panel a.

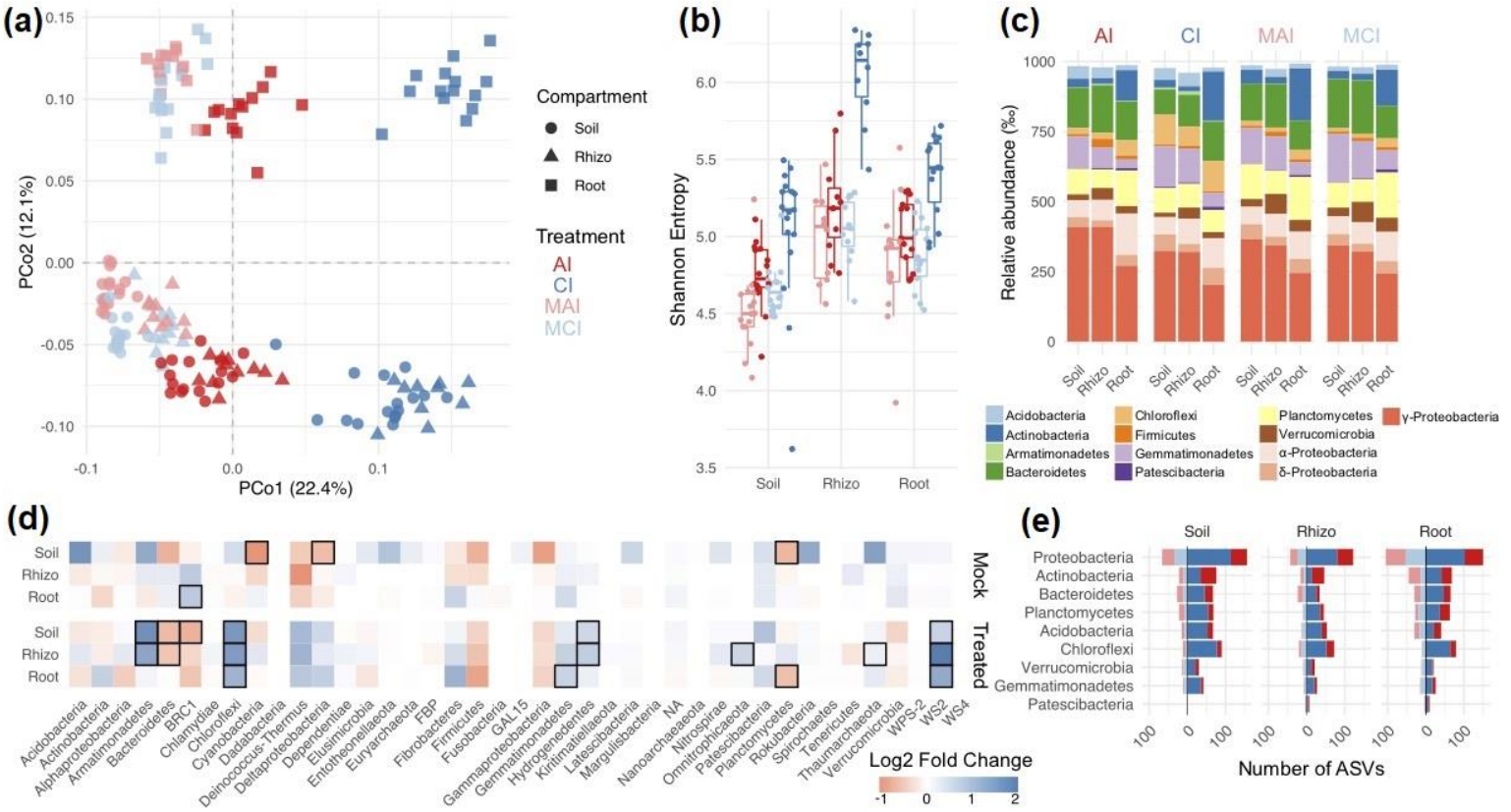

Figure 2.2. Microbial treatments differ significantly in community composition for plants growing in the glasshouse. Panels: (a), principal coordinate graph based on Bray-Curtis dissimilarities; (b), Shannon diversity of glasshouse samples; (c), phylum level distribution for microbiota from glasshouse samples; (d), differentially abundant phyla between soil treatments for mock and native microbiota where black boxes around tiles indicate a significant difference (adjusted $P < 0.05$) between soil treatments and the red color indicates a log fold change favoring the AI microbiota while blue favors CI microbiota; (e), number of differentially abundant ASVs when comparing AI vs. CI soil inoculum for both native and mock treatments where bars to the left indicate the comparison for the mock treatments while bars to the right indicate native treatments. The color scheme in panels b and e are consistent with panel a.

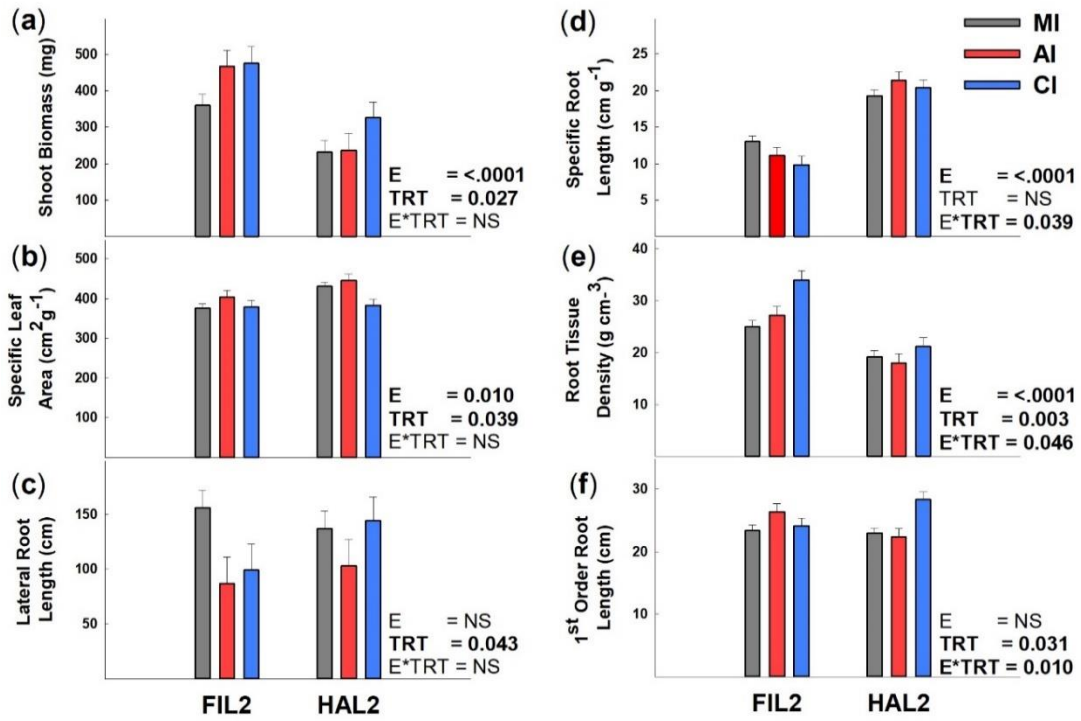

Figure 2.3. Effect of plant ecotype (E) and microbial treatment (TRT) and their interaction (E*TRT) on plant functional traits. Traits: (a), shoot biomass; (b), specific leaf area; (c), lateral root length; (d), specific root length; (e), root tissue density; (f), first order root length (data are means +S.E.).

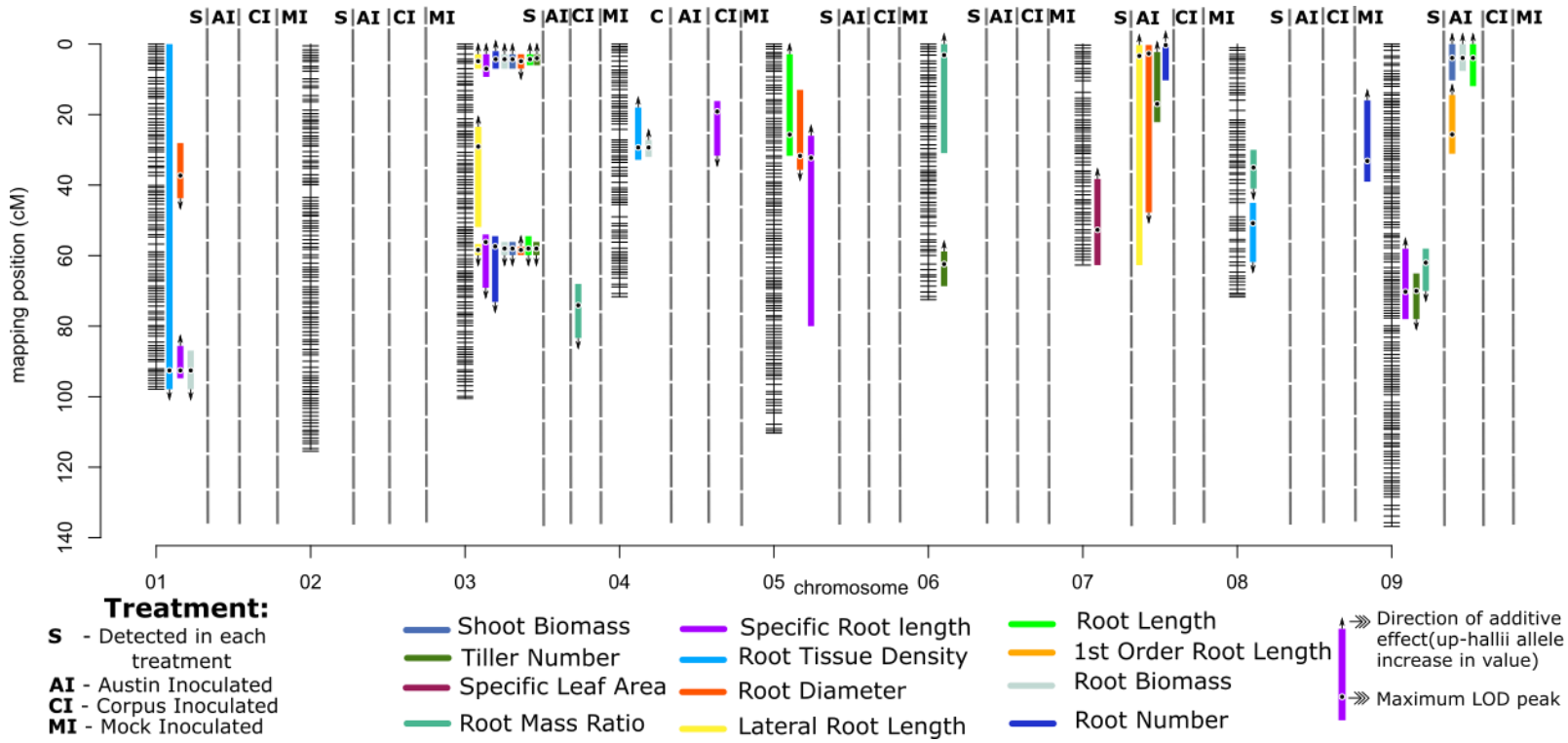

Figure 2.4. Genetic map of the *Panicum hallii* RIL population with locations of significant trait QTL by microbial treatment.

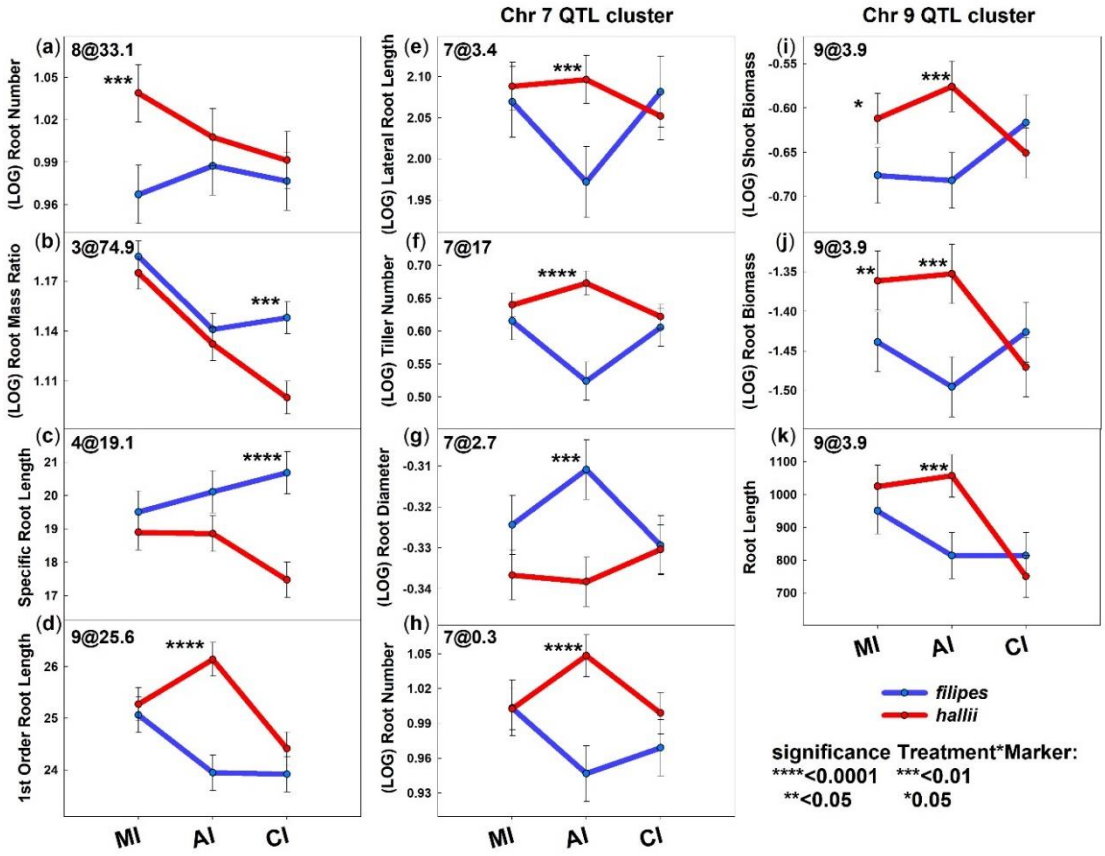

Figure 2.5. Tests of effect slices for significant Treatment x Marker interactions for traits in the full model analysis of QTL x treatment interactions using PROC mixed in SAS with QTL modeled on the marker nearest the QTL peak. Panels: (a), root number at 8@33.1; (b), root mass ratio at 3@74.9; (c), specific root length at 4@19.1; (d), first order root length at 9@25.6; (e), lateral root length at 7@3.4; (f), tiller number at 7@17.0; (g), root diameter at 7@2.7; (h), root number at 7@0.3; (i), shoot biomass at 9@3.9; (j), root biomass at 9@3.9; (k), root length at 9@3.9.

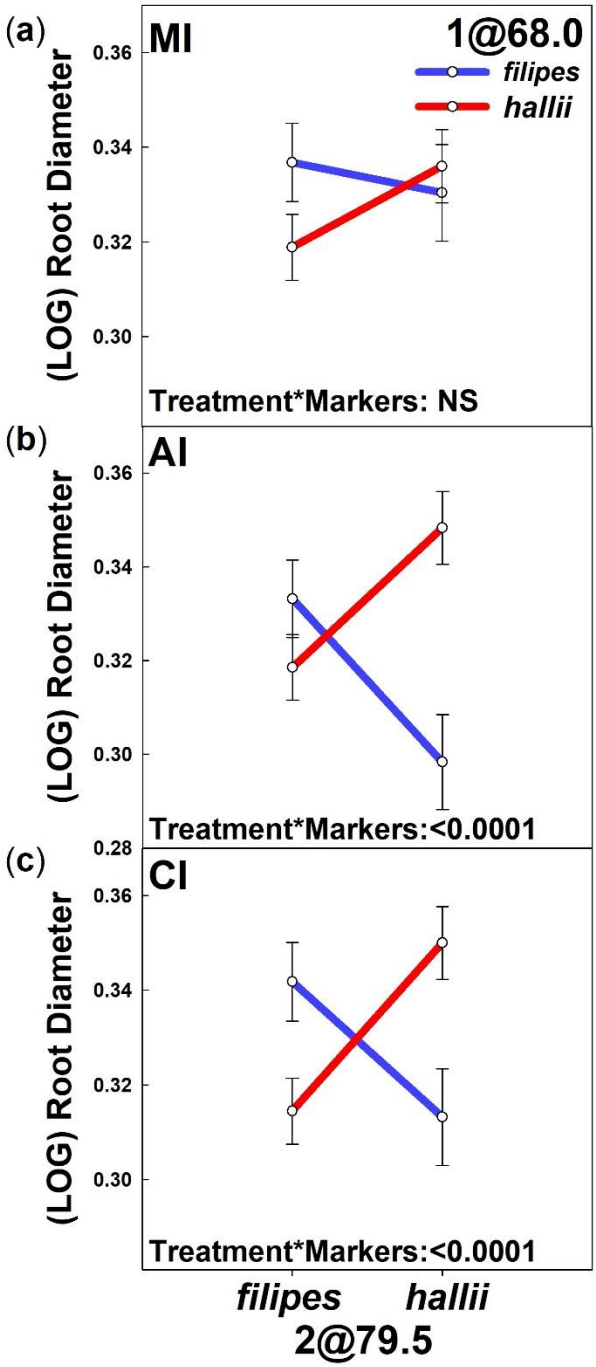

Figure 2.6. Pairwise epistatic QTL in the *P. hallii* RIL population detected only under Austin Inoculated and Corpus Inoculated treatments, with plotted points indicating two-locus genotype means ± 1SE for the two loci impacting root diameter. Root diameter QTL interactions for treatments: (a) Mock Inoculated (MI); (b), Austin Inoculated (AI); (c), Corpus Inoculated (CI).

Chapter 3: Quantitative genetics of host plant genome shape the root microbiome in a perennial grass

ABSTRACT

- Plants shape their root microbiomes in ways that can impact plant health, growth and local adaptation. Studying the impact of plant genetics on microbial communities from distinct native locations can show how plants interact with specific microbes and the extent to which host genetics affect overall microbial community diversity.
- We utilized a recombinant inbred line (RIL) mapping population produced by crossing upland and lowland ecotypes of *Panicum hallii* to explore how plant genetic architecture impacts root microbial communities. We used 16s rRNA sequencing to evaluated root microbial community composition of RILs grown in soils inoculated with microbial communities derived from native habitats and mock inoculated soils.
- We show that habitat of origin for microbial inocula changes the heritability for individual microbes (ASVs) and that root microbial community structure is distinct between treatments. We also found different plant genomic regions associated with abundance of individual microbes and community level structure across treatments.
- These results highlight the role of host genetics in shaping microbial community composition.

INTRODUCTION

Plants host a wide range of microbial communities in association with their root and shoot systems. These relationships are complex and multidirectional in their nature, and dependent upon the highly regulated expression of both plant and microbial genes. Whereas microbial communities associated with plant shoots are often dominated by a small number of bacterial clades suited to the arid and rapidly changing habitats of leaves, communities associated with plant roots can have larger degrees of diversity (Wagner et al., 2016; Toju et al., 2019). Soil contains some of the most complex and heterogeneous microbial habitats on the planet and plant root associated microbiomes are similarly complex as well. The root rhizosphere microbiota (microbes living in the soil region surrounding plant roots), the root rhizoplane microbiota (microbes living on the root surface that is in contact with the soil) and the root endosphere microbiota (microbes living within plant root tissue) are also distinct both from one another and the surrounding soil communities (Lundberg et al., 2012; Lang et al., 2019). Soil microbes aid plants by fixing atmospheric nitrogen, modulating plant hormonal signals, increasing the availability of soil borne nutrients and preventing plant disease by out-competing or deterring pathogenic microorganisms (Jacoby et al., 2017). Understanding the genetics behind how plants actively shape microbial diversity can be exploited in ways that can improve plant health, productivity and growth, aid in the understanding and prevention of plant diseases, enhance crop yields, and more broadly shed light on the impact of microbes on specific plant traits in both artificial and natural environments. The degree to which microbiomes contribute to plant health is becoming more widely recognized (Trivedi et al., 2020) and breeders in many crop systems are seeing gains by exploiting beneficial microbes (Bakker et al., 2012; Finkel et al., 2017).

There is increasing evidence that host genetics influence and interact with the microbiome and that this impact on microbial community structure varies by species and habitat. Plant microbiome studies have shown that both endophytic and epiphytic beneficial microbes (mutualists) can be attracted and detrimental microbes (pathogens) can be suppressed by plants (Andersen et al., 2018; Hartman et al., 2009; Raaijmakers et al., 2009). Many other microbes interacting with plants may be commensals presenting little cost or benefit to plants (Hartman & Tringe, 2019). For instance, the rhizosphere communities of two locally adapted Mimulus guttatus ecotypes were shown to be genetically influenced (Bowsher et al., 2020) and long-term persistence of host mediated microbiomes after transplantation to non-native horticultural soils has been observed in *Panicum virgatum* (Singer et al., 2019). Many of the studies conducted thus far on how plant genetics can shape root microbiomes have largely been done on few individuals, specific mutants, or in highly artificial settings involving synthetic microbial communities consisting of only a few organisms. The emergence of affordable high throughput sequencing is now allowing the broad characterization of entire plant microbiomes. Specifically, this allows detailed characterization of the many bacterial members of the microbiome on large numbers of individuals. Individual bacterial lineages can be identified by sequencing of the 16S rRNA gene and the amplicon sequence variants (ASVs) identified from these sequences can be used to identify specific bacteria. When these sequences are compared to a reference database, the bacterial taxonomic classification of each variant can be assigned and their abundance quantified by counting the occurrence of particular ASV reads. Combining these tools with quantitative genetic approaches to study large populations is a powerful approach to more effectively understand the scope of interactions between plant genetics and microbiomes.

Quantitative trait loci (QTL) mapping is a test for association between variation in plant genomes and variation in phenotypic traits. Given that QTL mapping only requires genotype and phenotype data across groups of individuals, and that root microbial community composition is effectively an extended plant phenotype of the plant, we can conduct QTL studies on bacterial counts of root microbes (Bergelson et al., 2019). In the root microbiome of any particular individual plant, each individual ASV can be present or absent; and if present, the abundance of each ASV can vary from plant to plant. QTL mapping provides a direct way to assess the genetic architecture that underlies the interaction between plant genes and microbial community composition and structure. Heritability is also measure of the amount of phenotypic variation present in a population that is due to genetics in contrast to other factors such as chance or the environment. Heritability is classified into two categories: broad-sense heritability (H2), which estimates contributions to the phenotype from all genetic sources; and narrow-sense heritability (h2), which estimates only the contributions that are due to additive genetic effects. Sets of genome-wide markers can be used to effectively estimate heritability among individuals (Wu et al., 2017). Heritability values range from 0 to 1, with 0 indicating no genetic control and 1 indicating complete genetic control of a given phenotype. Given the large amount of information about the presence of individual microbes and community level structure that can be extracted from microbiome DNA sequencing, these approaches can help to unravel the relationships between host genotype and microbiome community structure.

In this study, we examine plant genome – microbiome relationships in *Panicum hallii*, a perennial bunch grass native to North American. Its range covers a spread of diverse climates and habitats. *P. hallii* occurs naturally as two ecotypes that are classified as separate varieties: a xeric

upland ecotype, *P. hallii* var. *hallii* (hereafter referred to as *hallii*) and a mesic lowland ecotype, *P. hallii* var. *filipes* (hereafter referred to as *filipes*). Here, we obtain soil from the native environments of *P. hallii* ecotypes to serve as a source of microbial inoculum, creating treatments that contain microbes derived from the natural environment of each *P. hallii* ecotype. We blended these native microbiome inocula in both their live and heat killed forms with heat treated greenhouse soil to create two living native and two heat killed or mock soil treatments. To obtain sequences of root bacterial communities, we sampled the root systems of 293 recombinant inbred lines (RILs) produced from a cross between var. *hallii* and var. *filipes* grown under these four microbial inoculations. Our primary goals in this study are to (i) identify to what extent plant genetics affect overall microbial community diversity and the presence and abundance of individual bacteria, and (ii) to determine if these impacts are controlled by few or many genetic loci.

MATERIALS AND METHODS

We collected soil for inoculum from the native locations of the parental ecotypes (Lady Bird Johnson Wildflower Center in Austin, TX for var. *hallii* and Corpus Christi Botanical Garden, in Corpus Christi, TX for var. *filipes*). To prepare treatment soils (Inoculated), we mixed 1% by volume of native soil with a twice autoclaved horticultural soil mix of compost, decomposed granite and vermiculite (Thunder Dirt, Geo Growers, Austin, TX). To prepare control soils (Mock Inoculated), we mixed 1% by volume of twice autoclaved native soil with twice autoclaved horticultural soil mix. We used a cement mixer to thoroughly combine all soils and divided each treatment between two 400-liter covered trays and left them to incubate for two weeks indoors. We prepared four treatments in total: Austin Inoculated (AI), Corpus Inoculated (CI), Mock Austin

inoculated (MAI) and Mock Corpus Inoculated (MCI). After incubation, we transferred soil into 950 ml 3" x 8" Mini-Treepots (Stuewe and Sons, Tangent, OR) lined with sterile plastic bags perforated at the bottom for water drainage. We then randomized all pots into 20 cell racks and placed them in the greenhouse. We allowed pots to acclimate to greenhouse conditions for two weeks, and then transplanted seedlings into the pots. Full details of the experimental design can be found in Khasanova et al. (in prep/chapter 2).

For this study, we used a population of recombinant inbred lines derived from a cross between var. *hallii* and var. *filipes.* The development of this population is described in Khasanova et al., 2019. We sterilized seeds of both parents and 293 F7 RILs by treatment with 50% bleach followed by a rinse with sterile water, a rinse with 30% ethanol, and 5 additional rinses with sterile water. We then removed the seed coat by scarification with sandpaper, and placed seeds in petri dishes filed with wet sterilized sand. We sealed the petri dishes with parafilm and placed them on a greenhouse bench at the University of Texas at Austin in August 2018 (16-h days at 500 μE m −2 s −1, 28°C; 8-h nights at 24°C), rotating dishes daily to normalize growth. After five days, we transferred germinated seedlings over a three-day period to the prepared treatment plots and irrigated them from above with UV sterilized top water for the course of the 6-week experiment. We harvested plants at the tillering stage before panicle emergence over a 5-day period. During the harvest, we cleaned all soil particles from roots by affixing each plant to a clamping stand by the shoot base and spraying them with UV-sterilized water. We then separated the roots from the shoots just above the crown nodes and placed the intact root systems into 50 ml tubes filled with 90% ethanol and stored them at 4°C for future processing. After root phenotypes were measured, we aligned all roots vertically and removed a 1 cm section of the entire root system from the

midpoint and placed the cut sections into Eppendorf tubes. Tubes were stored at -80°C for until DNA extraction and 16S PCR amplification to determine bacterial root microbiota composition, including the root endosphere and the root rhizoplane (surface).

Microbial DNA extraction and 16S rRNA Sequencing and Sequence Analysis

We performed DNA extraction with a non-commercial low-cost soil DNA extraction method (Bollmann-Giola et al., 2020). We used the primer pair 515F-806R to amplify16S ribosomal RNA regions, and then sequenced barcoded samples on the Illumina novaseq platform. We used the R software package to perform microbial sequence analysis (R Core Team, 2020) and Cutadapt to remove adapter sequencing and primer binding sites (Martin, 2011). We then used DATA2 to infer amplicon sequence variants (ASVs), and de-chimerized them using the "consensus" method in DADA2 (Callahan et al., 2016). We retained ASVs 250-256 bp length for future analysis. We used the assignTaxonomy() function in DADA2 with Silva reference database (version 132) to assign taxonomic classification (Quast et al., 2013) and discarded ASVs assigned to mitochondrial and chloroplast lineages. The average number of reads per sample was 227,201 and we discarded all samples with coverage less than 10000 reads. Out of the resulting total of 582,831 ASVs, we removed all ASVs that were present in less than 5% of all samples, resulting in 4176 ASVs that were present in one or more treatments for use in the following analysis.

The resulting ASV data was corrected for batch effects with ComBat_seq (Zhang et al., 2020) by first correcting for the incubating tray effect within each treatment, and then for DNA extraction and PCR amplification plate effects across treatments by specifying treatments as biological covariates to preserve signal in the adjusted data. In order to account for differences in sequencing depth between samples, we normalized adjusted raw counts by dividing each ASV in

each sample by the number of reads and multiplying by 1000 (to place all counts in per mille scale). We estimated alpha diversity with Shannon entropy from the diversity() function in the package Vegan. We estimated Beta diversity by using the capscale() function in the package Vegan to perform principal coordinate analyses (PCoA) with Bray Curtis dissimilarities on log2 transformed abundances (Oksanen et al., 2020). We also conducted principal coordinate analyses on all ASVs within each treatment to generate multi-dimensional scales (MDS) for future QTL mapping. To create prevalence-abundance curves, we calculated abundance for each ASV as the average of normalized counts across all samples and prevalence as the ratio of the number of samples where each ASV was present divided by the number of samples.

In preparation for QTL mapping, we filtered all ASVs within each treatment to those that were present in ≥ 90% of sampled lines to generate a "core" microbiome set (Fig S1a, b). This core microbiome contained 160 unique ASVs in AI, 166 in MAI; 201 in CI; 189 in MCI—totaling 306 unique ASVs across all treatments. To more broadly explore the microbial community, we then filtered the data to generate an "extended" set of ASVs that were present in ≥ 40% of all lines in each treatment; resulting in 614 unique ASVs in MCI; 946 ASVs in CI; 674 ASVs in AI; 602 ASVs in MAI—totaling 1269 unique ASVs across treatments (Fig S1a, c). ASV's with prevalence values below 40% were insufficiently present to reliably conduct QTL mapping.

We used the bestNormalize package in R to perform normalization of the count data (Peterson & Cavanaugh, 2020) for all ASVs. ASVs with high prevalence were normally distributed. ASV's with lower prevalence exhibited a count distribution with a spike corresponding to the zero counts observed in a fraction of lines, following by a relatively normal distribution of counts. The absence of ASVs in any particular RIL or environment could be due to true absence,

sampling error related to sequencing depth, or possibly biological causes related to plant genotype. We decided to retain these zero values in our analysis to account for the possibility that they are biological in nature. We conducted QTL mapping on normalized ASV count values to detect QTL present in the AI, CI, MCI, and MAI treatments separately by using by using the R/qtl package (Broman & Sen, 2009). We used calc.genoprob with step=2 and map.function="kosambi" to calculate genotype probabilities every 2 cM. We used the "normal" model on core ASVs where count phenotypes were normally distributed. We also conducted QTL mapping on first 5 MDS values generated by PCoA that were normally distributed and on alpha diversity calculated as Shannon entropy. We used the scanone and scantwo functions with 1000 permutations followed by a stepwise QTL function to calculate penalties for main effects and interactions for each trait, and to perform a forward-backward search and account for epistasis with a maximum of 3 QTL. We set threshold values for type 1 error rates at alpha = 0.05 based on permutation. We also lowered our threshold to alpha = 0.1 to detect suggestive QTL and the 1.5 LOD drop interval of QTL was calculated with the qtlStats function. Overall, we performed more than 306 genomewide scans for ASV abundance. The reported p-values for genomes scans were corrected for multiple testing across SNPs (but not across taxa). We used the package Rqtl2 function est_herit () to calculated narrow sense heritability for each ASV abundance with a linear mixed model for all ASVs in the extended microbiome sets (Broman et al., 2018).

We used the extended microbiome to look for composite signal as measured by LOD scores at markers across ASVs. First, we used the scanone function with "np" (non-parametric model, given that many of the count phenotypes were not normally distributed) to calculate genome wide LOD scores. This approach converts count data into ranks and performs a generalized Wilcoxen

rank-sum type test (Kruglyak & Lander, 1995). Then, for each marker and pseudomarker, we summed LOD scores across all ASVs to get a new cumulative LOD score for a hotspot test. To calculate a significance threshold, we shuffled the LOD scores across markers within each ASV for all ASVs, summed LOD scores and retained the largest cumulative LOD score for each permutation. We performed this 1000 times to get an empirical distribution of null cumulative LOD scores, and set alpha = 0.05 for the permutation threshold.

RESULTS

We used ASVs derived from 16S rRNA amplicon sequencing to describe the root communities in our experimental inoculations. Microbiota varied significantly in alpha diversity between the treatments ($F=84.26$, $P < 0.0001$; Figure 3.1 b). Pairwise comparisons of means revealed no difference in alpha diversity between mock inoculated treatments (MAI and MCI). Alpha diversity in the Austin inoculated treatment (AI) was significantly different from corpus inoculated treatment (CI) and MAI, but not from MCI; and CI treatment was significantly different from all other treatments (Figure 3.1b). PCoA revealed robust divergence in beta diversity due to treatment (Figure 3.1 a) that were verified by Permanova ($R2 = 0.23$, $P < 0.001$).

For the core microbiome, native inoculated treatments had a 0.63-fold increase of unique ASVs relative to mock inoculated treatments. Out of 306 ASVs, 72 were unique for CI, 19 for AI, 20 for MCI and 12 to MAI (Figure A6 b). For the extended microbiome, native inoculated treatments had a 3.7-fold increase of unique ASV relative to mock inoculated treatments. Out of 1269 ASVs 406 were unique to CI, 104 to AI, 54 for MAI and 41 for MCI (Figure A6 c). Estimated narrow-sense heritability for the ASVs in the both the core and extended microbiomes ranged from 0 – 22% (Figure 3.2 a-d). Out of 1269 in the extended microbiome ASVs, 931 ASVs had 0

heritability at least in one treatment, and only 52 of these were present in each treatment. Plots comparing heritability of the first 60 most heritable ASVs between CI and MCI, and the first 60 most heritable ASVs between AI and MCI showed that heritability is often changed by the inoculation environment (Figure 3.2 e, f). In the core microbiome, bacteria from17 phyla were present, with Proteobacteria, Planctomycetes, Bacteriodes and Actinobacteria having the highest relative abundance (Figure A7).

We detected seven QTL in total for beta diversity from multidimensional scaling (MDS) from PCoA, with each QTL explaining 4.0 – 10.5 percent of total variation (Figure 3.3, Table 3.1). Two QTL for MDS5 for MCI treatment were detected on chromosome three, with the *hallii* allele driving positive effects at one QTL, and the *filipes* allele driving positive effects at the second QTL. Two QTL, one in each native soil inoculated treatment (CI and AI) had overlapping confidence intervals on chromosome six, with the *hallii* allele contributing to higher MDS values. In addition, three suggestive QTL (alpha= 0.10) were detected for the AI treatment: two for MDS3 on chromosomes two and six, with the *filipes* allele contributing to higher MDS values; and one for MDS4 on chromosome five, with the *hallii* allele contributing to higher MDS values. No QTL were detected for alpha diversity.

We detected a total of 56 QTL for individual ASVs present in the core microbiome across all treatments (Figure 3.4, Table 3.2). Nineteen of these QTL were present in the CI treatment, five in AI, 18 in MCI and 14 in MAI. Most ASVs had only one detected QTL—except for three ASVs that had two QTL—and each QTL explained from 5-10% of variation for the abundance of their respective ASV. QTL were detected on all 9 chromosomes, with only 7 QTL occupying unique positions. The other 49 had overlapping confidence intervals with at least one other QTL. A few

large hotspots were detected. The two largest had twelve and six QTL clustered on chromosomes three and four respectively. All of these QTL were from the CI, MAI, MCI treatments and none from the AI treatment. The third cluster on chromosome 9 contained 6 QTL, with all treatments represented. These QTL represented 9 of the 17 phyla detected in the core microbiome. QTL for *BRC1*, *Planctomycetes* and *Proteobacteria* were detected in all four treatments; QTL for *Acidobacteria, Bacteriodetes, Firmicutes* and *Gemmatimonadetes* were detected in 2-3 treatments; and QTL for *Chloroflexi* and *Thaumarchaeota* were detected in one treatment (Table 3.2).

Quantitative genetic analyses of omics data often generate genetic mapping results for hundreds to thousands of phenotypes. A common question is to ask whether there are common features of the genetic architecture or genomic regions impacting many phenotypes. Such genomic "hotspots" have been detected for transcript and metabolite abundance but are relatively unexplored for microbial communities. One challenge in studies of hotspots is the statistical thresholding of significance – only large effects are detected for most phenotypes. To aggregate information across ASVs, we summed the LOD scores across all ASVs to see if for some markers there were many QTL for ASVs that we could not detect due to lack of power from any single ASV genomescan. Mapping on the composite signal of LOD sums for each marker across all ASVs in the extended microbiome resulted in multiple peaks within each treatment (Figure 5). All but one of PCoA MDS QTL overlapped with these composite peaks. Given the small LOD scores of detected QTLs in core microbiome, this result suggests that multiple ASVs are clustered in hotspot that are not detected in individual QTL analysis, possibly as a result of the detection power.

DISCUSSION

Host genetics can drive root microbiome community assembly and recruitment. Several recent studies have shown genetic variation within plant species for attributes of the microbiome including the abundance of specific microbes and total microbial community diversity (Bergelson et al., 2018; Tabrett & Horton, 2020). Here, we conducted a QTL study using a *P. hallii* RIL mapping population grown in soils inoculated with microbiomes from native *P. hallii* habitats to examine how plant host genetics impact communities of root associated bacteria. Our previous work (Khasanova et al., in prep) showed that the microbiota from the natural habitat of the RIL parental lines are distinct and thus serve as suitable inoculum for experimental treatments to quantify the effects of host genetics on different microbiota. In this greenhouse experiment, we found that individual root microbes differ in presence and abundance depending upon the source of microbial inoculum and plant genetics. Surprisingly, we found a number of hotspot genomic regions that affected overall microbiome community composition. Moreover, we found that many loci are involved in driving changes in abundance of individual ASVs. Overall, our results suggest that plant host genetics play a role in shaping root bacterial communities.

Most studies on the bacterial members of root microbiomes have focused on members of the rhizosphere communities and have reported large ranges of diversity, from < 100 to more than 55,000 operational taxonomic units (Mendes et al., 2013). While the composition and function of rhizosphere, rhizoplane and endosphere communities are different, ultimately, the members of the endosphere arise from members of the rhizosphere that are either allowed in by the plant or are able to infiltrate plant tissues. Here, we found a total of 582,831 ASVs, indicating complex root surface and endosphere communities. To more closely look at dominant community members, we

removed all ASVs that were present in less than 5% of all samples, resulting in 4176 ASVs used in this study. Out of our four treatments, we found the highest alpha diversity in the CI soils, which contained inoculum from a mesic environment, followed by AI and mock communities. It has been shown in native prairies that soil hydrology drives bacterial diversity, and wetter environments are higher in bacterial diversity in native prairies (Griffin et al., 2020).

We found low levels of heritability across the majority of ASVs. This is consistent with other studies that have found low heritability of alpha diversity in maize leaf, in alpha and beta diversity in maize rhizosphere, and individual microbes in maize rhizosphere (Wallace at al., 2018; Walters et al., 2018; Peiffer et al., 2013). While heritability's are low in this study, they vary considerably between individual ASVs and across the treatments. Single ASVs that are relatively heritable in one treatment, can have much lower heritability in another context, or vice versa (Fig 2e, f). A possible cause of this is overall community structure differences between each treatment – it may be that the degree of host control or the abundance of a particular ASV depends on ecological aspects of the microbial community. Microbes in general are highly interdependent upon other members of the community and individual ASVs may find their prevalence or abundance greatly impacted by other members of the community.

To evaluate the genetic architecture of how host genotype shapes community structure, we evaluated metrics of both alpha and beta diversity. Other studies have shown that plants alter their root microbiomes in a manner that is host-dependent. It has been found that host genotype drives rhizosphere composition in barley (Bulgarelli et al., 2015), differences in alpha diversity in potato (Weinert et al., 2011) and variation in beta diversity in maize (Peiffer et al., 2013). For alpha diversity, we mapped no QTL for Shannon entropy in any treatments. However, for beta diversity,

we mapped QTL on PCoA multi-dimensional scales in the AI, CI and MCI treatments (Figure 3.4). For the native inoculated treatments, we found a shared QTL on chromosome 6, suggesting that this is a general microbiome effect where host genetics interacts with the native microbiomes on a community level. We also detected three additional QTL for the AI treatment showing location specific microbiome interactions. Two QTL were detected for the MCI treatment in the same genomic region of root and shoot phenotypic QTL from our previous work, which is also the same genomic region as the large hotspot containing single ASV QTL for the CI and MCI treatments.

To evaluate how host genetics interacts with specific microbes, we mapped QTL for the abundance of individual ASVs that were highly prevalent in the root microbial community. For the core microbiome of 306 unique ASVs, we found significantly more QTL for CI, MCI and MAI treatments than in the AI treatment. Some QTL for single ASVs occupy unique locations in the genome, but we also found evidence of hotspots that control multiple ASVs across different treatments, where QTL have overlapping confidence intervals (Figure 3.3). It should be noted, that these QTL are only for core microbiome members, that were present in 90% or more of all samples in any given treatment. Interestingly, about half of these QTL are for ASVs that were present in all four treatments, but QTL for these ASVs were only detected in one of the four treatments. This indicates that aspects of community structure or soil habitat impacted by our inoculation treatment can play a role in how individual microbes interact with plant genetics. Given that these QTL are of small effect, it is possible that we do not have enough power to detect other QTL that do not meet threshold.

Since differences exist within the communities of every individual plant, some degree of beta diversity exists between all samples. While some QTL were detected for metrics of beta diversity, this does not account for the many differences of small effect that may exist for individual ASVs. We hypothesis that there could be genomic regions with widespread impacts on the microbial community that are too diffuse and complex to easily detect. To examine the culmination of these many small genome – microbiome interactions, we decided to sum the LOD scores for all ASVs in the extended microbiome set (Figure 5). This approach is similar to testing community level interactions and it is still possible that individual loci may control many ASVs or that multiple ASVs act in concert. We found that summed LOD scores of all small effect ASVs exceeded threshold in the same genomic regions where we detected almost all of the PCoA QTLs in the same treatments. This is further evidence that these regions are involved in community assembly. This method detected additional regions in addition to the ones that matched our previous results, suggesting that there are many ASV QTL we cannot detect with single ASV analysis, and that community factors play a role in host genotype – microbiome interactions.

In this study we examined the genetic architecture of plant root microbiome interactions in a *Panicum hallii* mapping population. The *hallii* and *filipes* parents of this population are locally adapted to their home xeric and mesic environments respectively. When plant populations diverge in response to encountering novel environments, they must adapt to not only abiotic changes, but biotic changes as well, such as soil microbiomes. Different microbes play different roles in different environments, and what constitutes a beneficial root microbiome in a xeric environment may be different than one that would be beneficial in a mesic environment. Thus, as plants diverge to inhabit new environments, they may also diverge in the types of microbes they are able to recruit

or exclude. We have shown that *P. hallii* possess variation in the ability to interact with microbiomes which may contribute to local adaptation by yielding distinct advantages in inhabiting new environments such as the ability to associate with microbes that alleviate drought stress or to keep out new pathogens encountered. Future work in this system could add further understanding of microbial factors involved in local adaptation.

TABLES

Table 3.1. Main effects of QTL detected on multidimensional scaling (MDS) from PCoA within each treatment.

Treatment	MDS	Marker	Chromosome	LOD	% Var	Effect	SE	Donor of Positive allele
AI	MDS3	Chr06_2732462	6@10.9	6.96	10.57	0.328	0.056	*hallii*
AI	MDS3	*Chr02_55619688	2@115.5	2.76	4.05	-0.13	0.036	*filipes*
AI	MDS3	*Chr06_427744	6@0.0	2.98	4.39	-0.186	0.049	*filipes*
AI	MDS4	*Chr05_14001313	5@58.4	2.62	4.23	0.155	0.044	*hallii*
CI	MDS5	Chr06_3608105	6@16.7	2.90	4.82	0.186	0.050	*hallii*
MCI	MDS5	Chr03_5669221	3@14.5	5.15	7.88	0.199	0.040	*hallii*
MCI	MDS5	Chr03_15127510	3@46.7	4.35	6.61	-0.174	0.038	*filipes*

* indicates suggestive QTL detected with alpha=0.1;
MDS - Multidimensional scaling from PCoA

Table 3.2. QTL for ASVs of core microbiome detected within each treatment.

TRT	ASV	CHR	LOD	% VAR	Phylum	Class	Order	Family	Genus
AI	67	9@105.16	2.87	5.49	*Planctomycetes*	*Planctomycetacia*	*Planctomycetales*	NA	NA
AI	33	1@21.19	3.32	6.32	*Proteobacteria*	*Deltaproteobacteria*	*Myxococcales*	*BIrii41*	NA
AI	346	9@60.93	3.04	5.81	*Proteobacteria*	*Alphaproteobacteria*	*Thalassobaculales*	*Thalassobaculaceae*	*Thalassobaculum*
AI	421	5@80.69	3.01	5.75	*Proteobacteria*	*Alphaproteobacteria*	*Rhizobiales*	*Rhizobiales_Incertae_Sedis*	*Nordella*
AI	482	5@60.40	2.89	5.53	*Proteobacteria*	*Alphaproteobacteria*	*Micropepsales*	*Micropepsaceae*	NA
CI	36	3@2.86	3.13	5.98	*Acidobacteria*	*Subgroup_6*	NA	NA	NA
CI	95	7@27.46	3.53	6.71	*Actinobacteria*	*Actinobacteria*	*Propionibacteriales*	*Nocardioidaceae*	*Aeromicrobium*
CI	131	3@85.94	4.22	7.97	*Bacteroidetes*	*Bacteroidia*	*Cytophagales*	*Microscillaceae*	NA
CI	159	3@6.98	3.64	6.91	*Bacteroidetes*	*Bacteroidia*	*Cytophagales*	*MWH-CFBk5*	NA
CI	8	3@2.86	3.31	6.3	*Bacteroidetes*	*Bacteroidia*	*Cytophagales*	*Microscillaceae*	*Chryseolinea*
CI	79	9@95.07	4.22	7.96	*Firmicutes*	*Bacilli*	*Bacillales*	*Bacillaceae*	*Bacillus*
CI	23	3@2.86	3.1	5.92	*Gemmatimonadetes*	*Gemmatimonadetes*	*Gemmatimonadales*	*Gemmatimonadaceae*	NA
CI	294	4@27.21	3.42	6.52	*Planctomycetes*	*Planctomycetacia*	*Pirellulales*	*Pirellulaceae*	*Pir4_lineage*
CI	470	1@42.13	3.26	6.22	*Planctomycetes*	*Planctomycetacia*	*Pirellulales*	*Pirellulaceae*	*Pirellula*
CI	1019	6@26.11	3.39	6.46	*Proteobacteria*	*Alphaproteobacteria*	NA	NA	NA

Table 3.2 (Continue)

TRT	ASV	CHR	LOD	% VAR	Phylum	Class	Order	Family	Genus
CI	178	3@8.34	3.86	7.31	*Proteobacteria*	*Gammaproteobacteria*	*Gammaproteobacteria__Incertae_Sedis*	Unknown_Family	*Acidibacter*
CI	183	9@25.10	3.11	5.94	*Proteobacteria*	*Alphaproteobacteria*	*Rhizobiales*	*Xanthobacteraceae*	NA
CI	287	1@46.74	3.25	6.2	*Proteobacteria*	*Gammaproteobacteria*	*R7C24*	NA	NA
CI	287	3@55.27	3.26	6.21	*Proteobacteria*	*Gammaproteobacteria*	*R7C24*	NA	NA
CI	322	1@68.70	3.8	7.2	*Proteobacteria*	*Alphaproteobacteria*	*Rhizobiales*	*Rhizobiales_Incertae_Sedis*	*Bauldia*
CI	340	3@19.25	4	7.57	*Proteobacteria*	*Gammaproteobacteria*	*Xanthomonadales*	*Xanthomonadaceae*	*Arenimonas*
CI	42	7@55.68	3.71	7.04	*Proteobacteria*	*Gammaproteobacteria*	*Pseudomonadales*	*Pseudomonadaceae*	*Pseudomonas*
CI	567	5@41.12	3.49	6.64	*Proteobacteria*	*Gammaproteobacteria*	*R7C24*	NA	NA
CI	366	5@55.15	3.37	6.41	*Thaumarchaeota*	*Nitrososphaeria*	*Nitrososphaerales*	*Nitrososphaeraceae*	*Candidatus_Nitrocosmicus*
MAI	117	9@98.47	3.1	5.91	*Actinobacteria*	*Actinobacteria*	*Propionibacteriales*	*Nocardioidaceae*	*Nocardioides*
MAI	277	1@70.73	3.44	6.54	*Actinobacteria*	*Actinobacteria*	*Propionibacteriales*	*Nocardioidaceae*	*Nocardioides*
MAI	73	5@4.01	3.83	7.26	*Bacteroidetes*	*Bacteroidia*	*Cytophagales*	*Hymenobacteraceae*	*Pontibacter*

Table 3.2 (Continue)

TRT	ASV	CHR	LOD	% VAR	Phylum	Class	Order	Family	Genus
MAI	145	9@128.44	3.71	7.04	*Firmicutes*	*Bacilli*	*Bacillales*	*Planococcaceae*	NA
MAI	193	1@51.34	3.11	5.93	*Gemmatimonadetes*	*S0134_terrestrial_group*	NA	NA	NA
MAI	78	9@130.86	4.5	8.47	*Gemmatimonadetes*	*Gemmatimonadetes*	*Gemmatimonadales*	*Gemmatimonadaceae*	*Gemmatimonas*
MAI	213	1@35.06	3.11	5.94	*Planctomycetes*	*Planctomycetacia*	*Planctomycetales*	NA	NA
MAI	54	4@42.81	3.17	6.05	*Planctomycetes*	*Planctomycetacia*	*Pirellulales*	*Pirellulaceae*	*Pir4_lineage*
MAI	70	3@0.00	3.24	6.17	*Planctomycetes*	*Planctomycetacia*	*Pirellulales*	*Pirellulaceae*	*Rhodopirellula*
MAI	17	3@19.25	2.96	5.66	*Proteobacteria*	*Alphaproteobacteria*	*Rhizobiales*	*Rhizobiaceae*	*Allorhizobium_Neorhizobium_Pararhizobium_Rhizobium*
MAI	175	5@103.75	3.23	6.16	*Proteobacteria*	*Gammaproteobacteria*	*CCD24*	NA	NA
MAI	186	3@82.28	3.22	6.14	*Proteobacteria*	*Gammaproteobacteria*	*Betaproteobacteriales*	*Burkholderiaceae*	*Xylophilus*
MAI	338	2@1.61	3.68	6.98	*Proteobacteria*	*Deltaproteobacteria*	*Myxococcales*	*Sandaracinaceae*	*Sandaracinus*
MAI	338	7@3.35	3.1	5.93	*Proteobacteria*	*Deltaproteobacteria*	*Myxococcales*	*Sandaracinaceae*	*Sandaracinus*
MCI	110	5@51.14	3.27	6.23	*Actinobacteria*	*Actinobacteria*	*Pseudonocardiales*	*Pseudonocardiaceae*	*Pseudonocardia*

Table 3.2 (Continue)

TRT	ASV	CHR	LOD	% VAR	Phylum	Class	Order	Family	Genus
MCI	120	3@10.50	3.19	6.09	*Actinobacteria*	*Actinobacteria*	*Propionibacteriales*	*Nocardioidaceae*	*Nocardioides*
MCI	14	9@92.09	3.34	6.36	*Actinobacteria*	*Actinobacteria*	*Micrococcales*	*Microbacteriaceae*	NA
MCI	189	9@86.81	3.34	6.36	*Actinobacteria*	*Actinobacteria*	*Micrococcales*	*Intrasporangiaceae*	*Ornithinimicrobium*
MCI	55	3@5.41	3.59	6.81	*Actinobacteria*	*Actinobacteria*	*Streptomycetales*	*Streptomycetaceae*	*Streptomyces*
MCI	196	4@51.56	3.37	6.42	*Bacteroidetes*	*Bacteroidia*	*Sphingobacteriales*	*KD3-93*	NA
MCI	490	2@77.38	3.47	6.61	*Bacteroidetes*	*Bacteroidia*	*Cytophagales*	*Cyclobacteriaceae*	NA
MCI	157	5@40.25	3.23	6.16	*BRC1*	NA	NA	NA	NA
MCI	90	4@48.97	3.13	5.98	*BRC1*	NA	NA	NA	NA
MCI	81	4@44.86	3.05	5.83	*Chloroflexi*	*Chloroflexia*	*Thermomicrobiales*	*JG30-KF-CM45*	NA
MCI	252	4@51.56	4.12	7.8	*Firmicutes*	*Bacilli*	*Bacillales*	*Bacillaceae*	*Paucisalibacillus*
MCI	213	3@6.98	3.2	6.1	*Planctomycetes*	*Planctomycetacia*	*Planctomycetales*	NA	NA
MCI	267	2@62.14	3.46	6.58	*Proteobacteria*	*Alphaproteobacteria*	*Rhizobiales*	*D05-2*	NA
MCI	267	8@5.70	3.02	5.77	*Proteobacteria*	*Alphaproteobacteria*	*Rhizobiales*	*D05-2*	NA
MCI	284	3@17.16	5.27	9.85	*Proteobacteria*	*Gammaproteobacteria*	NA	NA	NA
MCI	370	2@71.96	3.05	5.83	*Proteobacteria*	*Alphaproteobacteria*	*Puniceispirillales*	*Puniceispirillales__Incertae_Sedis*	*Constrictibacter*

Table 3.2 (Continue)

TRT	ASV	CHR	LOD	% VAR	Phylum	Class	Order	Family	Genus
MCI	69	7@15.36	3.1	5.92	*Proteobacteria*	*Gammaproteobacteria*	*Betaproteobacteriales*	*Nitrosomonadaceae*	*IS-44*
MCI	91	2@103.33	3.17	6.05	*Proteobacteria*	*Deltaproteobacteria*	*Myxococcales*	*BIrii41*	NA

FIGURES

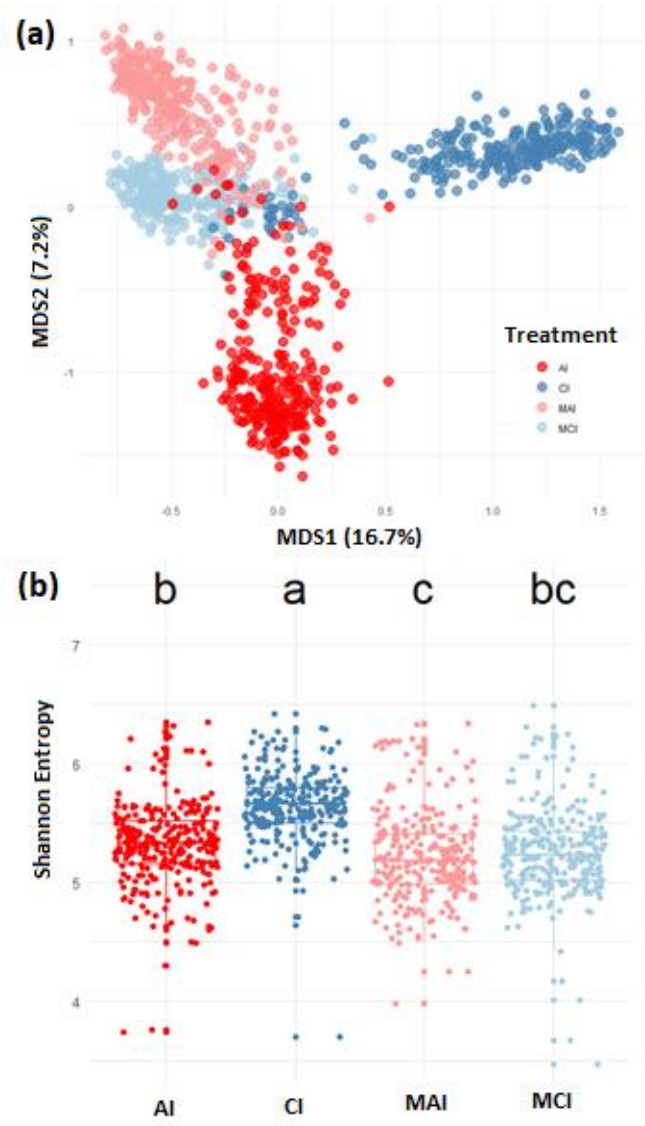

Figure 3.1. Beta and alpha diversity of bacterial root community structure of each treatment. Panels: (a), Principal coordinate analysis (PCoA) based on Bray-Curtis dissimilarities of beta diversity in microbial composition for experimental treatments; (b), Shannon entropy as a measure of alpha diversity in microbial composition for experimental treatments.

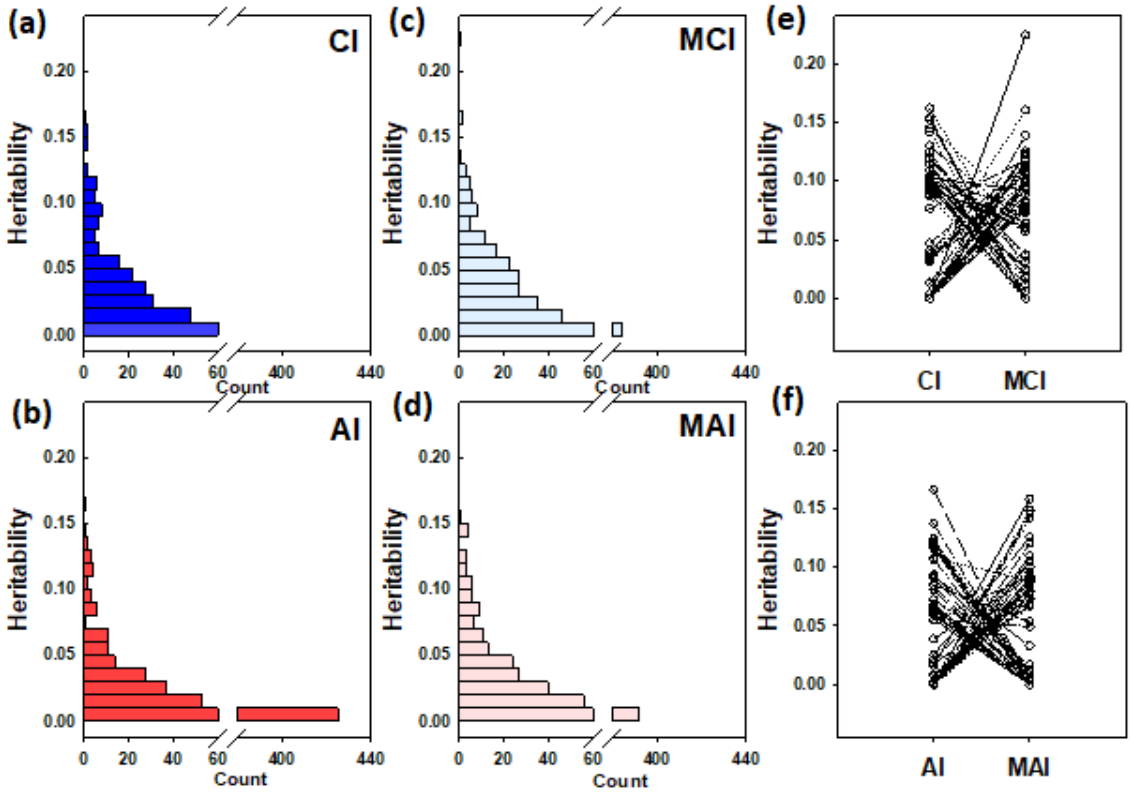

Figure 3.2. Narrow sense heritability (h2) of extended microbiome ASV abundance in each treatment. Panels: (a), Corpus Inoculated (CI); (b), Austin Inoculated (AI); (c), Mock corpus inoculated (MCI); (d), Mock Austin inoculated (MAI); (e), reaction plot of first 60 most heritable ASVs in CI and MCI treatments; (f), reaction plot of first 60 most heritable ASVs in AI and MAI treatments.

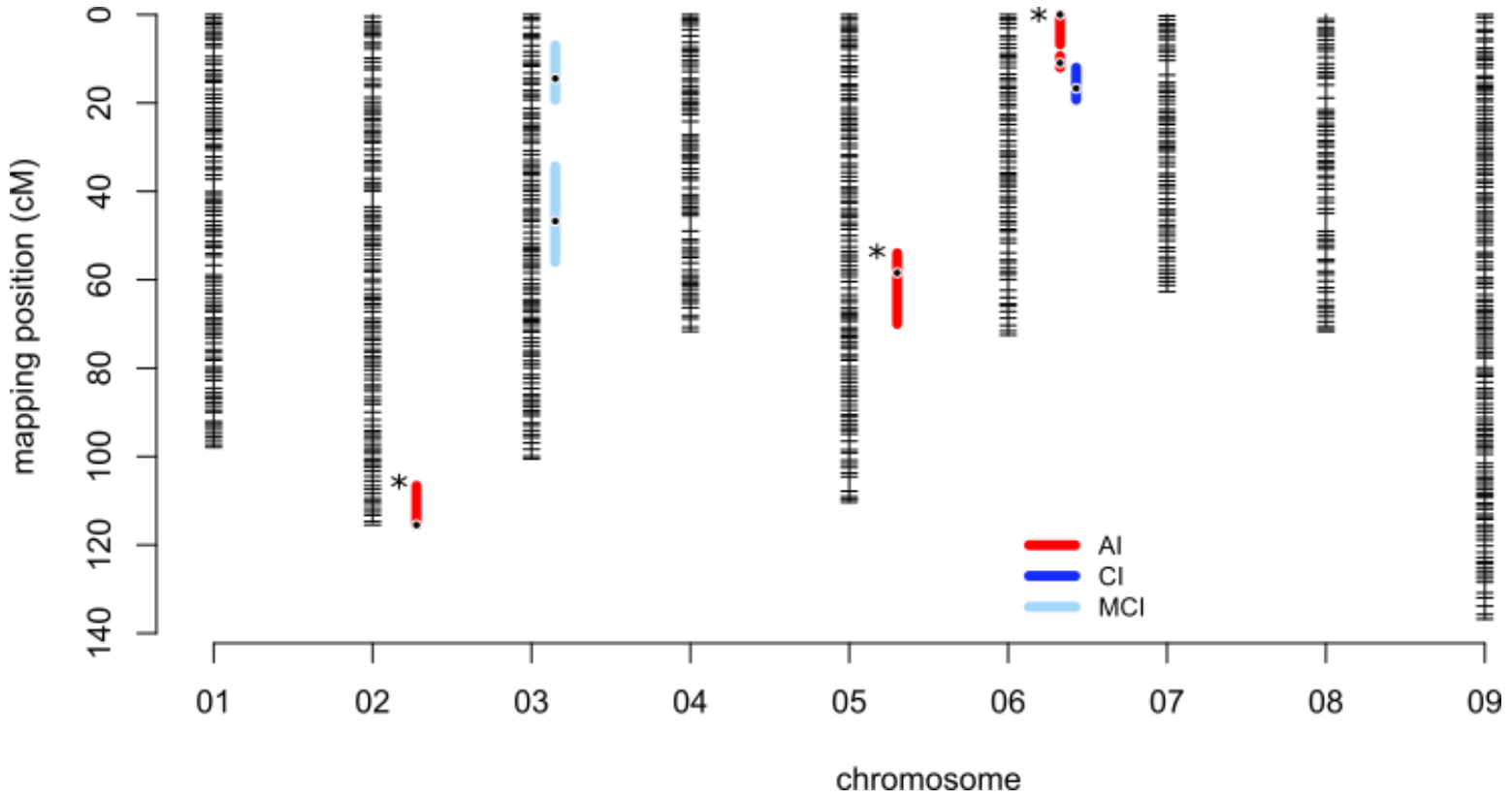

Figure 3.3. Genetic map of *Panicum hallii* RIL population with significant QTL for multidimensional scaling (MDS) from PCoA within each treatment. * indicates suggestive QTL detected with alpha=0.1.

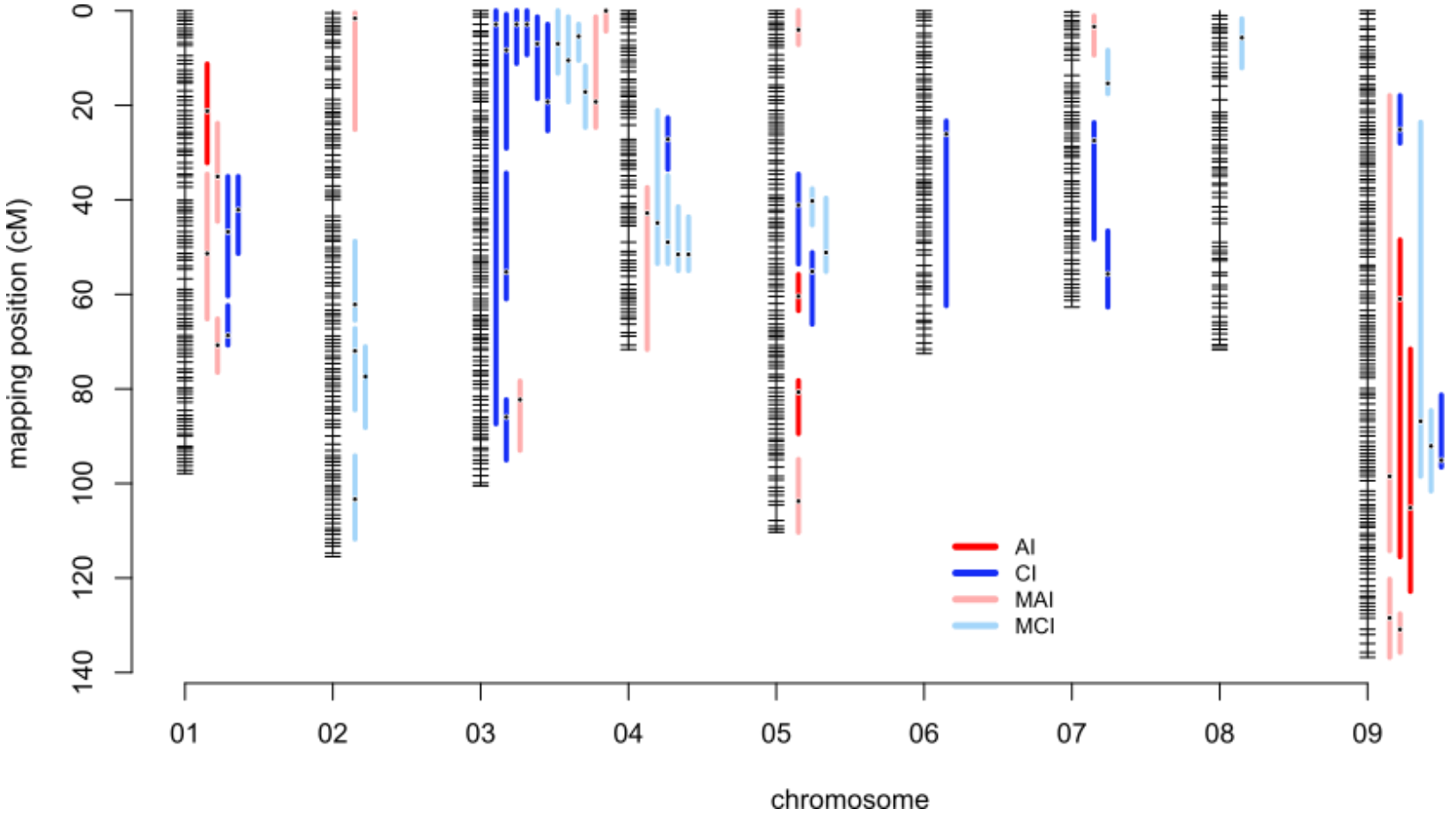

Figure 3.4. Genetic map of *Panicum hallii* RIL population with significant QTL for ASVs detected within each treatment for the core microbiome.

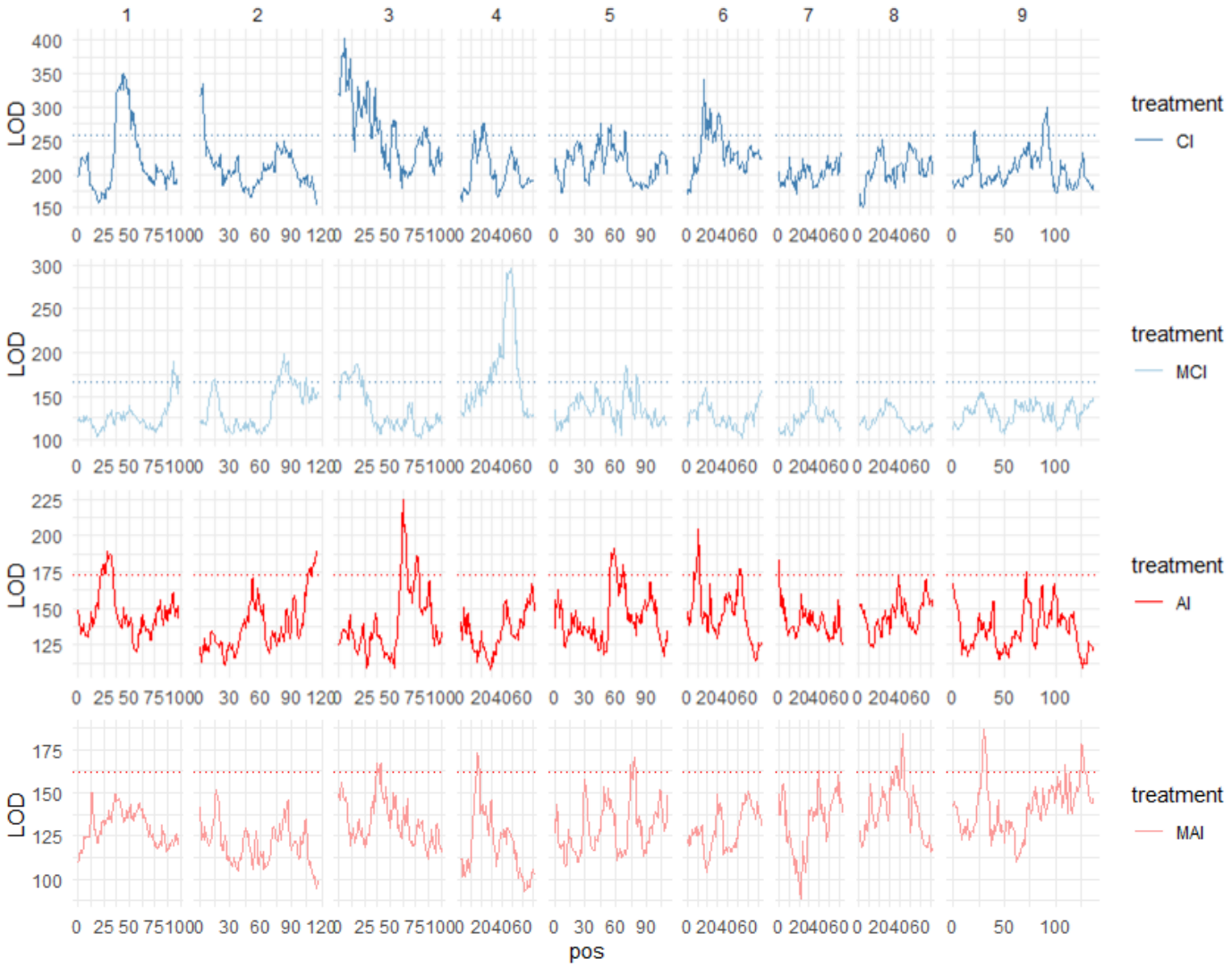

Figure 3.5. Composite signal of LOD sums for each marker across all ASVs in extended microbiome for each treatment.

Appendices

SUPPLEMENTAL MATERIAL FOR CHAPTER 1.

Supplementary Appendix A1.

Development of the RIL mapping population

We developed a population of recombinant inbred lines (RILs) in order to evaluate the genetic basis of divergence between *hallii* and *filipes*. The parents of the RIL mapping population were genotypes selected from populations of the upland and lowland ecotypes of *P. hallii*. The upland parent (HAL2-11, hereafter referred to as HAL2) was a one-generation selfed progeny of an individual selected from a glasshouse planting of seed collected from a natural population of *hallii* located at the Lady Bird Johnson Wildflower Center (Austin, TX, USA; 30.16°N, 97.87°W). The lowland parent (FIL2) was selected from a glasshouse planting of seed collected from a natural population of *filipes* located near the coastal city of Corpus Christi, Texas (27.65°N, 97.40°W). FIL2 and HAL2 represent the genome reference genotypes for *filipes* and *hallii* respectively (https://phytozome.jgi.doe.gov/pz/portal.html#!info?alias=Org_Phallii) and are largely homozygous individuals. A cross of these two genotypes, with HAL2 as the maternal parent, yielded an F1 hybrid and self-fertilized seed obtained from this individual was used to establish a large F2 population (Lowry, 2012). A number of these F2 progeny were selected at random and propagated repeatedly via single seed descent until the F6 generation. DNA was obtained from leaf tissue of F6 seedlings and submitted for whole genome resequencing at the DOE Joint Genome Institute through the Community Science Program. F7 seed was subsequently collected from the sequenced F6 individuals for this experiment.

SNPs were called from whole genome resequencing of 356 RILs on four Illumina 2x150 runs at 12x coverage. Libraries were quality filtered using the fastx toolkit 'fastq_quality_filter' program with a quality threshold of 33. Filtered reads were mapped to a soft masked *P. hallii*

reference genome (FIL-2 V2.0) using bwa mem with the default parameters. Mapped reads were filtered by samtools –Shb with a quality of 20. Bam files were indexed, sorted and duplicates were removed with picard. Reads adjacent to insertions / deletions were masked using GATK RealignerTargetCreator and reads were re-sorted and re-indexed prior to SNP calling. SNPs were called via GATK haplotypeCaller independently for each library, producing a gVCF for each. These were merged and re-genotyped by GATK's genotypeGVCF and condensed into a 0/1/2 (alternate allele counts) matrix with vcfTools. Genotype data from 335 RILs were included in the output genotype matrix. The resultant matrix was processed in R. SNPs with >10% and <80% homozygotes and <5% NA and <20% heterozygotes were retained.

We applied a 3-step sliding window approach for marker calling: 1) The genome was broken into 200 marker windows (overlapping by 100 markers) and the proportion of each genotype was calculated. 2) Training data was constructed, retaining the 100 strongest heterozygous sites and a random sampling of 100 of the sites with > the mean proportion of each homozygote; 3) A random forest machine learning model was fit to the training data (the R caret package) and used to predict the genotypes of all sliding window intervals resulting in a 3361 marker matrix. Raw sequence data was deposited in the NCBI short read archive under the BioProject ID in Table A4.

Genetic map construction

To build the genetic map, we culled the genotype matrix such that no two markers could have a pairwise recombination fraction <0.005. This culling procedure minimized the amount of segregation distortion and missing data within any 0.5 cM window. Linkage groups were formed from the resulting 1278 marker matrix. Markers were ordered within linkage groups using a travelling salesperson problem solver as implemented through the concorde program and parsed through the TSPMap function tspOrder (Monroe et al., 2017). We then fine-tuned the resulting genetic map first by culling the genotype matrix to a 711-marker grid where no markers resided

<1cM from an adjacent marker, then looking at improving the fine-order of markers using the ripple algorithm. Finally, chromosomes were named and oriented to maximize the similarity with the physical position of markers in the FIL2 genome annotation (phytozome.net).

Supplementary Appendix A2.

Greenhouse experiment

Seeds of 174 F7 RILs and the two parental genotypes were scarified with sandpaper and placed on wet sand in round petri dishes on September 5, 2016 and allowed to germinate in a greenhouse located at the University of Texas at Austin, Brackenridge Field Lab (12-h days at 500 μE m −2 s −1, 28°C; 12-h nights at 24°C). On the 7th day after sowing, seedlings were transferred to 6 cm x 30 cm Cone-Tainers (Stuewe and Sons, Tangent, OR). Cone-Tainers were lined with 1 mil plastic liners (perforated at the bottom for drainage) to facilitate separation of the plant and root systems from the container during harvest. Cone-tainers were filled with Field and Fairway Profile (The Turf Trade, NJ, USA) media. Plants were then assigned to a completely randomized block design within three blocks on a single greenhouse bench. Plants were bottom watered by block by soaking to saturation every three days with Grow liquid nutrient solution (DynaGro, Richmond, CA) to promote seedling growth. Plants were harvested within three days of a common developmental stage defined as when a fully expanded flag leaf with a visible ligule was observable on any tiller with an emerging panicle. The plant in its plastic bag was pulled from the pot gently to prevent damage to the root system. Then the bag was cut open and the profile substrate was gently removed by shaking the plant on wire mesh followed by light washing of the root system in a bucket of tap water. Shoot material was separated from root material. The tiller height (from base of the plant to the node of the flag leaf on the tiller with the emergent panicle), leaf length and area of the flag leaf of the main tiller were measured and tiller number was counted at the time of harvest. Total root number was counted and then the root system was spread out in a clear acrylic water filled tray and scanned at a 600 dpi resolution using an EPSON Scanner (Model 12000XL, Epson America, Inc., San Jose, CA, USA) calibrated for use with WinRhizo Pro 2015 root image analysis software (Regent Instruments Inc., Canada). The Lagarde's local threshold parameter in the analysis software was enabled to ensure detection of thin and pale roots

and the diameter class size was set to 0.25 mm. Root trait data was obtained from scans using WinRhizo Pro 2015 software and included total root length (cm), total root volume (cm3), and average root diameter (mm). Leaf, shoot and root tissue was collected separately, dried for 96 hours in an oven at 55°C, and weighed to obtain biomass.

Specific root length (SRL; total root length / root biomass (cm g-1)), root tissue density (RTD; root biomass / total root volume (g cm-3)), root mass ratio (RMR, root biomass / total biomass) and specific leaf area (SLA; fresh leaf area / dry mass of the leaf (cm2 g-1)) were calculated for each plant.

Confirming root and shoot biomass QTL in a field study

Seed of selected lines were germinated and established in the greenhouse using the procedure outlined above for the RIL planting and subsequently transplanted into the field at the age of one month. Eight biological replicates of each line and eight replicates of the parental genotypes were planted on May 10, 2016 under both restrictive and well-watered irrigation treatments ((10 RILs + 2 parents) x 8 biological replicates x 2 irrigation levels = 192 plants).

The field experiment was conducted at a site located within the Brackenridge Field Laboratory property of the University of Texas in Austin, TX, USA (N 30.2845, W 97.7809). The site elevation is 133 m above sea level and soils are Yazoo sandy loam greater than 1.2 m deep. The mean maximum temperature (August) is ~35.0 °C and the mean minimum temperature (January) is ~ 3.0 °C. This experiment was co-planted in vacant space within an existing *P. hallii* experiment which was established at a site capable of providing two separate levels of irrigation. The site contains 32 differentially irrigated 'beds' which are separated underground by 1.2-meter-deep plastic sheeting (Regal Plastics, Austin, TX, USA) to prevent the spread of applied irrigation water. Irrigation was applied by dripline (0.9 GPH, 12" emitter spacing, Rain Bird, Azusa, CA). The treatment period occurred from June through August with the restrictive treatment receiving 4.5 fold less irrigation in both number of irrigation events and total amount of water applied.

Plants were harvested towards the end of the summer growing season in August over a three-day period. To account for differences in size of the plants, an equal volume of the soil under each plant was harvested using a ‘shovelomics’ device that regulated shovel angle and depth while extracting plants from the field soil. Plants with roots attached were rinsed clean of soil over a metal screen. Shoots were separated from roots, dried at 55°C for 4 days before weighing for biomass.

Table A1. Pearson Correlation Coefficients for genetic correlations in the *Panicum hallii* RIL population.

Trait	ED	TN	RTN	SHMASS	RTMASS	SRL	RTD	HEIGHT	LFLG	RMR	SLA	RTDM	RTLG
TN	0.116												
RTN	0.039	**0.669**											
SHMASS	**0.215**	**0.545**	**0.758**										
RTMASS	0.132	**0.615**	**0.789**	**0.921**									
SRL	**-0.192**	**-0.115**	-0.05	-0.021	**-0.15**								
RTD	**0.195**	**0.195**	**0.191**	**0.281**	**0.336**	**-0.544**							
HEIGHT	0.119	**0.285**	**0.598**	**0.824**	**0.719**	0.118	0.136						
LFLG	0.015	**0.2**	**0.573**	**0.759**	**0.678**	0.135	0.109	**0.769**					
RMR	**-0.281**	-0.005	-0.121	**-0.424**	-0.085	**-0.267**	0.029	**-0.495**	**-0.399**				
SLA	**-0.331**	0.079	0.001	-0.223	-0.095	**0.259**	**-0.288**	-0.114	-0.047	**0.388**			
RTDM	0.125	-0.071	**-0.183**	**-0.260**	**-0.163**	**-0.696**	-0.115	**-0.317**	**-0.338**	**0.290**	-0.135		
RTLG	0.057	**0.566**	**0.772**	**0.905**	**0.925**	**0.185**	**0.198**	**0.762**	**0.734**	**-0.196**	0.003	**-0.450**	
RTVOL	0.120	**0.614**	**0.802**	**0.911**	**0.975**	-0.059	**0.150**	**0.722**	**0.670**	-0.107	-0.045	-0.134	**0.934**

ED, panicle emergence; TN, tiller number; RTN, root number; SHMASS, shoot biomass; RTMASS, root biomass; SRL, specific root length; RTD, root tissue density; HEIGHT, plant height; LFLG, leaf length; RMR, root mass ratio; SLA, specific leaf area; RTDM, root diameter; RTLG, root length. Significant correlations are indicated in bold text.

Table A2. Principal component (PC) loadings of measured traits in the *Panicum hallii* RIL population.

Trait	**PC1**	**PC2**	**PC3**
Panicle Emergence (day)	0.158	0.378	-0.51
Shoot Biomass (g)	0.97	0.065	-0.118
Tiller Number (count)	0.607	0.215	0.373
SLA ($cm^2\ g^{-1}$)	-0.119	-0.423	0.699
Plant Height (cm)	0.84	-0.153	-0.22
Leaf Length (cm)	0.793	-0.224	-0.137
Root Biomass (g)	0.943	0.191	0.174
Root Number (count)	0.836	0.082	0.252
SRL ($cm\ g^{-1}$)	0.039	-0.951	-0.08
RTD ($g\ cm^{-3}$)	0.273	0.563	-0.139
Root Diameter (mm)	-0.337	0.707	0.131
Root Volume (cm^3)	0.937	0.101	0.202
Root Length (m)	0.954	-0.136	0.132
RMR (ratio)	-0.336	0.263	0.773

SLA, specific leaf area; SRL, specific root length;
RTD, root tissue density; RMR, root mass ratio.

Table A3. Main and epistatic effects of the first three principal component QTL for the *Panicum hallii* RIL population.

Principal Component	Chr	Peak (cM)	1.5 Lod Interval	LOD	% var	Effect	SE	Donor of Positive allele	QTL Cluster (CL)
PC1	5	58.6	56-60	7.19	14.42	-1.215	0.209	*filipes*	CL5.1
	5	136.0	135-142	6.34	12.67	-1.049	0.206	*filipes*	CL5.3
	9	66.1	58-84	3.51	6.7	-0.664	0.164	*filipes*	CL9.1
	Epi5:5			3.14	6.0	0.812	0.212		
PC2	1	88.7	83-93	4.51	8.26	-0.458	0.099	*filipes*	CL1.1
	3	34.2	18-36	4.97	9.14	-0.533	0.109	*filipes*	CL3.1
	5	1.1	0-4	4.13	7.52	0.457	0.103	*filipes*	
	8	58.0	42-74	3.45	6.24	0.392	0.097	*filipes*	
PC3	7	67.0	65-72	12.14	25.05	0.676	0.084	*hallii*	CL7.2
	8	18.5	16-26	3.59	6.60	0.354	0.085	*hallii*	CL8.1

Chr, chromosome; Peak, cM (centimorgan) position of the QTL peak; LOD, logarithm of odds; % var, present of variance explained; SE, one standard error; PC1, principal component 1; PC2, principal component 2; PC3, principal component 3; Epi, epistasis.

Table A4. Raw sequence data deposited in NCBI short read archive under the BioProject ID.

RIL (id)	Bioproject ID	Biosample ID
1	PRJNA403347	SAMN07621924
2	PRJNA403345	SAMN07621336
4	PRJNA368209	SAMN06266727
5	PRJNA368210	SAMN06266737
7	PRJNA426989	SAMN08220570
9	PRJNA368211	SAMN06266860
12	PRJNA426952	SAMN08220594
15	PRJNA368212	SAMN06266633
17	PRJNA403402	SAMN07621245
18	PRJNA368213	SAMN06266822
19	PRJNA426938	SAMN08220598
23	PRJNA402629	SAMN07621152
24	PRJNA403343	SAMN07621460
28	PRJNA402626	SAMN07621218
31	PRJNA402613	SAMN07621188
35	PRJNA368214	SAMN06266715
36	PRJNA403344	SAMN07621520
41	PRJNA426971	SAMN08220612
46	PRJNA403362	SAMN07621308
48	PRJNA427015	SAMN08220579
51	PRJNA403373	SAMN07621470
53	PRJNA402600	SAMN07620946
54	PRJNA402599	SAMN07621148
55	PRJNA426954	SAMN08220593
56	PRJNA427017	SAMN08220558
58	PRJNA402646	SAMN07621020
60	PRJNA402660	SAMN07621361
61	PRJNA368215	SAMN06266709
62	PRJNA402603	SAMN07621213
63	PRJNA368216	SAMN06266772
65	PRJNA402633	SAMN07621394
66	PRJNA426965	SAMN08220614
67	PRJNA427014	SAMN08220580
68	PRJNA368217	SAMN06266668
69	PRJNA403360	SAMN07621309
70	PRJNA426984	SAMN08220626
71	PRJNA403434	SAMN07621381

Table A4. (continue)

RIL (id)	Bioproject ID	Biosample ID
73	PRJNA368218	SAMN06266696
75	PRJNA426960	SAMN08220565
77	PRJNA403429	SAMN07621726
79	PRJNA426974	SAMN08220549
81	PRJNA403348	SAMN07621335
82	PRJNA426970	SAMN08220613
83	PRJNA368219	SAMN06266839
84	PRJNA403350	SAMN07621323
85	PRJNA368220	SAMN06266968
89	PRJNA427018	SAMN08220578
90	PRJNA426933	SAMN08220619
93	PRJNA368221	SAMN06266960
95	PRJNA403342	SAMN07621657
96	PRJNA426975	SAMN08220629
99	PRJNA368222	SAMN06266824
100	PRJNA403349	SAMN07621047
101	PRJNA368223	SAMN06267001
102	PRJNA403363	SAMN07620997
104	PRJNA402589	SAMN07620959
105	PRJNA368224	SAMN06266740
106	PRJNA403356	SAMN07621022
107	PRJNA427000	SAMN08220573
108	PRJNA403403	SAMN07621270
109	PRJNA402608	SAMN07621479
110	PRJNA426997	SAMN08220572
113	PRJNA403398	SAMN07621244
114	PRJNA368225	SAMN06266677
115	PRJNA403375	SAMN07620971
117	PRJNA426946	SAMN08220563
120	PRJNA402650	SAMN07621008
125	PRJNA402597	SAMN07621475
131	PRJNA403400	SAMN07621145
132	PRJNA402588	SAMN07620869
134	PRJNA402596	SAMN07621259
136	PRJNA402615	SAMN07621177
137	PRJNA427005	SAMN08220623
141	PRJNA427011	SAMN08220604
142	PRJNA403397	SAMN07621174
144	PRJNA368226	SAMN06266817

Table A4. (continue)

RIL (id)	Bioproject ID	Biosample ID
145	PRJNA402606	SAMN07621080
151	PRJNA427001	SAMN08220582
156	PRJNA403358	SAMN07621322
157	PRJNA426990	SAMN08220586
158	PRJNA403419	SAMN07621070
159	PRJNA403405	SAMN07621163
160	PRJNA402611	SAMN07621147
161	PRJNA427012	SAMN08220603
165	PRJNA426939	SAMN08220634
178	PRJNA402587	SAMN07620870
179	PRJNA402632	SAMN07621058
180	PRJNA426967	SAMN08220548
181	PRJNA403370	SAMN07621284
183	PRJNA368227	SAMN06266761
184	PRJNA403414	SAMN07621078
186	PRJNA368228	SAMN06266861
187	PRJNA426942	SAMN08220618
190	PRJNA426973	SAMN08220611
192	PRJNA402586	SAMN07621103
195	PRJNA368229	SAMN06266863
198	PRJNA402657	SAMN07620968
201	PRJNA368230	SAMN06266869
202	PRJNA402585	SAMN07620970
205	PRJNA402618	SAMN07621230
206	PRJNA368231	SAMN06266649
207	PRJNA426979	SAMN08220569
208	PRJNA426982	SAMN08220587
213	PRJNA368232	SAMN06266806
220	PRJNA427022	SAMN08220601
231	PRJNA402649	SAMN07621495
236	PRJNA427010	SAMN08220621
238	PRJNA426963	SAMN08220615
239	PRJNA402634	SAMN07621490
245	PRJNA402595	SAMN07621271
247	PRJNA427008	SAMN08220555
252	PRJNA368233	SAMN06266889
253	PRJNA402591	SAMN07621283
256	PRJNA368234	SAMN06266892
258	PRJNA427019	SAMN08220577

Table A4. (continue)

RIL (id)	Bioproject ID	Biosample ID
259	PRJNA402434	SAMN07621291
262	PRJNA368235	SAMN06266991
263	PRJNA402639	SAMN07621044
266	PRJNA426981	SAMN08220627
267	PRJNA403388	SAMN07621186
270	PRJNA368236	SAMN06266900
277	PRJNA368237	SAMN06266814
280	PRJNA402605	SAMN07621212
281	PRJNA427020	SAMN08220559
283	PRJNA368238	SAMN06266662
285	PRJNA403379	SAMN07621333
288	PRJNA402647	SAMN07621009
291	PRJNA402625	SAMN07620865
292	PRJNA402614	SAMN07621187
293	PRJNA403351	SAMN07621046
297	PRJNA402653	SAMN07621362
298	PRJNA426969	SAMN08220588
299	PRJNA403365	SAMN07621296
302	PRJNA402593	SAMN07621474
303	PRJNA403386	SAMN07621239
304	PRJNA403406	SAMN07621257
306	PRJNA426980	SAMN08220550
307	PRJNA403409	SAMN07621116
308	PRJNA402648	SAMN07621959
309	PRJNA403435	SAMN07621380
311	PRJNA426968	SAMN08220589
312	PRJNA402604	SAMN07621478
314	PRJNA426985	SAMN08220609
317	PRJNA402598	SAMN07621149
318	PRJNA426995	SAMN08220571
319	PRJNA426945	SAMN08220617
320	PRJNA426951	SAMN08220545
322	PRJNA403430	SAMN07621217
323	PRJNA402643	SAMN07621372
324	PRJNA403368	SAMN07620983
325	PRJNA426978	SAMN08220568
328	PRJNA368239	SAMN06266771
330	PRJNA403458	SAMN07621346
332	PRJNA403376	SAMN07620944

Table A4. (continue)

RIL (id)	Bioproject ID	Biosample ID
333	PRJNA402628	SAMN07621153
334	PRJNA426936	SAMN08220635
336	PRJNA403383	SAMN07621210
337	PRJNA427009	SAMN08220622
338	PRJNA403428	SAMN07621443
339	PRJNA402592	SAMN07620958
341	PRJNA368240	SAMN06266859
342	PRJNA403422	SAMN07621228
344	PRJNA368241	SAMN06266934
345	PRJNA403423	SAMN07621069
348	PRJNA368242	SAMN06266650
349	PRJNA368243	SAMN06266870
352	PRJNA426959	SAMN08220590
353	PRJNA403401	SAMN07621281
354	PRJNA402443	SAMN07621268
355	PRJNA426958	SAMN08220631
356	PRJNA402664	SAMN07621348
357	PRJNA402658	SAMN07621500
360	PRJNA427023	SAMN08220620
363	PRJNA403359	SAMN07621011
365	PRJNA363831	SAMN06264661
366	PRJNA426962	SAMN08220616
367	PRJNA402619	SAMN07621176
368	PRJNA402621	SAMN07621483
369	PRJNA426944	SAMN08220562
371	PRJNA363832	SAMN06265096
372	PRJNA363833	SAMN06265097
374	PRJNA403377	SAMN07621347
378	PRJNA363834	SAMN06264660
379	PRJNA363835	SAMN06265098
380	PRJNA403340	SAMN07621060
381	PRJNA427013	SAMN08220556
382	PRJNA403364	SAMN07621678
383	PRJNA426937	SAMN08220599
385	PRJNA363836	SAMN06264659
387	PRJNA363837	SAMN06265099
388	PRJNA426935	SAMN08220560
390	PRJNA426964	SAMN08220547
391	PRJNA402642	SAMN07621747

Table A4. (continue)

RIL (id)	Bioproject ID	Biosample ID
394	PRJNA403392	SAMN07621294
399	PRJNA363838	SAMN06264658
402	PRJNA403378	SAMN07621334
403	PRJNA363839	SAMN06265100
406	PRJNA426948	SAMN08220544
407	PRJNA427004	SAMN08220554
411	PRJNA403366	SAMN07621295
413	PRJNA426966	SAMN08220566
416	PRJNA402655	SAMN07620980
417	PRJNA426961	SAMN08220630
418	PRJNA403369	SAMN07621469
420	PRJNA426949	SAMN08220632
421	PRJNA403367	SAMN07620996
423	PRJNA403411	SAMN07621248
425	PRJNA426998	SAMN08220625
426	PRJNA363840	SAMN06265101
427	PRJNA427016	SAMN08220557
430	PRJNA402640	SAMN07621033
431	PRJNA403353	SAMN07621035
434	PRJNA426996	SAMN08220583
436	PRJNA402590	SAMN07620886
439	PRJNA403355	SAMN07621023
441	PRJNA403346	SAMN07621970
442	PRJNA363841	SAMN06264761
443	PRJNA402623	SAMN07621146
444	PRJNA403415	SAMN07621249
447	PRJNA402617	SAMN07621482
451	PRJNA402607	SAMN07621746
457	PRJNA403427	SAMN07621043
458	PRJNA426943	SAMN08220597
459	PRJNA402624	SAMN07621164
460	PRJNA426956	SAMN08220546
463	PRJNA403421	SAMN07621229
464	PRJNA363842	SAMN06265102
466	PRJNA363843	SAMN06265103
471	PRJNA426976	SAMN08220610
472	PRJNA403374	SAMN07621117
473	PRJNA426977	SAMN08220628
474	PRJNA363844	SAMN06264760

Table A4. (continue)

RIL (id)	Bioproject ID	Biosample ID
476	PRJNA427003	SAMN08220581
477	PRJNA426987	SAMN08220552
478	PRJNA363845	SAMN06265104
479	PRJNA403426	SAMN07621056
481	PRJNA426994	SAMN08220606
482	PRJNA427002	SAMN08220605
483	PRJNA402610	SAMN07621201
487	PRJNA403407	SAMN07621162
488	PRJNA402661	SAMN07621958
489	PRJNA403381	SAMN07621211
491	PRJNA363846	SAMN06265105
492	PRJNA363847	SAMN06264759
493	PRJNA426992	SAMN08220585
494	PRJNA363848	SAMN06265303
668	PRJNA403399	SAMN07621282
669	PRJNA402630	SAMN07621489
671	PRJNA363849	SAMN06265304
675	PRJNA403433	SAMN07621392
679	PRJNA426983	SAMN08220551
681	PRJNA403396	SAMN07621700
682	PRJNA363850	SAMN06264758
683	PRJNA363851	SAMN06265305
684	PRJNA363852	SAMN06265306
687	PRJNA402609	SAMN07621079
689	PRJNA402663	SAMN07620956
691	PRJNA363853	SAMN06264757
694	PRJNA426988	SAMN08220607
702	PRJNA403418	SAMN07621077
704	PRJNA403425	SAMN07621057
707	PRJNA426940	SAMN08220633
708	PRJNA402627	SAMN07621395
714	PRJNA427021	SAMN08220602
716	PRJNA363854	SAMN06265307
718	PRJNA403413	SAMN07621142
719	PRJNA363855	SAMN06265308
722	PRJNA403391	SAMN07621306
727	PRJNA402641	SAMN07621032
728	PRJNA426941	SAMN08220561
729	PRJNA403393	SAMN07621293

Table A4. (continue)

RIL (id)	Bioproject ID	Biosample ID
730	PRJNA426955	SAMN08220592
737	PRJNA426991	SAMN08220553
742	PRJNA363856	SAMN06265106
754	PRJNA402602	SAMN07621258
755	PRJNA403384	SAMN07621321
758	PRJNA403432	SAMN07621393
759	PRJNA363857	SAMN06264756
760	PRJNA363858	SAMN06265309
768	PRJNA363859	SAMN06265310
770	PRJNA402659	SAMN07620957
771	PRJNA363860	SAMN06265311
772	PRJNA363861	SAMN06265199
773	PRJNA402636	SAMN07621383
774	PRJNA363862	SAMN06265312
775	PRJNA363863	SAMN06264657
777	PRJNA403382	SAMN07621238
781	PRJNA402656	SAMN07620969
782	PRJNA403424	SAMN07621442
783	PRJNA363864	SAMN06265313
786	PRJNA363865	SAMN06265314
791	PRJNA402631	SAMN07621059
792	PRJNA403372	SAMN07621104
793	PRJNA363866	SAMN06265198
794	PRJNA363867	SAMN06265315
795	PRJNA363868	SAMN06265316
798	PRJNA363869	SAMN06264755
799	PRJNA403466	SAMN07621319
802	PRJNA403408	SAMN07621144
803	PRJNA363870	SAMN06265317
804	PRJNA363871	SAMN06265318
805	PRJNA363872	SAMN06264656
808	PRJNA363873	SAMN06265319
811	PRJNA402654	SAMN07620981
814	PRJNA403394	SAMN07621185
816	PRJNA363874	SAMN06265320
818	PRJNA403395	SAMN07621175
819	PRJNA363875	SAMN06264754
820	PRJNA403404	SAMN07621269
825	PRJNA363876	SAMN06265321

Table A4. (continue)

RIL (id)	Bioproject ID	Biosample ID
826	PRJNA363877	SAMN06265322
829	PRJNA402601	SAMN07620945
831	PRJNA402651	SAMN07620995
833	PRJNA363878	SAMN06265323
834	PRJNA402662	SAMN07621501
838	PRJNA363879	SAMN06264655
841	PRJNA363880	SAMN06265326
850	PRJNA363881	SAMN06265147
853	PRJNA363882	SAMN06265327
854	PRJNA403417	SAMN07621150
858	PRJNA363883	SAMN06265328
862	PRJNA402620	SAMN07621219
863	PRJNA363884	SAMN06264654
867	PRJNA403416	SAMN07621151
868	PRJNA403431	SAMN07621216
872	PRJNA363885	SAMN06265329
874	PRJNA363886	SAMN06265330
878	PRJNA363887	SAMN06265331
880	PRJNA403387	SAMN07621198
881	PRJNA403385	SAMN07621199
887	PRJNA403390	SAMN07621307
893	PRJNA402622	SAMN07621165
898	PRJNA403412	SAMN07621143
906	PRJNA402635	SAMN07621045
909	PRJNA403371	SAMN07620982

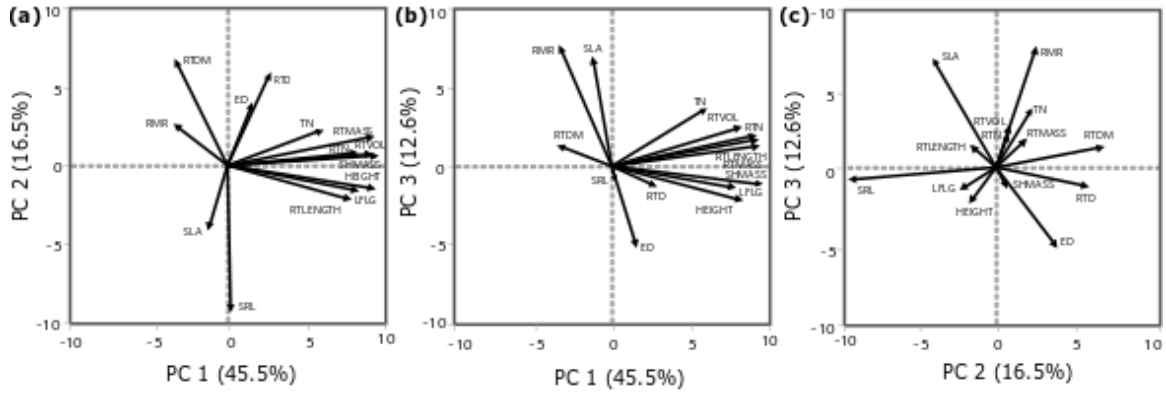

Figure A1. Principal component analysis of shoot and root traits for the *Panicum hallii* RIL population. Traits: PC, principal component; RMR, root mass ratio; SLA, specific leaf area; SRL, specific root length; RTLRNGTH, root length; LFLG, leaf length; HEIGHT, plant height; SHMASS, shoot biomass; RTMASS, root biomass; RTVOL, root volume; RTN, root number; TN, tiller number; RTD, root tissue density; ED, emergence day; RTDM, root diameter.

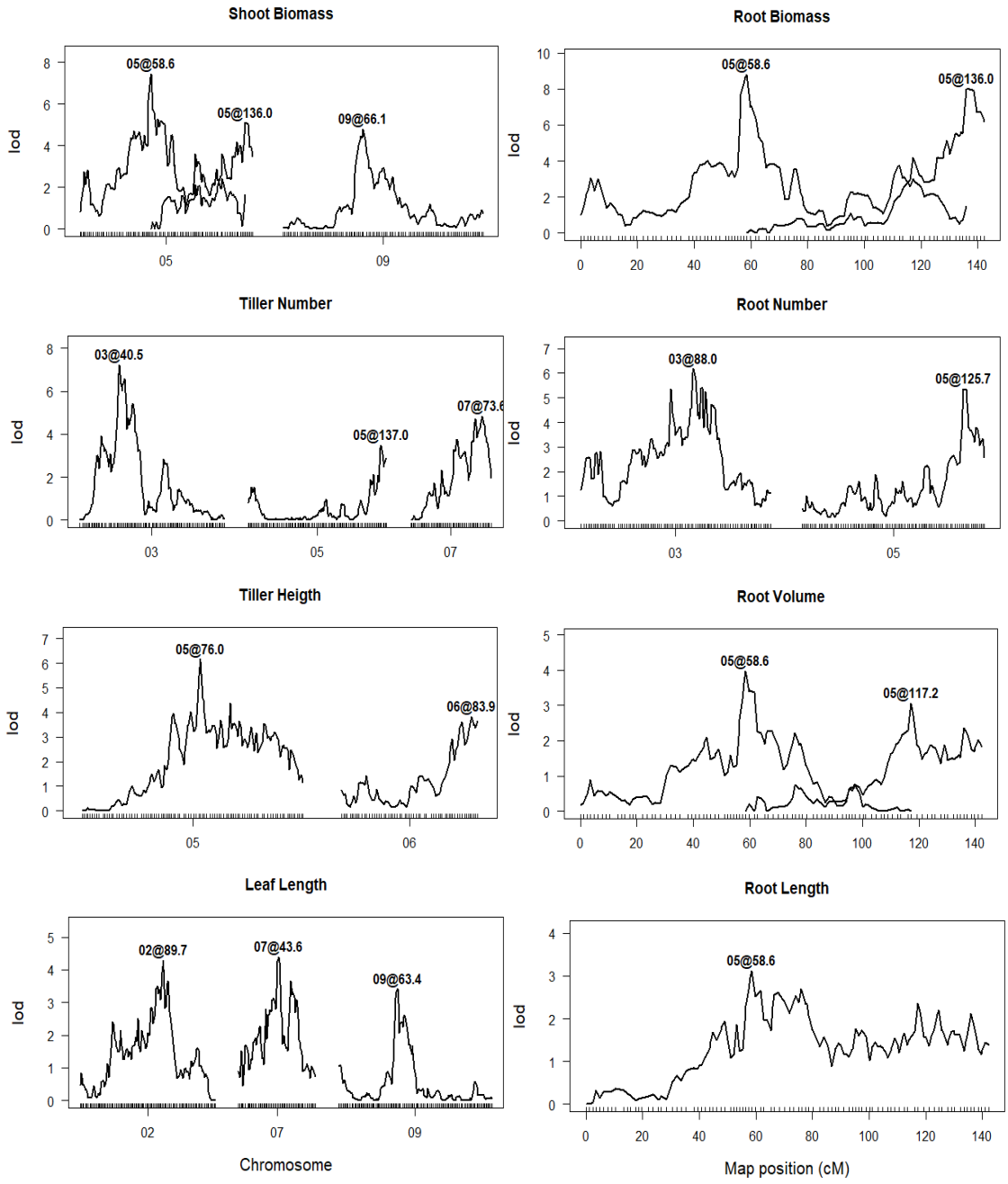

Figure A2. Conditional LOD profile plots of detected QTL for shoot and root traits and first three principle components of a *P. hallii* RIL mapping population resulting from the final model of stepwise QTL mapping.

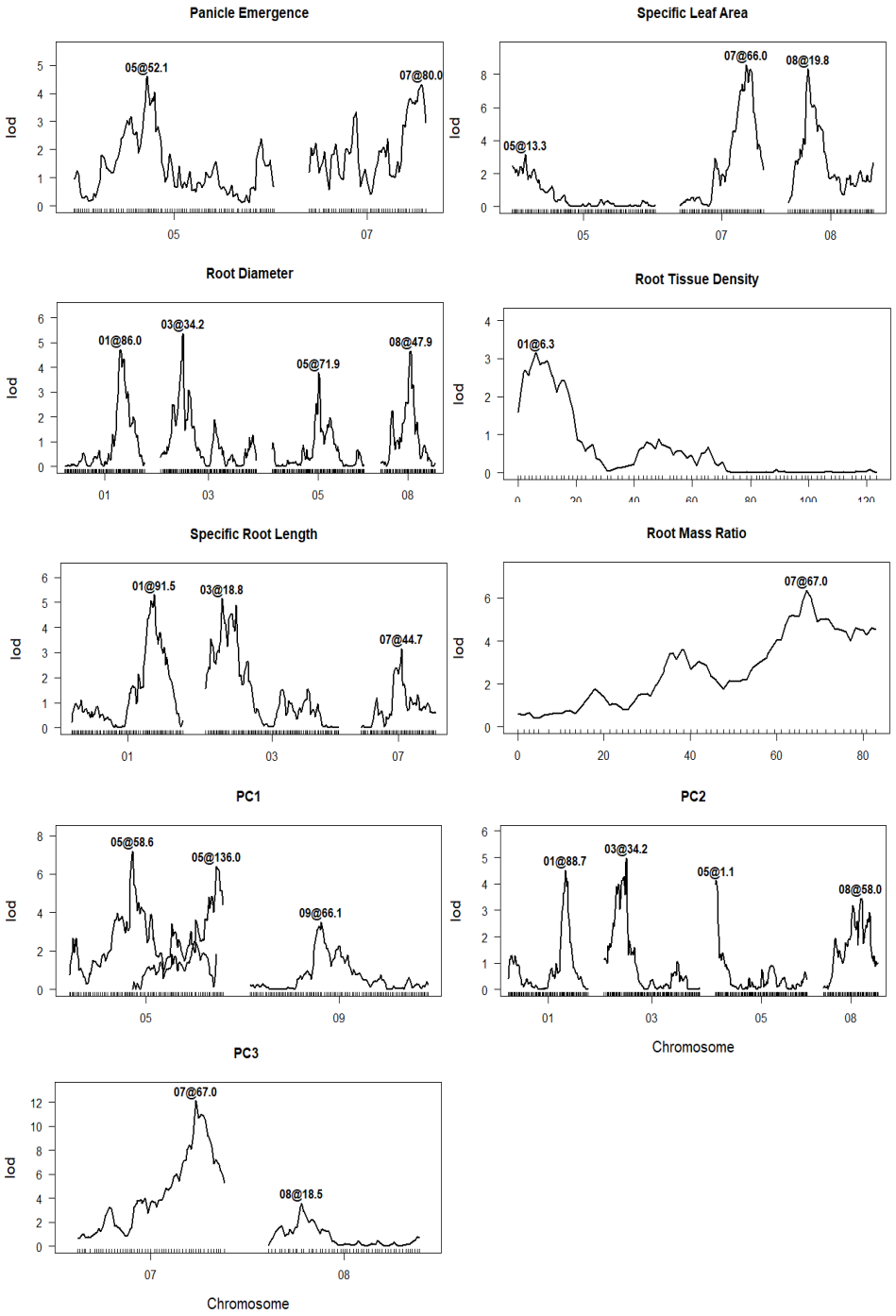

Figure A2. (continue)

SUPPLEMENTAL MATERIAL FOR CHAPTER 2.

Table A5. Nutrient and mineral composition of native soils used for microbial inoculum.

	Austin, TX	Corpus Christy, TX	units
pH	6.4	8.2	-
Conductivity	271	482	µmho/cm
Nitrate-N	26	14	ppm
Phosphorus	19	9	ppm
Potassium	271	360	ppm
Calcium	4	7	ppm
Magnesium	239	755	ppm
Sulfur	24	33	ppm
Sodium	12	353	ppm
Iron	11.3	7.96	ppm
Zinc	1.6	1.42	ppm
Manganese	82.37	3.19	ppm
Copper	0.8	0.77	ppm
Boron	0.34	1.4	ppm
Organic Matter	4.94	2.10	%

Table A6. Means + SE for the parental ecotypes, RILs, RIL range and broad-sense heritability (H2 + SE) for Mock Inoculated (MI), Austin Inoculated (AI), and Corpus Inoculated (CI) microbial treatments.

Trait	Treat-ment	FIL2 Mean±SE	HAL2 Mean±SE	RIL Mean±SE	RIL range	H^2±SE
Shoot Biomass	MI	361±30	233±30	318±8	26-924	0.04±0.04
(mg)	AI	468±43	237±46	353±11	31-992	0.04±0.04
	CI	476±46	326±43	301±10	30-895	0.03±0.03
Tiller Number	MI	4.3±0.3	4±0.3	5.2±0.1	1-11.5	0.07±0.05
(count)	AI	5±0.47	4.3±0.5	5.7±0.12	43843	0.08±0.05
	CI	5.2±0.5	5±0.47	5.0-0.11	43843	0.10±0.06
SLA	MI	376±11	431±11	400±2.5	251-515	0.11±0.06
(cm^2g^{-1})	AI	404±16	445±17	400±2.7	249-512	0.04±0.05
	CI	379±17	382±16	400±3.2	73-535	0.07±0.05
Root Biomass	MI	80±8	43±9	61±2	5-179	0.04±0.05
(mg)	AI	87±12	36±13	59±2	5-198	0.09±0.05
	CI	90±13	51±12	48±1	4-176	0.08±0.05
Root Number	MI	12.7±0.7	10.5±0.7	11.4±0.2	3-22	0.11±0.06
(count)	AI	13±1	11.2±1.1	12.2±0.2	2-26	0.09±0.06
	CI	14.2±1.1	12.1±1	10.9±0.23	2-27	0.03±0.04
SRL	MI	13±0.8	19.3±0.8	20.4±0.27	9.3-35.9	0.15±0.06
($cm\ g^{-1}$)	AI	11.1±1.1	21.4±1.2	20.4±0.35	7.3-43.2	0.15±0.06
	CI	9.8±1.2	20.4±1.1	19.8±0.32	8.3-41.7	0.18±0.07
RTD	MI	25±1.2	19.8±1.2	34.6±0.38	18.8-59.9	0.06±0.05
($g\ cm^{-3}$)	AI	27.2±1.7	18±1.8	34.7±0.46	16.5-57.8	0.09±0.05
	CI	34±1.8	21.2±1.7	35.0±0.47	9.4-60.8	0.07±0.05
Root Diameter	MI	0.63±0.01	0.59±0.01	0.44±0.003	0.35-0.64	0.12±0.06
(mm)	AI	0.67±0.02	0.59±0.03	0.44±0.003	0.33-0.63	0.07±0.05
	CI	0.63±0.03	0.55±0.02	0.44±0.003	0.35-0.67	0.05±0.05
Lateral Root	MI	156±16	137±16	198-5.9	1-919	0.06±0.05
Length (cm)	AI	87±24	103±24	187±6.8	5-721	0.01±0.04
	CI	99±24	144±22	158±5.6	15-721	0.04±0.04
1st Order Root	MI	23.4±0.9	23±0.8	25.2±0.21	17-40	0.01±0.03
Length (cm)	AI	26.4±1.3	22.4±1.3	25.1±0.25	14-38	0.03±0.04
	CI	24.1±1.3	28.4±1.2	24.3±0.22	13-44	0.08±0.06
Root Length	MI	955±99	828±99	1159±34	65-3033	0.02±0.04
(cm)	AI	893±140	729±151	1124±37	70-3194	0.07±0.05
	CI	875±151	1020±140	909±41	140-3167	0.02±0.04
RMR	MI	16.9±0.9	15.6±0.9	15.8±0.18	7-27	0.11±0.06
(ratio)	AI	15.2±1.3	12.8±1.4	14.2±0.19	6-27	0.15±0.07
	CI	15.7±1.4	13.7±1.3	14.0±0.20	6-44	0.04±0.04

Table A7. P-values for genetic and microbial treatment effects of root and shoot traits for the *Panicum hallii* parental ecotypes across three microbial treatments (Mock Inoculates, Austin Inoculated and Corpus Inoculated).

Trait	**Effect**	**df**	**F-value**	***P*-value**
Shoot Biomass	Ecotype	1, 48	26.36	**<0.0001**
(mg)	Treatment	2, 48	3.89	**0.027**
	Ecotype x Treatment	2, 48	0.92	0.405
Tiller Number	Ecotype	1, 48	1.05	0.313
(count)	Treatment	2, 48	2.66	0.080
	Ecotype x Treatment	2, 48	0.15	0.863
SLA	Ecotype	1, 47	7.14	**0.010**
(cm^2g^{-1})	Treatment	2, 47	3.46	**0.039**
	Ecotype x Treatment	2, 47	1.60	0.212
Root Biomass	Ecotype	1, 48	19.93	**<0.0001**
(mg)	Treatment	2, 48	0.38	0.689
	Ecotype x Treatment	2, 48	0.19	0.828
Root Number	Ecotype	1, 48	6.16	**0.016**
(count)	Treatment	2, 48	1.35	0.269
	Ecotype x Treatment	2, 48	0.02	0.979
SRL	Ecotype	1, 48	113.01	**<0.0001**
(cm g-1)	Treatment	2, 48	0.67	0.520
	Ecotype x Treatment	2, 48	3.47	**0.039**
RTD	Ecotype	1, 47	48.12	**<0.0001**
(g cm-3)	Treatment	2, 47	6.45	**0.003**
	Ecotype x Treatment	2, 47	3.32	**0.046**
Root Diameter	Ecotype	1, 48	11.81	**0.001**
(mm)	Treatment	2, 48	1.09	0.343
	Ecotype x Treatment	2, 48	0.37	0.694
Lateral Root	Ecotype	1, 46	0.67	0.415
Length (cm)	Treatment	2, 46	3.36	**0.043**
	Ecotype x Treatment	2, 46	1.41	0.255
1sr Order Root	Ecotype	1, 46	0	0.989
Length (cm)	Treatment	2, 46	3.74	**0.031**
	Ecotype x Treatment	2, 46	5.01	**0.010**
Root Length	Ecotype	1, 48	0.20	0.652
(cm)	Treatment	2, 48	0.45	0.641
	Ecotype x Treatment	2, 48	0.74	0.480
RMR	Ecotype	1, 48	3.87	0.055
(ratio)	Treatment	2, 48	2.21	0.122
	Ecotype x Treatment	2 ,48	0.12	0.890

Table A8. Comparison of "base" and "GxE" linear mixed models to evaluate the impact of the microbiome on the quantitative genetic architecture of our measured traits (The Diagonal model allows Va or Vaa to vary by treatment).

Trait	**Treatment**	**V_a**	**V_{aa}**	**Residual**	**Test of GxE (model favored)**	**AIC**	**LogLik**	**P-Value**
Shoot Biomass (mg)	Base model	2478±954	2505±526	20141±1153	No GxE	837	-415	
	MI	473±605	342±778	20289±2825	Diagonal model	777	-385	**0.001**
	AI	1429±1220	0.00±1205	35880±4745				
	CI	103±571	620±816	26176±3317				
Tiller Number (count)	Base model	0.54±0.16	0.21±0.05	2.52±0.14	No GxE	818	-406	
	MI	0.19±0.11	0.00±0.08	2.65±0.35	Diagonal model	743	-368	**0.001**
	AI	0.34±0.18	0.00±0.14	4.11±0.55				
	CI	0.35±0.16	0.00±0.10	3.07±0.42				
SLA (cm^2g^{-1})	Base model	273±81	58±28	1786±100	No GxE	831	-412	
	MI	189±85	0.00±54	1533±208	Diagonal model	797	-395	**0.001**
	AI	93±72	0.00±68	2067±269				
	CI	180±108	0.00±86	2568±341				
Root Biomass (mg)	Base model	111±38	73±18	806±45	No GxE	826	-10	
	MI	40±36	0.24±35	1039±138	Diagonal model	768	-381	**0.001**
	AI	123±65	0.00±46	1291±179				
	CI	18±24	41±24	703±98				
Root Number (count)	Base model	1.57±0.53	0.84±0.23	11.55±0.65	No GxE	830	-412	
	MI	1.26±0.57	0.00±0.36	10.51±1.42	Diagonal model	780	-387	**0.001**
	AI	1.41±0.78	0.26±0.66	16.53±2.38				
	CI	0.39±0.43	0.00±0.48	15.21±1.93				

Table A8. (continue)

Trait	Treatment	V_a	V_{aa}	Residual	Test of GxE (model favored)	AIC	LogLik	P-Value
SRL ($cm\ g^{-1}$)	Base model	5.36±1.43	2.10±0.46	15.32±0.88	No GxE	773	-383	
	MI	2.99±1.15	0.00±0.60	16.67±2.32	Diagonal model	634	-314	**0.001**
	AI	4.71±1.84	0.00±0.99	27.10±3.80				
	CI	4.7±1.67	0.00±0.79	21.32±3.05				
RTD ($g\ cm^{-3}$)	Base model	4.90±1.64	1.42±0.68	45.00±2.53	No GxE	843	-418	
	MI	2.43±1.57	0.00±1.34	40.34±5.26	Diagonal model	811	-402	**0.001**
	AI	5.38±2.66	0.00±1.83	52.39±7.09				
	CI	3.78±2.36	0.00±2.27	56.98±8.02				
Root Diameter (µm)	Base model	342±118	261.60±56	2157±123	No GxE	836	-415	
	MI	239±118	47.31±93	2201±324	Diagonal model	742	-368	**0.001**
	AI	230±137	10.05±113	3210±433				
	CI	178±124	0.00±110	3337±437				
Lateral Root Length (cm)	Base model	571±7.46	426±148	8888±501	No GxE	829	-411	
	MI	570±371	0.00±316	9525±1243	Diagonal model	807	-400	**0.001**
	AI	164±313	0.00±404	12956±1625				
	CI	164±234	171±325	8218±1158				
1st Order Root Length (cm)	Base model	0.31±0.21	0.29±0.17	13.70±0.76	No GxE	853	-423	
	MI	0.13±0.29	0.00±0.39	13.08±1.61	Diagonal model	851	-422	0.936
	AI	0.44±0.48	0.00±0.53	16.74±2.14				
	CI	0.10±0.32	0.86±0.60	11.65±1.86				

Table A8. (continue)

Trait	Treatment	V_a	V_{aa}	Residual	Test of GxE (model favored)	AIC	LogLik	P-Value
Root Length (m)	Base model	2.55±0.99	2.46±0.54	22.54±1.28	No GxE	818	-406	
	MI	0.71±0.87	0.00±1.00	31.93±4.01	Diagonal model	757	-375	**0.001**
	AI	2.48±1.49	0.00±1.20	35.35±4.68				
	CI	0.37±0.59	0.00±0.74	23.78±2.98				
RMR (ratio)	Base model	1.91±0.50	0.14±0.13	9.77±0.54	No GxE	778	-386	
	MI	1.03±0.47	0.00±0.30	8.72±1.18	Diagonal model	751	-372	**0.001**
	AI	1.43±0.56	0.00±0.30	8.32±1.17				
	CI	0.58±0.51	0.00±0.52	16.06±2.07				

Table A9. QTL effects (main and epistatic) of for the *Panicum hallii* RIL population.

Trait	Detected at Treatment	Chr	Peak (cM)	1.5 Lod Interval	LOD	% var	Effect	SE	Donor of Positive allele	GxE (Mixed Model)
Shoot	MI	3	4.3	2.8-6	9.7	13.9	0.10	0.019	*hallii*	n
Biomass	MI	3	58	56-60	11.7	16.6	-0.15	0.020	*filipes*	n
(g)	MI	Epi3@4.3:3@58.0			6.8	9.2	0.11	0.020		Y
Tiller	MI	3	4	3-6	7.4	9.8	0.05	0.012	*hallii*	n
number	MI	3	58	56-60	9.4	12.6	-0.08	0.012	*filipes*	n
(count)	MI	6	62.4	59-69	6.8	4.8	0.03	0.008	*hallii*	n
	MI	9	70	65-78	6.5	4.4	-0.03	0.008	*filipes*	n
	MI	Epi3@4.0:3@58.0			4.9	6.3	0.06	0.013		Y
	AI	9	70.2	68-80	3.3	4.9	-0.04	0.010	*filipes*	n
	CI	9	59.5	52-78	3.5	5.5	-0.04	0.010	*filipes*	n
SLA	MI	7	52.7	38-63	5.8	8.7	13.19	2.503	*hallii*	n
(cm^2g^{-1})	AI	7	42.7	24-61	3.2	4.9	11.13	2.891	*hallii*	n
	CI	7	60.4	49-63	6.2	9.5	17.17	3.032	*hallii*	n
Root	MI	1	92.6	87-98	3	4.0	-0.06	0.016	*filipes*	n
Biomass	MI	3	4.3	3-7	6.3	8.6	0.08	0.022	*hallii*	n
(g)	MI	3	58	56-60	8.5	11.9	-0.14	0.022	*filipes*	n
	MI	Epi3@4.3:3@58.0			4.7	6.3	0.11	0.023		n
	AI	*1	90	0-97	3.2	4.5	-0.07	0.018	*filipes*	n
	AI	*4	29.3	27-32	3.2	4.5	0.07	0.018	*hallii*	n
	CI	*3	57.4	51-65	2.6	4.1	-0.06	0.018	*filipes*	n
Root	MI	*3	4.3	2-7	4.9	6.8	0.04	0.011	*hallii*	n
Number	MI	3	57.4	54-73	7.6	10.8	-0.07	0.012	*filipes*	n
(count)	MI	*Epi3@4.3:3@57.4			2.2	2.9	0.04	0.012		n

Table A9. (continue)

Trait	Detected at Treatment	Chr	Peak (cM)	1.5 Lod Interval	LOD	% var	Effect	SE	Donor of Positive allele	GxE (Mixed Model)
SRL	MI	1	92.6	86-95	4.2	4.9	1.12	0.252	*hallii*	n
(cm g^{-1})	MI	3	7	3-9	13.2	16.4	2.08	0.316	*hallii*	n
	MI	3	56.1	54-69	6.5	7.6	-0.41	0.322	*filipes*	n
	MI	5	32.3	26-80	3.4	3.9	0.98	0.248	*hallii*	n
	MI	Epi3@7.0:3@56.1			5.9	6.9	1.73	0.328		n
	AI	3	11.2	4-25	6.7	9.7	2.22	0.390	*hallii*	n
	AI	*9	70.2	58-78	2.7	3.7	1.19	0.340	*hallii*	n
	CI	3	4	3-10	10.9	14.8	2.41	0.398	*hallii*	n
	CI	*3	51.9	51-60	4.9	6.3	-0.24	0.397	*filipes*	n
	CI	*Epi3@4.0:@51.9			4	5.1	1.77	0.411		n
RTD	MI	*1	92.6	0-98	2.6	4.0	-1.43	0.408	*filipes*	n
(g cm^{-3})	AI	4	29.3	18-32	3.5	5.1	1.91	0.475	*hallii*	n
	AI	8	50.8	45-62	3.2	4.7	-1.77	0.458	*filipes*	n
	CI	8	62.8	60-69	3.5	5.4	-1.96	0.483	*filipes*	n
Root	MI	1	37.3	28-44	4	4.5	-0.01	0.002	*filipes*	n
Diameter	MI	3	4.3	3-6	16.8	20.9	-0.02	0.003	*filipes*	n
(mm)	MI	3	58.4	54-60	11.6	13.8	0.02	0.003	*hallii*	n
	MI	5	31.7	13-36	3.1	3.5	-0.01	0.002	*filipes*	n
	MI	Epi3@4.3:3@58.4			10.7	12.6	-0.03	0.003		n
	AI	3	4.8	3-7	13.6	18.5	-0.03	0.004	*filipes*	n
	AI	3	58.4	57-60	9.2	12.1	0.02	0.004	*hallii*	n
	AI	Epi3@4.8:3@58.4			8.5	11.0	-0.03	0.004		n

Table A9. (continue)

Trait	Detected at Treatment	Chr	Peak (cM)	1.5 Lod Interval	LOD	% var	Effect	SE	Donor of Positive allele	GxE (Mixed Model)
Root	CI	3	4.8	3-7	17.1	21.9	-0.04	0.004	*filipes*	n
Diameter	CI	3	58.4	54-60	7.9	9.4	0.02	0.004	*hallii*	n
(mm)	CI	Epi3@4.8:3@58.4			6.7	7.8	-0.02	0.004		n
Lateral	MI	*3	4.8	3-7	11.1	14.7	0.11	0.024	*hallii*	n
Root	MI	*3	29.1	23-52	3.3	4.1	0.08	0.021	*hallii*	n
Length	MI	*3	58.4	57-60	13.1	17.6	-0.18	0.024	*filipes*	n
(cm)	MI	*Epi3@4.8:3@58.4			9.5	12.5	0.17	0.024	*hallii*	n
Root	MI	3	4.3	3-7	6.9	9.7	195.25	45.630	*hallii*	n
Length	MI	3	58	54-60	6.7	9.4	#####	46.890	*filipes*	n
(cm)	MI	5	25.7	3-32	3	4.1	123.30	33.150	*hallii*	n
	MI	Epi3@4.3:3@58.4			4.6	6.3	220.75	47.590	*hallii*	n
	AI	*5	24.2	13-29	2.7	4.0	131.38	36.980	*hallii*	n
RMR	MI	8	35	30-41	3.1	4.5	-0.02	0.005	*filipes*	n
(Ratio)	MI	9	62	58-70	3.6	5.2	-0.02	0.005	*filipes*	n
	CI	6	3.1	0-31	3.1	4.6	0.02	0.006	*hallii*	n

With * indicating suggestive QTL detected with alpha=0.1. GxE (Mixed Model) – Treatment x Marker interactions using PROC mixed in SAS**.** Y indicates QTL that were significant by mixed model between treatments. Treatments: Mock Inoculated (MI), Austin Inoculated (AI), Corpus Inoculated (CI).

Table A10. Full model analysis of QTL–treatment interactions using PROC mixed in SAS with QTL modeled on the marker nearest the QTL peak.

Trait	Effect	Num DF	Den DF	F-Value	P-Value
Shoot Biomass (g)	Treatment	2	446	0.16	0.8497
	3@4.3	1	446	25.79	**<0.0001**
	Treatment x 3@4.3	2	446	1.26	0.2835
	3@58.0	1	446	43.29	**<0.0001**
	Treatment x 3@58.0	2	446	2.01	0.1346
	*9@3.9	1	446	3.1	0.0791
	* Treatment x 9@3.9	2	446	7.87	**0.0004**
	3@4.3 x 3@58.0	1	446	32.09	**<0.0001**
	Treatment x 3@4.3 x 3@58.0	2	446	4.49	**0.0117**
Tiller number (count)	Treatment	2	394	0.88	0.4149
	3@4.0	1	394	26.22	**<0.0001**
	Treatment x 3@4.0	2	394	0.94	0.3924
	3@58.0	1	394	33.42	**<0.0001**
	Treatment x 3@58.0	2	394	1.61	0.2018
	6@62.4	1	394	7.2	**0.0076**
	Treatment x 6@62.4	2	394	0.64	0.5295
	7@17.0	1	394	7.89	**0.0052**
	Treatment x 7@17.0	2	394	9.94	**<0.0001**
	9@70.0	1	394	18.63	**<0.0001**
	Treatment x 9@70.0	2	394	0.61	0.543
	3@4.0 x 3@58.0	1	394	24.74	**<0.0001**
	Treatment x 3@4.0 x 3@58.0	2	394	3.47	**0.0321**
SLA (cm^2g^{-1})	Treatment	2	522	0.23	0.7965
	7@52.7	1	522	39.06	**<0.0001**
	Treatment x 7@52.7	2	522	1.33	0.2664

Table A10. (continue)

Trait	Effect	Num DF	Den DF	F-Value	P-Value
Root Biomass (g)	Treatment	2	389	1	0.3701
	1@92.6	1	389	6.42	**0.0117**
	Treatment x 1@92.6	2	389	1.33	0.2662
	3@4.3	1	389	7.6	**0.0061**
	Treatment x 3@4.3	2	389	0.4	0.6688
	3@58.0	1	389	20.47	**<.0001**
	Treatment x 3@58.0	2	389	1.78	0.1697
	*4@29.3	1	389	9.92	**0.0018**
	* Treatment x 4@29.3	2	389	1.25	0.2889
	9@3.9	1	389	3.58	0.0593
	Treatment x 9@3.9	2	389	10.19	**<0.0001**
	3@4.3 x 3@58.0	1	389	16.74	**<0.0001**
	Treatment x 3@4.3 x 3@58.0	2	389	2.61	0.0749
Root Number (count)	Treatment	2	416	0.49	0.6147
	*3@4.3	1	416	9.61	**0.0021**
	* Treatment x 3@4.3	2	416	0.43	0.6499
	3@57.4	1	416	23.44	**<0.0001**
	Treatment x 3@57.4	2	416	0.81	0.4467
	7@0.3	1	416	5.63	**0.0181**
	Treatment x 7@0.3	2	416	6.95	**0.0011**
	8@33.1	1	416	4.73	**0.0302**
	Treatment x 8@33.1	2	416	3.11	**0.0457**
	*3@4.3 x 3@57.4	1	416	13.48	**0.0003**
	* Treatment x 3@4.3 x 3@57.4	2	416	1.79	0.1686

Table A10. (continue)

Trait	Effect	Num DF	Den DF	F-Value	P-Value
SRL	Treatment	2	358	0.31	0.7359
(cm g^{-1})	1@92.6	1	358	8.9	**0.003**
	Treatment x 1@92.6	2	358	0.27	0.7652
	3@7.0	1	358	57.27	**<0.0001**
	Treatment x 3@7.0	2	358	1.05	0.3527
	3@56.1	1	358	4.22	**0.0407**
	Treatment x 3@56.1	2	358	1.4	0.2482
	4@19.1	1	358	9.85	**0.0018**
	Treatment x 4@19.1	2	358	5.63	**0.0039**
	5@32.7	1	358	9.6	**0.0021**
	Treatment x 5@32.7	2	358	0.23	0.7973
	*9@70.2	1	358	12.46	**0.0005**
	* Treatment x 9@70.2	2	358	1.36	0.2583
	3@7.0 x 3@56.1	1	358	15.91	**<0.0001**
	Treatment x 3@7.0*3@56.1	2	358	0.93	0.397
RTD	Treatment	2	415	0.21	0.8091
(g cm^{-3})	*1@92.6	1	415	3.6	0.0586
	* Treatment x 1@92.6	2	415	1.13	0.3238
	4@29.3	1	415	12.36	**0.0005**
	Treatment x 4@29.3	2	415	0.13	0.8802
	8@50.8	1	415	11	**0.001**
	Treatment x 8@50.8	2	415	1.8	0.1668

Table A10. (continue)

Trait	Effect	Num DF	Den DF	F-Value	P-Value
Root	Treatment	2	358	0.43	0.6506
Diameter	1@37.3	1	358	3.13	0.0778
(mm)	Treatment x 1@37.3	2	358	2.13	0.1201
	1@68.0	1	358	0.17	0.6813
	Treatment x 1@68.0	2	358	0.36	0.7012
	2@78.8	1	358	1.23	0.2683
	Treatment x 2@78.8	2	358	3.13	**0.0449**
	3@4.8	1	358	70.19	**<0.0001**
	Treatment x 3@4.8	2	358	1.37	0.2542
	3@58.4	1	358	39.18	**<0.0001**
	Treatment x 3@58.4	2	358	0.07	0.9362
	5@31.7	1	358	11.19	**0.0009**
	Treatment x 5@31.7	2	358	1.15	0.318
	7@0.3	1	358	7.2	**0.0076**
	Treatment x 7@0.3	2	358	3.65	**0.027**
	1@68.0 x 2@78.8	1	358	28.41	**<0.0001**
	Treatment x1@68.0 x 2@78.8	2	358	3.27	**0.0393**
	3@4.8 x 3@58.4	1	358	56.49	**<.0001**
	Treatment x 3@4.8 x 3@58.4	2	358	0.8	0.4521
Lateral	Treatment	2	434	0.79	0.4558
Root	*3@4.8	1	434	23.23	**<0.0001**
Length	* Treatment x 3@4.8	2	434	2.03	0.1331
(cm)	*3@29.1	1	434	11.07	**0.001**
	* Treatment x 3@29.1	2	434	0.51	0.6017

Table A10. (continue)

Trait	Effect	Num DF	Den DF	F-Value	P-Value
Lateral	*3@58.4	1	434	47.88	**<.0001**
Root	* Treatment x 3@58.4	2	434	3.84	**0.0221**
Length	*7@3.4	1	434	1.6	0.2072
(cm)	* Treatment x 7@3.4	2	434	4.21	**0.0155**
	*3@4.8 x 3@58.4	1	434	48.61	**<0.0001**
	* Treatment x 3@4.8 x 3@58.4	2	434	5.55	**0.0042**
1st Order	Treatment	2	517	6.25	**0.0021**
Root	9@25.6	1	517	9.89	**0.0018**
Length(cm)	Treatment x 9@25.6	2	517	5.98	**0.0027**
Root	Treatment	2	415	5.19	**0.0059**
Length	3@4.8	1	415	20.18	**<0.0001**
(cm)	Treatment x 3@4.8	2	415	0.01	0.9933
	3@58.0	1	415	22.15	**<0.0001**
	Treatment x 3@58.0	2	415	0.89	0.4108
	5@25.7	1	415	17.53	**<0.0001**
	Treatment x 5@25.7	2	415	0.62	0.5407
	9@3.9	1	415	2.46	0.1179
	Treatment x 9@3.9	2	415	6.27	**0.0021**
	3@4.8 x 3@58.0	1	415	20.94	**<0.0001**
	Treatment x 3@4.8 x 3@58.0	2	415	1.7	0.1834

Table A10. (continue)

Trait	Effect	Num DF	Den DF	F-Value	P-Value
RMR	Treatment	2	362	26.94	**<0.0001**
(Ratio)	3@74.1	1	362	4.88	**0.0278**
	Treatment x 3@74.1	2	362	4.28	**0.0145**
	6@3.1	1	362	7.28	**0.0073**
	Treatment x 6@3.1	2	362	1.16	0.3137
	8@35.0	1	362	17.11	**<0.0001**
	Treatment x 8@35.0	2	362	0.63	0.5306
	9@62.0	1	362	3.18	0.0753
	Treatment x 9@62.0	2	362	2.29	0.1023
*indicates QTL detected with alpha =0.1					

Table A11. Tests of effect slices of significant TRT x Marker interaction in the full model analysis of QTL x treatment interactions using PROC mixed in SAS with QTL modeled on the marker nearest the QTL peak.

Trait	Effect	Treatment	Num DF	Den DF	F-Value	P-Value
Shoot Biomass (g)	* Treatment x 9@3.9	MI	1	446	3.77	0.0529
		AI	1	446	10.17	**0.0015**
		CI	1	446	1.06	0.3031
	Treatment x 3@4.3 x 3@58.0	MI	3	446	15.82	**<0.0001**
		AI	3	446	11.68	**<0.0001**
		CI	3	446	6.26	**0.0004**
Tiller Number (count)	Treatment x 7@17.0	MI	1	394	0.66	0.416
		AI	1	394	25.32	**<0.0001**
		CI	1	394	0.3	0.5872
	Treatment x 3@4.0 x 3@58.0	MI	3	394	9.84	**<0.0001**
		AI	3	394	11.48	**<0.0001**
		CI	3	394	4.45	**0.0043**
Root Biomass (g)	Treatment x 9@3.9	MI	1	389	3.88	**0.0496**
		AI	1	389	13.08	**0.0003**
		CI	1	389	1.27	0.2599
Root Number (count)	Treatment x 7@0.3	MI	1	416	0	0.9768
		AI	1	416	17.15	**<0.0001**
		CI	1	416	1.48	0.2252
	Treatment x 8@33.1	MI	1	416	10.76	**0.0011**
		AI	1	416	0.86	0.3537
		CI	1	416	0.46	0.4985
SRL ($cm\ g^{-1}$)	Treatment x 4@19.1	MI	1	358	0.74	0.3904
		AI	1	358	3.06	0.0809
		CI	1	358	20.33	**<0.0001**

Table A11. (continue)

Trait	Effect	Treatment	Num DF	Den DF	F-Value	P-Value
Root Diameter (mm)	Treatment x 7@0.3	MI	1	358	2.64	0.1052
		AI	1	358	13	**0.0004**
		CI	1	358	0.02	0.8993
	Treatment x 1@68.0 x 2@78.8	MI	3	358	2.25	0.0818
		AI	3	358	8.4	**<0.0001**
		CI	3	358	9.11	**<0.0001**
Lateral Root Length (cm)	* Treatment x 7@3.4	MI	1	434	0.19	0.6598
		AI	1	434	8.17	**0.0045**
		CI	1	434	0.46	0.496
	* Treatment x 3@4.8 x 3@58.4	MI	3	434	20.95	**<0.0001**
		AI	3	434	8.81	**<0.0001**
		CI	3	434	4.64	**0.0033**
1st Order Root Length (cm)	Treatment x 9@25.6	MI	1	517	0.2	0.6551
		AI	1	517	21.51	**<0.0001**
		CI	1	517	1.08	0.2982
Root Length (cm)	Treatment x 9@3.9	MI	1	415	1.03	0.3097
		AI	1	415	10.85	**0.0011**
		CI	1	415	0.74	0.3887
RMR (ratio)	Treatment x 3@74.1	MI	1	362	0.56	0.4564
		AI	1	362	0.43	0.5104
		CI	1	362	12.85	**0.0004**

*indicates QTL detected with alpha =0.1. Treatments: Mock Inoculated (MI), Austin Inoculated (AI), Corpus Inoculated (CI).

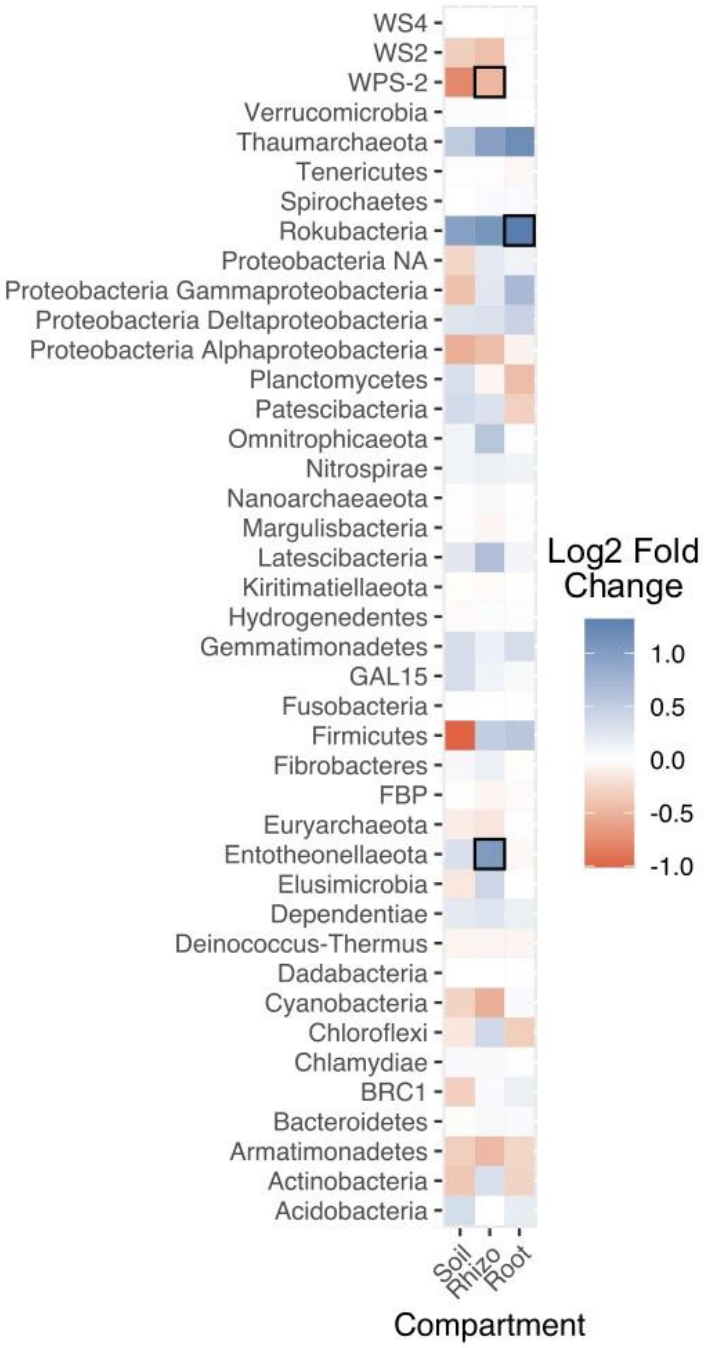

Figure A3: Phylum level differences with plants growing in their native habitats. Black boxes around tiles indicate a significant different between Austin Inoculated (AI) and Corpus Inoculated (CI) environments (adjusted P value < 0.05). A red color indicates a higher abundance in the AI environment, while a blue indicates higher abundance in the CI environment.

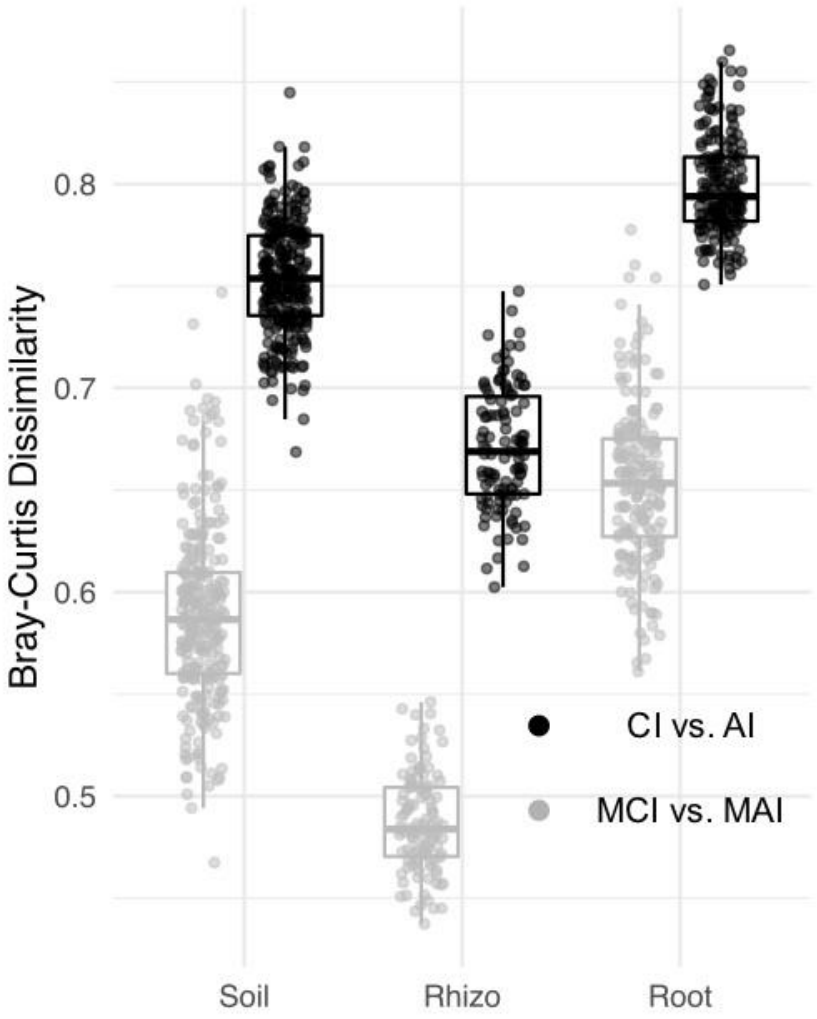

Figure A4. Mock treatment microbiota are more similar than native treatment microbiota. The graph displays Bray-Curtis dissimilarities comparing inoculation within mock (Mock Austin Inoculated (MAI) vs. Mock Corpus Inoculated (MCI)) and native (Austin Inoculated (AI) vs. Corpus Inoculated (CI)) treatments levels.

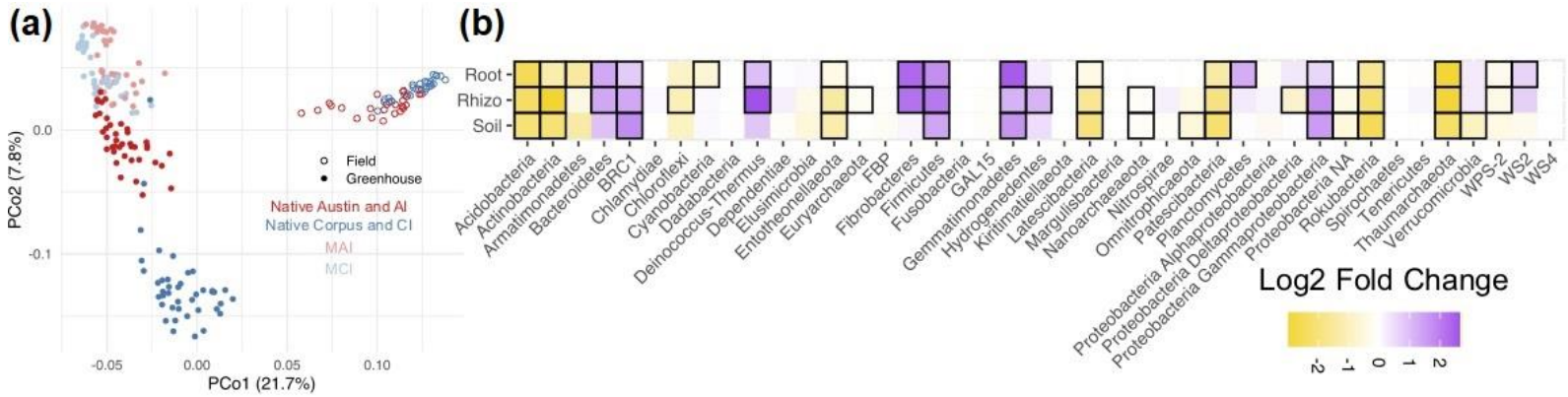

Figure A5. Field and glasshouse derived samples host non-identical microbiota. Panels: (a), PCoA graph displaying all samples collected in the study; (b), phylum level differences between glasshouse and field grown samples.

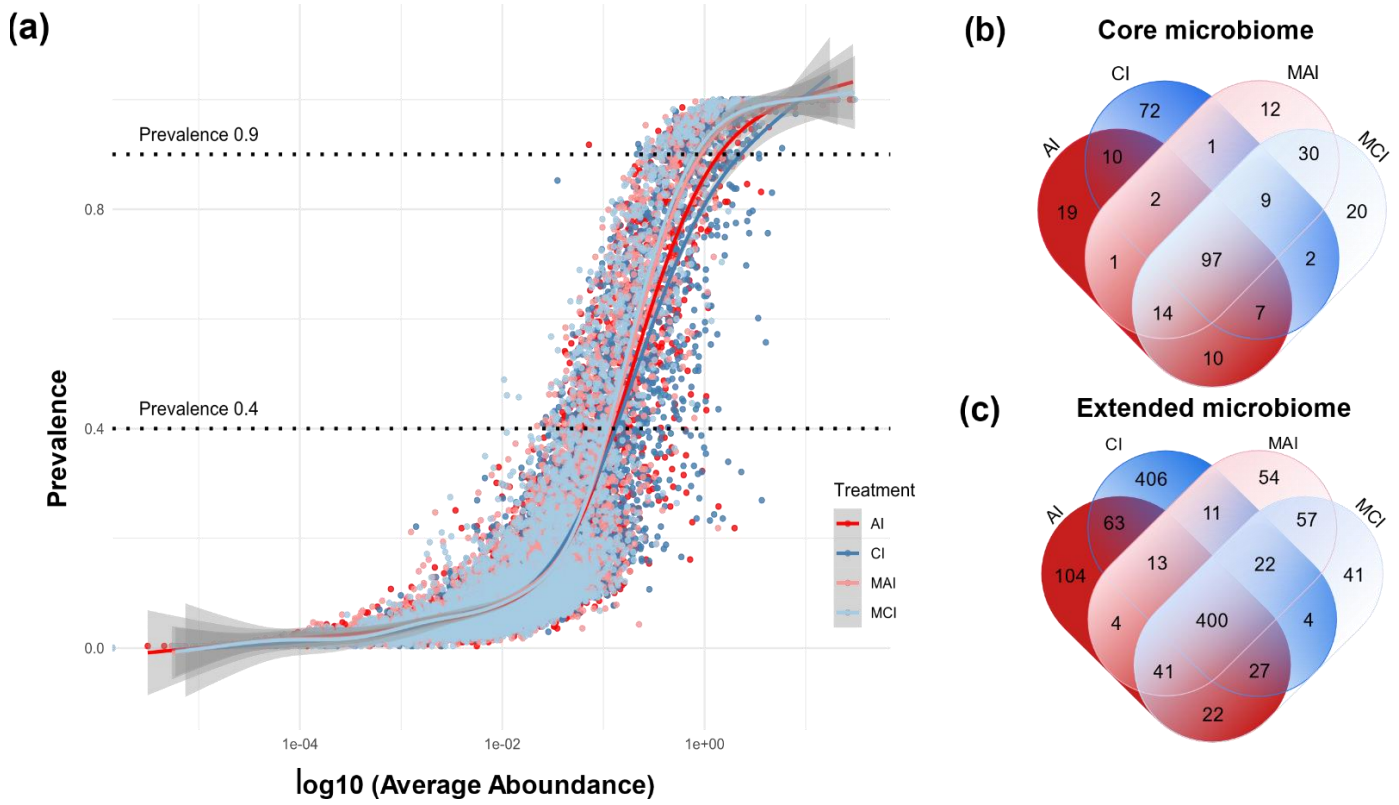

Figure A6. Selection of ASVs for QTL analysis. Panels: (a), scatter plot illustrating relationships between average abundance and prevalence in AI, CI, MAI and MCI microbial treatments with colored curves showing best fit for each treatment and dashed lines representing the 0.9 prevalence cutoff for the core microbiome and 0.4 prevalence cutoff for the extended microbiome; (b), Venn diagram showing shared and unique ASVs in the core microbiome; (c), Venn diagram showing shared and unique ASVs of the extended microbiome.

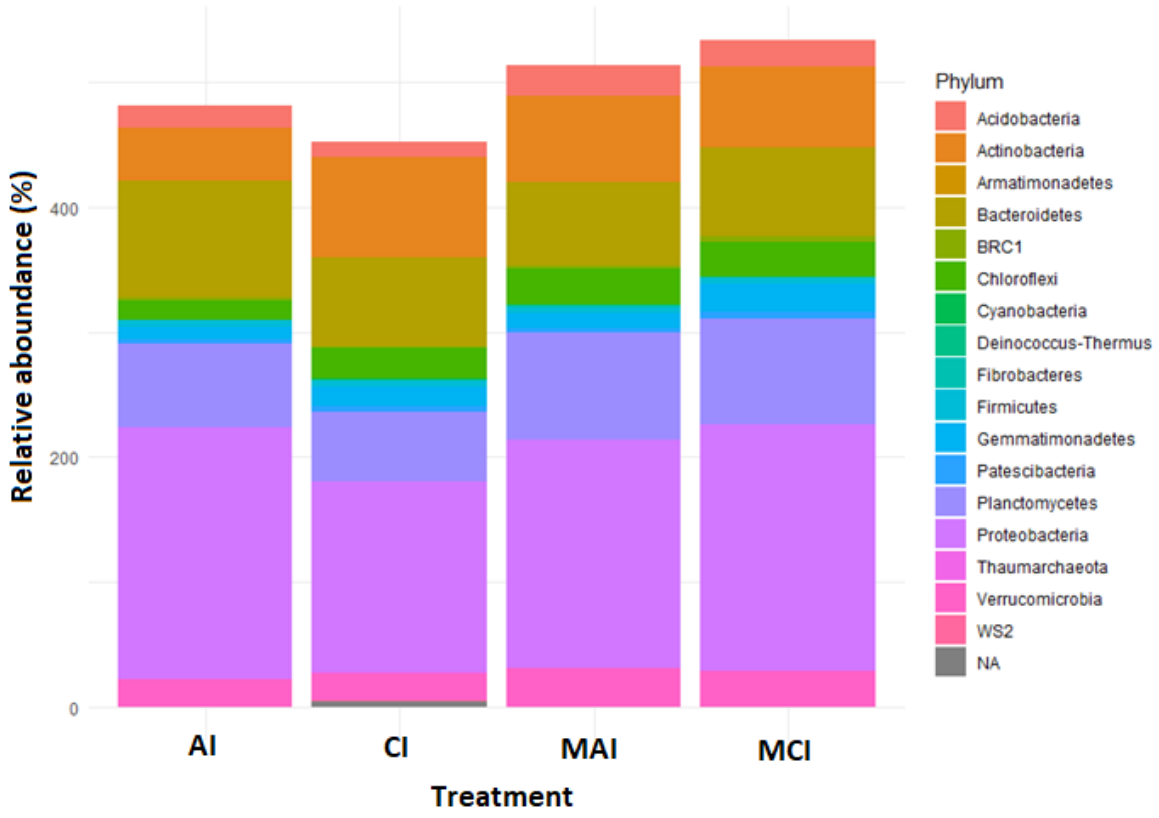

Figure A7. Relative abundance of phyla in the core microbiome in each treatment.

References

Andersen EJ, Ali S, Byamukama E, Yen Y, Nepal MP. **2018**. Disease resistance mechanisms in plants. *Genes* **9**.

Bakker MG, Manter DK, Sheflin AM, Weir TL, Vivanco JM. **2012**. Harnessing the rhizosphere microbiome through plant breeding and agricultural management. *Plant and Soil* **360**: 1–13.

Balachowski JA, Bristiel PM, Volaire FA. **2016**. Summer dormancy, drought survival and functional resource acquisition strategies in California perennial grasses. *Annals of Botany* **118**: 357–368.

Baruch Z. **1994**. Responses to drought and flooding in tropical forage grasses. I. Biomass allocation, leaf growth and mineral nutrients. *Plant and Soil* **164**: 87–96.

Benning JW, Moeller DA. **2020**. Microbes, mutualism, and range margins: testing the fitness consequences of soil microbial communities across and beyond a native plant's range. *New Phytologist*.

Bergelson J, Mittelstrass J, Horton MW. **2019**. Characterizing both bacteria and fungi improves understanding of the Arabidopsis root microbiome. *Scientific Reports* **9**: 1–11.

Bischoff A, Crémieux L, Smilauerova M, Lawson CS, Mortimer SR, Dolezal J, Lanta V, Edwards AR, Brook AJ, Macel M, *et al.* 2006. Detecting local adaptation in widespread grassland species - The importance of scale and local plant community. *Journal of Ecology* **94**: 1130–1142.

Bollmann-Giolai A, Giolai M, Heavens D, Macaulay I, Malone J, Clark MD. 2020. A low-cost pipeline for soil microbiome profiling. Microbiology Open **9**: 1–22.

Bouteillé M, Rolland G, Balsera C, Loudet O, Muller B. **2012**. Disentangling the intertwined genetic bases of root and shoot growth in arabidopsis. *PLoS ONE* **7**.

Bowsher AW, Kearns PJ, Popovic D, Lowry DB, Shade A. **2020**. Locally adapted mimulus ecotypes differentially impact rhizosphere bacterial and archaeal communities in an environment-dependent manner. *Phytobiomes Journal* **4**: 53–63.

Brodie ED, Moore AJ, Janzen FJ. **1995**. Visualizing and quantifying natural selection. *Trends in Ecology & Evolution* **10**: 313–318.

Broman KW, Gatti DM, Simecek P, Furlotte NA, Prins P, Sen Ś, Yandell BS, Churchill GA. **2018**. R/qtl2: software for mapping quantitative trait loci with high-dimensional data and multi-parent populations. *Genetics* **211**:495-502

Broman KW, Sen S. 2009. *A guide to QTL mapping with R/Qtl*. New York, USA: Springer.

Brumbarova T, Ivanov R. **2019**. The Nutrient Response Transcriptional Regulome of Arabidopsis. *iScience* **19**: 358–368.

Bulgarelli D, Garrido-Oter R, Münch PC, Weiman A, Dröge J, Pan Y, McHardy AC, Schulze-Lefert P. **2015**. Structure and function of the bacterial root microbiota in wild and domesticated barley. *Cell Host and Microbe* **17**: 392–403.

Burke JM, & Arnold ML. 2001. Genetics and the fitness of hybrids. *Annu. Rev. Genet*. **35**: 31–52.

Callahan BJ, McMurdie PJ, Rosen MJ, Han AW, Johnson AJA, Holmes SP. 2016. DADA2: High-resolution sample inference from Illumina amplicon data. *Nature Methods* **13**: 581–583.

Carmo-Silva AE, Francisco A, Powers SJ, Keys AJ, Ascensão L, Parry MAJ, Arrabaça MC. **2009**. Grasses of different C4 subtypes reveal leaf traits related to drought tolerance in their natural habitats: Changes in structure, water potential, and amino acid content. *American Journal of Botany* **96**: 1222–1235.

Chapin S, Autumn K, Pugntairet F. **1993**. Evolution of Suites of Traits in Response to Environmental Stress. *American Naturalist* **142**: S78–S92.

Chen T, Nomura K, Wang X, Sohrabi R, Xu J, Yao L, Paasch BC, Kremer J, Cheng Y, Zhang L, *et al*. 2020. HHS Public Access. **580**: 653–657.

Cheng J, Chu P, Chen D, Bai Y. **2016**. Functional correlations between specific leaf area and specific root length along a regional environmental gradient in Inner Mongolia grasslands. *Functional Ecology* **30**: 985–997.

Clausen J. **1951**. *Stages in the evolution of plant species.* Ithaca, NY, USA: Cornell University Press.

Comas LH, Becker SR, Cruz VM V, Byrne PF, Dierig DA. **2013**. Root traits contributing to plant productivity under drought. *Frontiers in plant science* **4**: 442.

Cornelissen JHC, Lavorel S, Garnier E, Díaz S, Buchmann N, Gurvich DE, Reich PB, Steege H Ter, Morgan HD, Heijden MG a. Van Der, *et al.* 2003. A handbook of protocols for standardised and easy measurement of plant functional traits worldwide. *Australian Journal of Botany* **51**: 335.

Covarrubias-Pazaran G. 2018. Software update: Moving the R package sommer to multivariate mixed models for genome-assisted prediction. *bioRxiv preprint*

Des Marais DL, Hernandez KM, Juenger TE. **2013**. Genotype-by-environment interaction and plasticity: Exploring genomic responses of plants to the abiotic environment. *Annual Review of Ecology, Evolution, and Systematics* **44**: 5–29.

Des Marais DL, Lasky JR, Verslues PE, Chang TZ, Juenger TE. 2017. Interactive effects of water limitation and elevated temperature on the physiology, development and fitness of diverse accessions of Brachypodium distachyon. New Phytologist **214**: 132–144.

De Souza RSC, Armanhi JSL, Arruda P. **2020**. From Microbiome to Traits: Designing Synthetic Microbial Communities for Improved Crop Resiliency. *Frontiers in Plant Science* **11**: 1–7.

Edwards J, Santos-Medellín C, Nguyen B, Kilmer J, Liechty Z, Veliz E, Ni J, Phillips G, Sundaresan V. **2019**. Soil domestication by rice cultivation results in plant-soil feedback through shifts in soil microbiota. *Genome Biology* **20**: 1–14.

Edwards J, Johnson C, Santos-Medellín C, Lurie E, Podishetty NK, Bhatnagar S, Eisen JA, Sundaresan V, Jeffery LD. **2015**. Structure, variation, and assembly of the root-associated microbiomes of rice. *Proceedings of the National Academy of Sciences of the United States of America* **112**: E911–E920.

Egamberdieva D, Wirth SJ, Shurigin V V., Hashem A, Abd Allah EF. **2017**. Endophytic bacteria improve plant growth, symbiotic performance of chickpea (Cicer arietinum L.) and induce suppression of root rot caused by Fusarium solani under salt stress. *Frontiers in Microbiology* **8**: 1–13.

Eissenstat DM, Wells CE, Yanai RD, Whitbeck JL. **2000**. Building roots in a changing environment: Implications for root longevity. *New Phytologist* **147**: 33–42.

Enquist BJ, Niklas KJ. **2002**. Global allocation aules for patterns of biomass partitioning in seed plants. *Science* **295**: 1517–1520.

Fierer N. **2017**. Embracing the unknown: Disentangling the complexities of the soil microbiome. *Nature Reviews Microbiology* **15**: 579–590.

Finkel OM, Salas-González I, Castrillo G, Conway JM, Law TF, Teixeira PJPL, Wilson ED, Fitzpatrick CR, Jones CD, Dangl JL. **2020**. A single bacterial genus maintains root development in a complex microbiome. *Nature* **587**:103–108.

Fishman L, Kelly AJ, Willis JH. **2002**. Minor quantitative trait loci underlie floral traits associated with mating system divergence in *Mimulus*. *Evolution; international journal of organic evolution* **56**: 2138–2155.

Friesen ML, Porter SS, Stark SC, Von Wettberg EJ, Sachs JL, Martinez-Romero E. **2011**. Microbially mediated plant functional traits. *Annual Review of Ecology, Evolution, and Systematics* **42**.

Gould FW. 1975. *The grasses of Texas*. College Station, TX, USA: Texas A&M University Press.

Gray MM, St. Amand P, Bello NM, Galliart MB, Knapp M, Garrett KA, Morgan TJ, Baer SG, Maricle BR, Akhunov ED, *et al*. 2014. Ecotypes of an ecologically dominant prairie grass (*Andropogon gerardii*) exhibit genetic divergence across the U.S. Midwest grasslands' environmental gradient. *Molecular Ecology* **23**: 6011–6028.

Griffin JS, Haug LA, Rivera VA, Hernandez Gonzalez LM, Kelly JJ, Miller WM, Wells GF, Packman AI. 2020. Soil hydrology drives ecological niche differentiation in a native prairie microbiome. FEMS Microbiology Ecology **96**: 1–11.

Hammer GL, Dong Z, McLean G, Doherty A, Messina C, Schussler J, Zinselmeier C, Paszkiewicz S, Cooper M. **2009**. Can changes in canopy and/or root system architecture explain historical maize yield trends in the U.S. corn belt? *Crop Science* **49**: 299–312.

Hartman K, Tringe SG. **2019**. Interactions between plants and soil shaping the root microbiome under abiotic stress. *Biochemical Journal* **476**: 2705–2724.

Hartmann A, Schmid M, van Tuinen D, Berg G. **2009**. Plant-driven selection of microbes. *Plant and Soil* **321**: 235–257.

Hendriks PW, Kirkegaard JA, Lilley JM, Gregory PJ, Rebetzke GJ. **2016**. A tillering inhibition gene influences root-shoot carbon partitioning and pattern of water use to improve wheat productivity in rainfed environments. *Journal of experimental botany* **67**: 327-340.

Hummel I, Pantin F, Sulpice R, Piques M, Rolland G, Dauzat M, Christophe A, Pervent M, Bouteillé M, Stitt M, *et al.* 2010. Arabidopsis Plants Acclimate to Water Deficit at Low Cost through Changes of Carbon Usage: An Integrated Perspective Using Growth, Metabolite, Enzyme, and Gene Expression Analysis. *Plant Physiology* **154**: 357–372.

Hund A, Ruta N, Liedgens M. **2009**. Rooting depth and water use efficiency of tropical maize inbred lines, differing in drought tolerance. *Plant and Soil* **318**: 311–325.

Iannucci A, Marone D, Russo MA, Vita P De, Miullo V, Ferragonio P, Blanco A, Gadaleta A, Mastrangelo AM. **2017**. Mapping QTL for Root and Shoot Morphological Traits in a Durum Wheat × *T. dicoccum* Segregating Population at Seedling Stage. **2017**.

Jacoby R, Peukert M, Succurro A, Koprivova A, Kopriva S. **2017**. The role of soil microorganisms in plant mineral nutrition—current knowledge and future directions. *Frontiers in Plant Science* **8**: 1–19.

Järemo J, Tuomi J, Nilsson P, Lennartsson T. 1999. Plant Adaptations to Herbivory: Mutualistic versus Antagonistic Coevolution. *Oikos* **84**: 313-320.

Jeuken MJW, Zhang NW, McHale LK, Pelgrom K, Den Boer E, Lindhout P, Michelmore RW, Visser RGF, Niks RE. 2009. Rin4 causes hybrid necrosis and race-specific resistance in an interspecific lettuce hybrid. Plant Cell **21**: 3368–3378.

Joly RJ, Adams WT, Stafford SG. **1989**. Phenological and morphological responses of mesic and dry site sources of coastal Douglas-fir to water deficit. *Forest Science* **35**: 987–1005.

Jones P, Garcia BJ, Furches A, Tuskan GA, Jacobson D. **2019**. Plant host-associated mechanisms for microbial selection. *Frontiers in Plant Science* **10**: 1–14.

Jtlovell/qtlTools. **2018**. Data Processing AND Plotting in Association with R/qtl. Available at: https://rdrr.io/github/jtlovell/qtlTools/. Last accessed 05 March 2018.

Juenger TE. **2013**. Natural variation and genetic constraints on drought tolerance. *Current Opinion in Plant Biology* **16**: 274–281.

Kaeppler SM, Parke JL, Mueller SM, Senior L, Stuber C, Tracy WF. **2000**. Variation among maize inbred lines and detection of quantitative trait loci for growth at low phosphorus and responsiveness to arbuscular mycorrhizal fungi. *Crop Science* **40**: 358–364.

Khasanova A, Lovell JT, Bonnette J, Weng X, Jenkins J, Yoshinaga Y, Schmutz J, Juenger TE. **2019**. The genetic architecture of shoot and root trait divergence between mesic and xeric ecotypes of a perennial grass. *Frontiers in Plant Science* **10**: 1–10.

Khasanova A, Edwards JA, Bonnette J, Schmutz J, Juenger TE. Quantitative genetic-by-microbiome interactions in a perennial grass affect functional traits. *In prep.*

Knight CA, Vogel H, Kroymann J, Shumate A, Witsenboer H, Mitchell-Olds T. **2006**. Expression profiling and local adaptation of *Boechera holboellii* populations for water use efficiency across a naturally occurring water stress gradient. *Molecular Ecology* **15**: 1229–1237.

Kooyers NJ, Greenlee AB, Colicchio JM, Oh M, Blackman BK. **2015**. Replicate altitudinal clines reveal that evolutionary flexibility underlies adaptation to drought stress in annual *Mimulus guttatus*. *New Phytologist* **206**: 152–165.

Kumar A., Bernier J., Verulkar S., Lafitte H. R., Atlin G. N. 2008. Breeding for drought tolerance: Direct selection for yield, response to selection and use of drought-tolerant donors in upland and lowland-adapted populations. *Field Crops Research* **107**: 221–231.

Labbé J, Jorge V, Kohler A, Vion P, Marçais B, Bastien C, Tuskan GA, Martin F, Le Tacon F. 2011. Identification of quantitative trait loci affecting ectomycorrhizal symbiosis in an interspecific F1 poplar cross and differential expression of genes in ectomycorrhizas of the two parents: Populus deltoides and Populus trichocarpa. *Tree Genetics and Genomes* **7**: 617–627.

Latta RG. 2009. Testing for local adaptation in *Avena barbata*: A classic example of ecotypic divergence. *Molecular Ecology* **18**: 3781–3791.

Lang M, Bei S, Li X, Kuyper TW, Zhang J. 2019. Rhizoplane Bacteria and Plant Species Co-determine Phosphorus-Mediated Microbial Legacy Effect. *Frontiers in Microbiology* **10**: 1–12.

Lankau RA, Keymer DP. 2018. Simultaneous adaptation and maladaptation of tree populations to local rhizosphere microbial communities at different taxonomic scales. *New Phytologist* **217**: 1267–1278.

Lau JA, Lennon JT. 2012. Rapid responses of soil microorganisms improve plant fitness in novel environments. *Proceedings of the National Academy of Sciences of the United States of America* **109**: 14058–14062.

Leimu R, Fischer M. 2008. A meta-analysis of local adaptation in plants. *PLoS ONE* **3**: 1–8.

Lehnert H, Serfling A, Enders M, Friedt W, Ordon F. 2017. Genetics of mycorrhizal symbiosis in winter wheat (Triticum aestivum). *New Phytologist* **215**: 779–791.

Lexer C, Fay MF. 2005. Adaptation to environmental stress: A rare or frequent driver of speciation? *Journal of Evolutionary Biology* **18**: 893–900.

Li Y, Wu X, Chen T, Wang W, Liu G, Zhang W, Li S, Wang M, Zhao C, Zhou H, *et al.* 2018. Plant phenotypic traits eventually shape its microbiota: A common garden test. *Frontiers in Microbiology* **9**: 1–13.

Littell RC, Milliken GA, Stroup WW, Wolfinger RD. 1996. SAS System for Mixed Models. New York. USA: SAS Institute Inc.

Love MI, Huber W, Anders S. 2014. Moderated estimation of fold change and dispersion for RNA-seq data with DESeq2 Genome Biology. **15(12)**:550.

Lovell JT, Jenkins J, Lowry DB, Mamidi S, Sreedasyam A, Weng X, Barry K, Bonnette J, Campitelli B, Daum C, *et al.* 2018. The genomic landscape of molecular responses to natural drought stress in *Panicum hallii*. *Nature Communications* **9**.

Lovell JT, Shakirov E V, Schwartz S, Lowry DB, Aspinwall MJ, Taylor SH, Bonnette J, Palacio-Mejia JD, Hawkes C V., Fay PA, *et al.* 2016. Promises and challenges of eco-physiological genomics in the field: tests of drought responses in switchgrass. *Plant Physiology* **172**: 734-748.

Lovell JT, Mullen JL, Lowry DB, Awole K, Richards JH, Sen S, Verslues PE, Juenger TE, McKay JK. **2015**. Exploiting Differential Gene Expression and Epistasis to Discover Candidate Genes for Drought-Associated QTLs in *Arabidopsis thaliana*. *The Plant Cell* **27**: 969–983.

Lovell JT, Juenger TE, D MS, Lasky JR, Platt A, Richards JH, Yu X, Easlon HM, Sen S, McKay JK. **2013**. Pleiotropy of FRIGIDA enhances the potential for multivariate adaptation. *Proceedings of the Royal Society B: Biological Sciences* **280**: 20131043.

Lowry DB, Behrman KD, Grabowski P, Morris GP, Kiniry JR, Juenger TE. **2014a**. Adaptations between ecotypes and along environmental gradients in *Panicum virgatum*. *The American naturalist* **183**: 682–92.

Lowry DB, Hernandez K, Taylor SH, Meyer E, Logan TL, Barry KW, Chapman JA, Rokhsar DS, Schmutz J, Juenger TE. **2014b**. The genetics of divergence and reproductive isolation between ecotypes of *Panicum hallii*. *New Phytologist* **205**: 402-414.

Lundberg DS, Lebeis SL, Paredes SH, Yourstone S, Gehring J, Malfatti S, Tremblay J, Engelbrektson A, Kunin V, Rio TG Del, *et al.* 2012. Defining the core Arabidopsis thaliana root microbiome. *Nature* **488**: 86–90.

Lowry DB, Purmal CT, Juenger TE. **2013**. A population genetic transect of *Panicum hallii* (*Poaceae*). *American Journal of Botany* **100**: 592–601.

Lowry DB. **2012**. Ecotypes and the controversy over stages in the formation of new species. *Biological Journal of the Linnean Society* **106**: 241–257.

Lynch M, Walsh B. 1998. ***Genetics and analysis of quantitative traits***. Sunderland, MA: Sinauer Associates.

Mace ES, Singh V, van Oosterom EJ, Hammer GL, Hunt CH, Jordan DR. **2012**. QTL for nodal root angle in sorghum (*Sorghum bicolor* L. Moench) co-locate with QTL for traits associated with drought adaptation. *Theoretical and Applied Genetics* **124**: 97–109.

Maherali H, Sherrard ME, Clifford MH, Latta RG. **2008**. Leaf hydraulic conductivity and photosynthesis are genetically correlated in an annual grass. *New Phytologist* **180**: 240–247.

Markesteijn L, Poorter L. **2009**. Seedling root morphology and biomass allocation of 62 tropical tree species in relation to drought- and shade-tolerance. *Journal of Ecology* **97**: 311–325.

Martin M. 2011. Cutadapt removes adapter sequences from high-throughput sequencing reads. *EMBnet J* **17.1**:10-12.

McMillan C. 1965. Ecotypic differentiation within 4 North American Prairie grasses. II. Behavioral variation within transplanted community fractions. *American Journal of Botany* **52**: 55–65.

Mendes R, Garbeva P, Raaijmakers JM. **2013**. The rhizosphere microbiome: Significance of plant beneficial, plant pathogenic, and human pathogenic microorganisms. *FEMS Microbiology Reviews* **37**: 634–663.

Midolo G, Wellstein C. **2020**. Plant performance and survival across transplant experiments depend upon temperature and precipitation change along elevation. *Journal of Ecology* **108**: 2107–2120.

Milano ER, Lowry DB, Juenger TE. **2016**. The Genetic Basis of Upland/Lowland Ecotype Divergence in Switchgrass (*Panicum virgatum*). *G3: Genes,Genomes,Genetics* **6**: 3561–3570.

Monroe JG, Allen Z, Tanger P, Mullen JL, Lovell JT, Moyers BT, Whitley D, McKay JK. 2017. TSPmap: A tool making use of traveling salesperson problem solvers in the efficient and accurate construction of high-density genetic linkage maps. *BioData Mining* **10**

Müller LM, Harrison MJ. **2019**. Phytohormones, miRNAs, and peptide signals integrate plant phosphorus status with arbuscular mycorrhizal symbiosis. *Current Opinion in Plant Biology* **50**: 132–139.

Oksanen J, Blanchet FG, Friendly M, Kindt R, Legendre P, McGlinn D, Minchin PR, O'Hara RB, Simpson GL, Solymos P, Stevens MHH, Szoecs E, Wagner H. 2020. vegan: *Community Ecology Package*. *R package version* 2.5-7. https://CRAN.R-project.org/package=vegan

Paredes SH, Gao T, Law TF, Finkel OM, Mucyn T, Teixeira PJPL, *et al*. 2018. Design of synthetic bacterial communities for predictable plant phenotypes. PLoS Biol **16(2)**: e2003962.

Palacio-Mejía JD, Grabowski PP, Ortiz EM, Silva-Arias GA, Haque T, Des Marais DL, Bonnette J, Lowry DB, Juenger TE. **2021**. Geographic patterns of genomic diversity and structure in the C 4 grass *Panicum Hallii* across its natural distribution. *Annals of Botany* **13**:1-19**.**

Peiffer JA, Spor A, Koren O, Jin Z, Tringe SG, Dangl JL, Buckler ES, Ley RE. **2013**. Diversity and heritability of the maize rhizosphere microbiome under field conditions. *Proceedings of the National Academy of Sciences of the United States of America* **110**: 6548–6553.

Pérez-Harguindeguy N, Diaz S, Garnier E, Lavorel S, Poorter H, Jaureguiberry P, Bret-Harte MSS, Cornwell WKK, Craine JMM, Gurvich DEE, *et al.* 2013. New Handbook for standardized measurment of plant functional traits worldwide. *Australian Journal of Botany* **61**: 167–234.

Pérez-Jaramillo JE, Carrión VJ, Bosse M, Ferrão LFV, De Hollander M, Garcia AAF, Ramírez CA, Mendes R, Raaijmakers JM. **2017**. Linking rhizosphere microbiome composition of wild and domesticated Phaseolus vulgaris to genotypic and root phenotypic traits. *ISME Journal* **11**: 2244–2257.

Pérez-Ramos IM, Volaire F, Fattet M, Blanchard A, Roumet C. **2013**. Tradeoffs between functional strategies for resource-use and drought-survival in Mediterranean rangeland species. *Environmental and Experimental Botany* **87**: 126–136.

Peterson RA, Cavanaugh JE. **2020**. Ordered quantile normalization: a semiparametric transformation built for the cross-validation era. *Journal of Applied Statistics* **47**: 2312–2327.

Phillips PC, Arnold SJ. **1999**. Hierarchical Comparison of Genetic Variance-Covariance Matrices. I. Using the Flury Hierarchy. *Evolution* **53**: 1506–1515.

Price AH, Steele KA, Gorham J, Bridges JM, Moore BJ, Evans JL, Richardson P, Jones RGW. **2002**. Upland rice grown in soil-filled chambers and exposed to contrasting water-deficit regimes. I. Root distribution, water use and plant water status. *Field Crops Research* **76**: 11–24.

Poorter H, Bühler J, Van Dusschoten D, Climent J, Postma JA. **2012**. Pot size matters: A meta-analysis of the effects of rooting volume on plant growth. *Functional Plant Biology* **39**: 839–850.

Quast C, Pruesse E, Yilmaz P, Gerken J, Schweer T, Yarza P, Peplies J, Glöckner FO. 2013. The SILVA ribosomal RNA gene database project: Improved data processing and web-based tools. *Nucleic Acids Research* **41**: 590–596.

R Core Team. **2020**. R: A language and environment for statistical computing. *R Foundation for Statistical Computing, Vienna, Austria*. URL https://www.R-project.org/.

Raaijmakers JM, Paulitz TC, Steinberg C, Alabouvette C, Moënne-Loccoz Y. **2009**. The rhizosphere: A playground and battlefield for soilborne pathogens and beneficial microorganisms. *Plant and Soil* **321**: 341–361.

Rajakaruna N. **2004**. The Edaphic Factor in the Origin of Plant Species. *International Geology Review* **46**: 471–478.

Reich PB. **2014**. The world-wide 'fast-slow' plant economics spectrum: a traits manifesto. *Journal of Ecology* **102**: 275–301.

Reich PB, Walters MB, Ellsworth DS. **1997**. From tropics to tundra: Global convergence in plant functioning. *Proceedings of the National Academy of Sciences* **94**: 13730–13734.

Rieseberg LH, Archer MA, Wayne RK. **1999**. Transgressive segregation, adaptation and speciation. *Heredity* **83**: 363–372.

Runquist RDB, Gorton AJ, Yoder JB, Deacon NJ, Grossman JJ, Kothari S, Lyons MP, Sheth SN, Tiffin P, Moeller DA. **2020**. Context dependence of local adaptation to abiotic and biotic environments: A quantitative and qualitative synthesis. *American Naturalist* **195**: 412–431.

Santhanam R, Luu VT, Weinhold A, Goldberg J, Oh Y, Baldwin IT. **2015**. Native root-associated bacteria rescue a plant from a sudden-wilt disease that emerged during continuous cropping. *Proceedings of the National Academy of Sciences of the United States of America* **112**: E5013–E5120.

Singer E, Vogel J, Northen T, Mungall C, Juenger T. 2020. Novel and emerging capabilities that can provide a holistic understanding of the phytobiome. Phytobiomes, in press.

Singer E, Bonnette J, Woyke T, Juenger TE. **2019**. Conservation of endophyte bacterial community structure across two panicum grass species. *Frontiers in Microbiology* **10**.

Stebbins GL. 1952. Aridity as a stimulus to plant evolution. *American Naturalist* **86**: 33–44.

Sukumar P, Legué V, Vayssières A, Martin F, Tuskan GA, Kalluri UC. **2013**. Involvement of auxin pathways in modulating root architecture during beneficial plant-microorganism interactions. *Plant, Cell and Environment* **36**: 909–919.

Tabrett A, Horton MW. **2020**. The influence of host genetics on the microbiome. *F1000Research* **9**.

Toju H, Kurokawa H, Kenta T. **2019**. Factors influencing leaf- and root-associated communities of bacteria and fungi across 33 plant orders in a grassland. *Frontiers in Microbiology* **10**: 1–14.

Tozer AKN, Carswell K, Griffiths WM, Crush JR, Cameron CA, Chapman DF, King W. 2017. Growth responses of diploid and tetraploid perennial ryegrass (*Lolium perenne*) to soil-moisture deficit, defoliation and a root-feeding invertebrate. *Crop & Pasture Science* **68**: 632–642.

Trivedi P, Leach JE, Tringe SG, Sa T, Singh BK. 2020. Plant–microbiome interactions: from community assembly to plant health. *Nature Reviews Microbiology* **18:** 607–621.

Valverde-Barrantes O J, Freschet GT, Roumet C, Blackwood CB. 2017. A Worldview of Root Traits: The Influence of Ancestry, Growth Form, Climate and Mycorrhizal

Association on the Functional Trait Variation of Fine-Root Tissues in Seed Plants. *New Phytologist* **215**: 1562–1573.

Via S, Hawthorne DJ. **2005**. Back to the future: Genetic correlations, adaptation and speciation. *Genetica* **123**: 147–156.

Vij S, Tyagi AK. **2007**. Emerging trends in the functional genomics of the abiotic stress response in crop plants: Review article. *Plant Biotechnology Journal* **5**: 361–380.

Vorholt JA, Vogel C, Carlström CI, Müller DB. **2017**. Establishing Causality: Opportunities of Synthetic Communities for Plant Microbiome Research. *Cell Host and Microbe* **22**: 142–155.

Wagner MR, Lundberg DS, Coleman-Derr D, Tringe SG, Dangl JL, Mitchell-Olds T. **2014**. Natural soil microbes alter flowering phenology and the intensity of selection on flowering time in a wild Arabidopsis relative. *Ecology Letters* **17**: 717–726.

Wagner MR, Lundberg DS, del Rio TG, Tringe SG, Dangl JL, Mitchell-Olds T. 2016. Host genotype and age shape the leaf and root microbiomes of a wild perennial plant. *Nat Commun* **7**: 1–15.

Wallace JG, Kremling KA, Buckler ES. **2018**. Quantitative genetic analysis of the maize leaf microbiome. *bioRxiv*: 208–224.

Waller FR. 1976. *A biosystematic study of* Panicum *section* Diffusa (Poaceae)*in North America*. PhD thesis, TexasA&M University, College Station, TX, USA.

Walters WA, Jin Z, Youngblut N, Wallace JG, Sutter J, Zhang W, González-Peña A, Peiffer J, Koren O, Shi Q, *et al.* 2018. Large-scale replicated field study of maize rhizosphere identifies heritable microbes. *Proceedings of the National Academy of Sciences of the United States of America* **115**: 7368–7373.

Weißhuhn K, Auge H, Prati D. **2011**. Geographic variation in the response to drought in nine grassland species. *Basic and Applied Ecology* **12**: 21–28.

Weinert N, Piceno Y, Ding GC, Meincke R, Heuer H, Berg G, Schloter M, Andersen G, Smalla K. **2011**. PhyloChip hybridization uncovered an enormous bacterial diversity in the rhizosphere of different potato cultivars: Many common and few cultivar-dependent taxa. *FEMS Microbiology Ecology* **75**: 497–506.

Weng X, Lovell JT, Schwartz SL, Cheng C, Haque T, Zhang L, Razzaque S, Juenger TE. **2019**. Complex interactions between day length and diurnal patterns of gene expression drive photoperiodic responses in a perennial C4 grass. *Plant Cell and Environment* **42**: 2165–2182.

Winer BJ. 1971. *Statistical Principles in Experimental Design*. 2nd ed. New York, USA: McGraw-Hill.

Withington JM, Reich PB, Oleksyn J, Eissenstat DM. **2006**. Comparisons of structure and life span in roots and leaves among temerate trees. *Ecological Monographs* **76**: 381–397.

Wu Y, Zheng Z, Visscher PM, Yang J. 2017. Quantifying the mapping precision of genome-wide association studies using whole-genome sequencing data. Genome Biology **18**: 1–10.

Yardeni G, Tessler N, Imbert E, Sapir Y. **2016**. Reproductive isolation between populations of Iris atropurpurea is associated with ecological differentiation. *Annals of Botany* **118**: 971–982.

Zhang Y, Parmigiani G, Johnson WE. **2020**. ComBat-seq: batch effect adjustment for RNA-seq count data. *NAR Genomics and Bioinformatics* **2**: 1–10.